Computational Approaches in Molecular and Systems Pharmacology: Application to Neurosignaling Membrane Proteins

by

Chang Liu

Bachelor of Science, Shandong University, China, 2012

Submitted to the Graduate Faculty of

School of Medicine in partial fulfillment

of the requirements for the degree of

Master of Science

University of Pittsburgh

2014

UNIVERSITY OF PITTSBURGH

School of Medicine

This thesis was presented

by

Chang Liu

It was defended on

July 29th, 2014

and approved by

Dr. Takis Benos, Associate Professor, Department of Computational and Systems biology, University of Pittsburgh

Dr. Donald DeFranco, Professor, Department of Pharmacology and Chemical Biology, University of Pittsburgh

Thesis Advisor: Dr. Ivet Bahar, Professor, Department of Computational and Systems Biology, University of Pittsburgh

Computational Approaches in Molecular and Systems Pharmacology:

Application to Neurosignaling Membrane Proteins

Chang Liu, MS

University of Pittsburgh, 2014

Computational Approaches in Molecular and Systems Pharmacology: Application to Neurosignaling Membrane Proteins

Chang Liu, M.S.

University of Pittsburgh, 2014

Computer-aided drug discovery methods have played a major role in the development of therapeutically important molecules for decades, and some more advanced and effective methods have been introduced in recent years. Those methods are generally classified as either molecular pharmacology methods or quantitative systems pharmacology methods.

In this thesis, with regard to molecular pharmacology computations, we assess the druggability of ionotropic glutamate receptors (iGluRs) N-terminal domains (NTDs) using molecular dynamics (MD) simulations. The simulations are performed in the presence of probe molecules that contain fragments shared by drug-like molecules. iGluRs are ligand-gated ion channels that mediate excitatory neurotransmission events in the central nervous system. Alterations in those receptors, especially in AMPA receptors (AMPARs) and NMDA receptors (NMDARs), are responsible for many neuron diseases like Huntington's diseases and Parkinson's diseases. Our study provides insights into the ligand-binding landscape of iGluR NTD dimers and monomers. Moreover, we build PMs for AMPARs and NMDARs, which are then used in a virtual screening scheme to identify lead compounds.

Our quantitative systems pharmacology studies focus on drug repurposing upon computational analysis of known drug-target interactions. We use the probabilistic matrix factorization (PMF) method for this purpose, which is particularly useful for analyzing large interaction networks. Our method is shown to outperform those recently introduced for identifying new drug-target associations. Finally, we integrate the results from our druggability

simulations and PMF calculations by comparing the drug candidates predicted to bind AMPARs or NMDARs by either of those methods.

In addition, we analyzed the structure and dynamics of sodium-coupled neurotransmitter transporters that share the leucine transporter (LeuT) fold. We explore how the collective motions predicted for LeuT using the elastic network models agree with the structural changes experimentally observed upon ligand binding.

TABLE OF CONTENTS

LIST OF TABLES

LIST OF FIGURES

PREFACE

I would like to sincerely thank my advisor Professor Ivet Bahar, for being a great mentor, whose patience, guidance, care and strong support, both academically and personally, have eventually made my overseas graduate life enjoyable and memorable, especially her strong support during my hard time. I learned a lot under her supervision such as critical thinking, independent researching and preciseness for academic research. It is my great honor to have had her as my supervisor and she will always be my life-long learning example and mental guide who will inspire me to work or study hard to achieve my goals.

Also, I would like to thank my thesis committee members Dr. Takis Benos and Dr. Donald DeFranco whose insightful comments and critiques have shaped my thoughts and ideas towards my research.

In addition, I would like to thank Dr. Ignacio General, Dr. Indira Shrivastava, Dr. Ahmet Bakan, Dr. Anindita Dutta and Murat Can Cobanoglu who taught me some useful techniques and gave me insightful ideas towards research, and who have encouraged me to learn new techniques. Moreover, I feel lucky to have had really helpful lab members, Dr. Mert Gur, Dr. Mary Cheng, Dr. Filippo Pullara, Dr. Bing Liu, Dr. Timothy Lezon and Dr. Elia Zomot and graduate students Mao, Kaitlyn and Cihan.

I feel lucky to have been accepted to the PIMB and happy to have met kind and helpful students and friends, and interact with the faculty and staff of the program. I would like to thank Susanna Goodwin who was always there to offer help and Dr. Jeffrey Hildebrand. Also, in the department of Computational and Systems Biology, I am grateful to Kelly, Sandy and Nancy for their help and patience.

A special acknowledgement goes to my roommate Jue Gong who helped me a lot during my hard times. The time we studied in the library together, had meals together and went to parties together is unforgettable. I also thank my best friends Mengdi Sun, Pu zhang, Shuchang Liu, Rittika, Kaitlyn, Wenzhi Mao, Ya Su , Xiaolong Shen, Qingyang Ding and Jingyi Zhang who accompanied me and made my graduate life colorful in Pittsburgh, whose friendship has meant so much to me and will last forever. I really cherish the time when we had meals together in Tong's Cuisine.

Finally, I would like to thank my dad Mr. Dazhen Liu and my mom Mrs. Hong Qiu who support me to do whatever I do and whose love is selfless and priceless. I hope they will be proud of me one day.

1.0 INTRODUCTION

Drug discovery and development is generally considered to be costly and time-consuming. A typical drug discovery and development cycle takes around 14 years (Myers and Baker 2001) and costs between 0.8 and 1.0 billion USD (Moses, Dorsey et al. 2005). Due to the rapid development in combinatorial chemistry and high-throughput screening technologies, it enables huge libraries of compounds to be screened and synthesized in a short time (Ou-Yang, Lu et al. 2012). However, because of the low efficiency and high failure rate in drug discovery, the output of developing a new drug is not positively proportional to the investment (Shekhar 2008). As a result, computational drug discovery has been developed to transform drug development, and has become an effective method to shorten the research cycle and reduce the cost and risk of failure.

Computer-aided drug design (CADD) is a general term that defines computational approaches and sources for the storage, management, analysis and modeling of compounds toward drug design. It includes many aspects of drug discovery, such as tools for assessing potential lead candidates systematically, computer programs for designing compounds and the development of digital repositories for investigating chemical interactions (Song, Lim et al. 2009).

The traditional and widely used computational drug discovery methods can be classified into two broad groups: structure-based drug design, ligand-based drug design. Structure-based drug design methods include molecular docking, molecular dynamics (MD) simulations and

structure-based pharmacophore modeling (PM). They all rely on knowledge of the target macromolecule structure. The target molecule is usually a protein for which a drug is to be designed, and its structural data are obtained from crystal structures, NMR data and homology models (Chen, Morrow et al. 2012). In the absence of three-dimensional structure for the target, and even in the case where the target is not known, ligand-based drug discovery tools, such as quantitative structure-activity relationship (QSAR) analyses, ligand-based PM, molecular field analysis and 2D or 3D similarity assessment between small molecules can offer insights into the construction of predictive models fit for lead discovery and optimization (Acharya, Coop et al. 2011). Chapter 3 presents MD-based druggability simulation approaches and their application to ionotropic glutamate receptors (iGluRs). We consider in particular two families of iGluRs: AMPA receptors (AMPAR) and NMDA receptors (NMDAR). These simulations use all-atom models in the presence of explicit water and organic probe molecules. Based on the captured "druggable" sites and the binding pause of the probes observed in druggability simulations, PMs are built, which, in turn, are used in virtual screenings for identifying small molecules that potentially serve as drugs for AMPARs and NMDARs.

Many biological functions rely on protein-protein interactions where the structure and dynamics of one or both proteins is affected during the course of binding. Therefore, an understanding of conformational flexibility of target proteins involved in protein-protein interaction and protein-ligand interaction is very important for structure-based drug design. Elastic network models (ENM) normal mode analysis (NMA) (Bahar, Atilgan et al. 1997), rooted in the statistical thermodynamics of polymer networks (Flory, Gordon et al. 1976), are broadly used to extract those more probable modes, which are near the global free energy minimum. Identification of these so-called 'soft modes' has been considered as a prerequisite for

structure-based drug design (Floquet, Marechal et al. 2006). A lot of work has indicated that in fact those soft modes conform to the structural changes associated with ligand binding and allosteric transitions demonstrating their relevance to function (Bahar, Lezon et al. 2010, Bahar, Lezon et al. 2010). Chapter 2 provides an overview of the assumptions and theory underlying these approaches and their application to leucine transporter (LeuT) and secondary transporters sharing the LeuT fold.

Drugs are frequently withdrawn from markets and this is mainly due to their side effects or toxicities. Drug molecules often interact with multiple targets, termed as polypharmacology, and the off-target interactions can cause adverse side-effects. The philosophy of drug design has been transformed from 'one drug, one target' to 'one drug, multiple targets' (Hopkins 2008). Polypharmacology emerged as the new paradigm of drug discovery (Hopkins 2008) and became a major focus in recent CADD studies. Polypharmacological phenomena includes: (a) a single drug acting on multiple targets on a unique disease pathway or (b) a single drug acting on multiple targets pertaining to multiple diseases' pathways (Hopkins 2007, Reddy and Zhang 2013). Moreover, polypharmacology for complex disease is likely to employ multiple drugs acting on distinct targets, that are part of a network regulating various physiological responses (Hopkins 2007). The aim of polypharmacological approaches is to discover the unknown off-targets for the existing drugs, a task also known as drug repurposing (Oprea and Mestres 2012). Chapter 4 provides details on the theory, assumptions and applications of probabilistic matrix factorization (PMF) method for predicting drug-target associations.

Most of the methods described above are used in the present study for investigating the structure, dynamics and/or drug-binding properties of the NMDAR and AMPAR families of proteins and LeuT fold family of proteins. NMDARs and AMPARs play a major role in

mediating neurotransmission events in the central nervous system. NMDARs have served as important drug targets due to their implication in neurodegenerative diseases and neurological disorders, while the druggability of AMPARs has remained unknown to date. Among LeuT-fold family proteins, dopamine transporter (DAT) has been an important drug target for drug abuse and addiction research, among other neurodegenerative disorders. Discovering the structural and dynamic bases of their function and their ligand-binding properties, and the identification of the potential drug candidates may potentially provide new insights into developing better novel therapeutic treatments.

1.1 COMPUTATIONAL METHODS IN MOLECULAR PHARMACOLOGY

Computer-aided drug discovery (CADD) has actively promoted the development of therapeutically significant small molecules for three decades. As mentioned above, CADD approaches are broadly classified into two major methods—structure-based methods and ligand-based methods. Structure-based approaches for drug design include ligand docking, PM and ligand design, all based on knowledge and/or modeling of the target protein structure, while ligand-based methods use ligand information only for predicting activity depending on similarities to already identified active ligands (Sliwoski, Kothiwale et al. 2014). The following paragraphs introduce the position of CADD in the drug discovery pipeline as well as the use of virtual screening, MD simulations, and PM in structure-based CADD, since those methods are used in our study.

1.1.1 CADD in the drug discovery pipeline

CADD can achieve a better hit rate of novel drug compounds, compared to traditional high-throughput screening (HTS) and combinatorial chemistry, due to the usage of more targeted search. It not only helps to understand the molecular basis of therapeutic activity but also to predict other possible activities which might improve therapeutic effects. In the drug discovery process, CADD has been employed for three main goals (Sliwoski, Kothiwale et al. 2014): (1) to filter large compound libraries into smaller ones which can be tested by experimentalists; (2) to design a new compound either by adding a functional group on a starting molecule or by putting chemical fragments together into novel chemotypes; and (3) to optimize lead compounds, whether to increase their affinity or optimize drug metabolism and pharmacokinetics properties including their absorption, distribution, metabolism, excretion and potential toxicity (ADMET).

The most common use of CADD is the screening of virtual compound libraries, known as virtual high-throughput screening (vHTS). This enables researchers to test a series of compounds and provide a reduced set for further tests. In this way, researchers can identify the same number of hits while (experimentally) screening less compounds as they skip those less likely compounds, thereby saving money and time. vHTS was first introduced in 1997 (Horvath 1997) and it triggered an increasing rate of publications on the applications of vHTS since then (Ripphausen, Nisius et al. 2010). The largest fraction of hits has been obtained for G-protein-coupled receptors (GPCRs) followed by kinases (Ripphausen, Nisius et al. 2010).

vHTS has several components, such as compounds selection by predicted biological activity through QSAR models or PM, chemical similarity searches and structure-based docking (Enyedy and Egan 2008). All those methods can rank hits from the screened virtual compound library. The ranking reflects the property of the compounds, such as the percentage of similarity

to a query compound or the predicted biological activity or in the case of docking, an estimate of the relative binding affinity (often expressed as scores) for each compound bound to the targeted protein (Joffe 1991).

There is a substantial cost benefit in the utilization of computational tools during the lead optimization phase of drug development. The cost for developing a new drug ranges from 400 million to 2 billion USD and the synthesis and test of lead analogs contribute a large proportion of the sum (Basak 2012). As a result, it is significant and beneficial to use computational methods in hit-to-lead optimization to cover a wider chemical space while dramatically decreasing the number of compounds that must be tested or synthesized *in vitro* (Sliwoski, Kothiwale et al. 2014). Optimization of a hit compound computationally includes a structure-based analysis of docking poses or energy profiles for hit analogs, ligand-based screening for compounds with similar chemical structure and properties or improved enhanced biological activity and prediction of biologically preferred ADMET properties. The comparably low cost of CADD, compared to chemical synthesis and biological characterization of compounds, makes it popular as a tool for generating more focused, reduced and diversified set of compounds in the the chemical space that is explored (Enyedy and Egan 2008).

1.1.2 Use of MD simulations in CADD

Molecular dynamics (MD) simulation can be used for binding site detection and characterization. The dynamics of proteins make it inappropriate to predict binding site using a single static structure. Several conformations are used to account for the conformational dynamics of a protein. Conventional MD can capture an ensemble of protein conformations starting with a single structure. MD simulations use classical Newtonian physics principles to compute a

trajectory of conformations of a target as a function of time. The trajectory is computed for a given number of atoms in small time steps, usually 1-10 fs (van Gunsteren and Berendsen 1990). Molecules simulated in classic MD approaches have a tendency of being trapped in local energy minima. To overcome this, some advanced MD algorithms including targeted-MD (Schlitter, Engels et al. 1994), SWARM-MD (Huber and van Gunsteren 1998), conformational flooding simulations (Grubmüller 1995), temperature accelerated MD simulations (Abrams and Vanden-Eijnden 2010) and replica exchange MD (Sugita and Okamoto 1999) have been introduced. In general, these methods permit us to jump over multiple minima on the energy surface of proteins, thus allowing for a more complete sampling of the conformational space. One example of success of MD simulations is the identification of a novel binding trench in HIV integrase, which led to the development of raltegravir, a drug used to treat HIV infection. The MD simulation of the inhibitor of the same protein, 5CITEP, captured a novel binding trench which was not detected with a static structure previously (Schames, Henchman et al. 2004). After the discovery, Merck developed the antiretroviral drug raltegravir (Summa, Petrocchi et al. 2008).

A major limitation in MD simulations is the time scale that can be explored, usually limited to nanoseconds-to-microseconds. More recently, the timescale has been extended to milliseconds (for small proteins) with the development of the special purpose machine Anton (Shaw, Deneroff et al. 2008). Such long simulations now provide more accurate visualization of drug binding events to their targets (Shan, Kim et al. 2011). Anton has been used successfully for full atomic resolution protein folding (Lindorff-Larsen, Piana et al. 2011). Advances in computer technology mean that protein flexibility can be accessed more efficiently, which may allow us to have a better understanding and descriptions of the effect of protein dynamics in biological function.

1.1.3 Pharmacophore modeling (PM) in CADD

A PM of the target binding site summarizes electronic and steric features required for optimal interaction of a ligand with a target (Sliwoski, Kothiwale et al. 2014). The typical properties that define a PM are hydrogen bond acceptors or donors, basic or acidic groups, partial charges, aliphatic hydrophobic moieties and aromatic hydrophobic moieties. Pharmacophore features have been widely used in lead optimization, virtual screening and *de novo* drug design (Yang 2010). A PM for a target binding site can be used to virtually screen a compound library like DrugBank containing all FDA-approved drugs, or STITCH database that contains information in small molecules/ligands characterized to date. In addition to interrogate such databases for filtering the inactive compounds, PM can be used to refine drug design.

Structure-based PM approaches are usually developed upon analyzing the target binding site or target-ligand complex structure (Sliwoski, Kothiwale et al. 2014). For instance, LigandScout (Wolber and Langer 2005) use protein-ligand complex data to map interactions between ligands and targets. Usually, there is an empirical scoring algorithm, which includes terms to account for van der Waals interactions, metal-ligand bonding, hydrogen bonding and desolvation effects (Wang, Liu et al. 1998) and the algorithm can automatically develop a PM from target-ligand complex.A successful application is that of Brvar et al. (Brvar, Perdih et al. 2010) who used a PM to identify novel inhibitors of bacterial DNA gyrase B, a target for antibacterial drugs. A PM learned from LigandScount was utilized to screen the ZINC database, which produced a novel class of thiazole-based inhibitors with IC_{50} value of 25 uM.

1.2 COMPUTATIONAL METHODS IN SYSTEMS PHARMACOLOGY

Systems biology approaches have long been used in pharmacology to understand drug action. The application of computational and experimental systems biology methods allows us to extend the definition of systems pharmacology (Zou, Zheng et al. 2013), which provides a field of study that provides us with a comprehensive view of drug action in humans. Systems pharmacology is rooted in molecular interactions between drugs and their targets in the cell, and includes network analyses at multiple scales of biological organization to explain both therapeutic and adverse effects of drugs (Zhao and Iyengar 2012). In the long run, advances in systems biology will assist in the development of new drugs and more effective therapies for patients. Systems biology approaches make contributions to several clinically driven applications in drug discovery. Here, we introduce five recent advances and major applications in this area: (1) analysis of drug-target networks, (2) prediction of drug-target interactions, (3) predictions of drug combination, (4) drug repurposing, (5) exploration of the side effects of drugs (Zou, Zheng et al. 2013).

1.2.1 Drug-target networks

Quantitative analysis of drug-target networks systematically helps disclose the patterns of interactions between drugs and targets. Drugs usually bind multiple rather than single molecular targets, a phenomenon known as polypharmacology (Hopkins 2007). Quantitative topological analyses of drug-target networks show an overabundance of ‘follow-up’ drugs, that is to say drugs target those proteins already targeted by other drugs (Zou, Zheng et al. 2013). Thus, many proteins are targeted by more than one drug, although those drugs have distinct chemical structures. These observations have significant implications for drug discovery and will lay the

ground for future CADD work. While single-target approach remains the main strategy currently, a large body of work has been done to facilitate the development of 'promiscuous drugs' which can bind multiple targets.

Integration of systems biology and polypharmacology offers the opportunities to expand current technologies to improve clinical efficacy and decrease adverse effects and toxicity of drugs. Advances in these fields are forming the foundation of the next paradigm in drug discovery, that is 'network pharmacology' (Hopkins 2008). Along these lines, Keiser et al. related receptors to each other quantitatively based on the chemical similarities between the ligands that they are interacting with. They have shown that targets without significant sequence or structure similarity are still linked quantitatively based on their bioactive ligands that they share (Keiser, Roth et al. 2007). This type of link between drugs and targets can be used to predict their biological function. Moreover, another computational framework developed by Li et al. can be used to build disease-specific drug-protein network and help study molecular signature differences between different classes of drugs under different diseases conditions (Li, Zhu et al. 2009).

1.2.2 Predictions of drug-target interactions

Since the observation of drug polypharmacology, this concept has motivated a large number of studies to predict and characterize drug- target associations (Oprea, Tropsha et al. 2007, Siegel and Vieth 2007, Bajorath 2008, Newman 2008, Miller, Dunham et al. 2009, Walsh and Fischbach 2009). Some groups have employed phenotypic and chemical similarities among molecules to identify those interacting with multiple targets (Wagner, Kitami et al. 2008, Young, Bender et al. 2008), and early drug candidates have been screened against molecular target

panels (Krejsa, Horvath et al. 2003). To identify new targets for known drugs, Campillos et al. looked for side-effects shared between two molecules and applied to marketed drugs (Campillos, Kuhn et al. 2008). Several new drug-drug relations have emerged between chemically dissimilar drugs having different therapeutic indications, implying that they are involved in new drug-target associations (Paolini, Shapland et al. 2006).

Unlike conventional approaches based on sequence or structural similarity between targets, Shoichet, Roth and coworkers developed a computational tool that predicts the pharmacological profile of drugs (Keiser, Setola et al. 2009). They introduced the 'similarity ensemble approach' (SEA) which defines each target by its set of known ligands, searches for drugs with chemical structure similar to the known ligands, and then eventually predicts new drug-target interactions. To integrate side-effect and pharmacogenomics similarities, Takarabe et al. made a comprehensive prediction and pointed to some potential drug-target associations that were not identified by previous methods (Takarabe, Kotera et al. 2012). In addition, it is shown by Cheng et al. that network-based inference methods perform best on predicting drug-target interactions after comparison of three supervised inference approaches (Cheng, Liu et al. 2012). In this regard, the important role of machine learning approaches such as active learning has been highlighted (Murphy 2011). The application of probabilistic matrix factorization (PMF), a widely used machine learning method, to the prediction of drug-target interactions will be discussed in details in Chapter 4.

1.2.3 Predictions of drug combinations

In recent years, combination therapies were shown to be more beneficial to patients than using a single drug (Jia, Zhu et al. 2009). Systems biology approaches have been used to describe and

predict potential drug combinations (Fitzgerald, Schoeberl et al. 2006). Dynamical modeling has already been used to simulate the effect of drug combinations and generate testable intervention methods experimentally (Iadevaia, Lu et al. 2010, Zou, Luo et al. 2011). However, due to lack of knowledge on the kinetics of biochemical reactions, these dynamic models are currently restricted to small scales. Given that target information is usually accessible, the combined effect of drugs on specific targets may be assessed by analyzing the interaction pattern of targets using a network perspective (Zou, Ji et al. 2012). Lee et al. showed that how the progressive rewiring of oncogenic signaling networks over time following EGFR inhibition makes breast tumors vulnerable to a second and later hit with DNA-damaging drugs, indicating that time- and order-dependent drug combinations might be more effective in killing cancer cells (Lee, Ye et al. 2012). Lehar et al. used large-scale simulations of bacterial metabolism to simulate the inhibitory effects of drug combinations and gave evidence that synergistic combinations are in general more specific to particular cellular phenotypes than are to single agents (Lehar, Krueger et al. 2009). Kwong et al. investigated a gated signaling model that provides a new framework to find synergistic drug combinations for melanoma (Kwong, Costello et al. 2012)

1.2.4 Drug repurposing

Drug repurposing, also called drug repositioning, one of the alternatives for drug discovery, is to explore new therapeutic applications for known drugs. The essential advantage for drug repurposing is that it can dramatically reduce the risks of drug development and promote repurposed drugs to advance to clinical phase more rapidly. For example, Iorio et al. developed a method that uses the similarities in the molecular activity signatures of all drugs so as to calculate pair-wise similarities between drugs in their drug mode and in their effects (Iorio,

Bosotti et al. 2010). Drugs were organized into a network based on the resulting similarity scores. Then, drugs were separated into groups of interconnected nodes (i.e., communities) using network theory. Those compounds with similar mode of action were grouped into same communities, which usually shared the same targets and pathways. By this method, drug repurposing shows its importance in collocating drugs within network communities, which identifies a shared molecular activity with other drugs in the same drug communities. Moreover, some systems biology methods based on genomics have been published, which aim at drug repurposing (Sirota, Dudley et al. 2011, Jin, Fu et al. 2012). Iskar et al. found a large set of drug-induced transcriptional modules from genome-wide microarray data of drug-treated human cell lines (Iskar, Zeller et al. 2013). Those identified modules show the conservation of transcriptional activities in response to drugs, which provides a hint for drug repurposing. Gottlieb et al. developed 'PREDICT' algorithm that could deal with both novel compounds and approved drugs (Gottlieb, Stein et al. 2011). This new approach is based on the assumption that similar drugs are involved in similar diseases, and uses the chemical similarity of drugs as well as disease-disease similarity measures for predicting novel drug indications.

1.2.5 Exploring the side effects of drugs

One of the major challenges for drug discovery is to predict the toxicity and side-effects of drugs in the early stage of drug development pipeline. Assessment of drug candidates can dramatically change when integrating biological data and systems biology methods. Lounkine et al. utilized a similarity ensemble approach, which computes whether a drug will bind to a target or not based on the chemical properties it shares with existing ligands, and predicted the activity of marketed drugs on unintended 'side-effect' targets (Lounkine, Keiser et al. 2012). Around half of their

predictions were validated by experiments and a correlation metric was developed to give more weight to those new off-targets that explained side effects of a certain drug better than any known existing target of the drug. Recently, Kuhn et al. have performed a large scale analysis to systematically predict and identify proteins that are implicated in drug side effects (Kuhn, Al Banchaabouchi et al. 2013). Clinical phenotypic data and existing drug-target interactions were integrated to find overrepresented protein side effect associations. They demonstrated that some individual proteins are responsible for regulating most of complex side effects. Yang et al. have developed a computational chemical-protein interactome, which mimics the interactions between drugs known to cause at least one type of severe side effect and a group of human proteins (Yang, Chen et al. 2009). They pointed out that those drugs that share similarities in their chemical-protein interactome profiles also share side-effects. Through exploration of the associations between drugs and off-targets, they also elucidated the molecular basis of several adverse events. There are other researches who adopted integrated systems biology and structural or chemoinformatics analyses, which proved to predict drug adverse effects (Chang, Xie et al. 2010, Chen, Lu et al. 2013).

2.0 ELASTIC NETWORK MODELS: THEORY AND APPLICATION TO LEUCINE TRANSPORTER

Proteins have the ability to go through a distribution of collective changes in conformation, or modes of motions at their equilibrium or native state, which accommodate their function (Bahar, Chennubhotla et al. 2007). Coarse-grained methods have been widely used in capturing those collective movements. Particularly, after the studies performed by Bahar and coworkers (Bahar, Atilgan et al. 1997, Haliloglu, Bahar et al. 1997) and Hinsen (Hinsen 1998), ENMs have been broadly used in association with normal mode analysis (NMA) and revealed that network models can capture global modes. The wide use of ENMs results from their three major advantages: simplicity, robustness of predicted modes of motions in the low frequency regime (the softest modes), and functional significance of these modes, as indicated by a large number of applications (Bahar, Lezon et al. 2009).

In this chapter, we describe the general theory and methods of ENMs, especially the Anisotropic Network Model (ANM), along with its application toward understanding the specific features and structural dynamics of leucine transporter (LeuT). Also, we compare the conformation sampling ability of ANM and MD simulations for LeuT.

2.1 ELASTIC NETWORK MODELS

2.1.1 Theory and methods

The principal assumption in ENMs is that the intrinsic dynamics of a protein is defined by its topology which is represented as a network of nodes and springs; the nodes match the coordinates of individual residues and the springs simulate the interactions between residues that stabilize the whole structure. The Gaussian network model (GNM) (Bahar, Atilgan et al. 1997, Haliloglu, Bahar et al. 1997) and the anisotropic network model (ANM) (Doruker, Atilgan et al. 2000, Atilgan, Durell et al. 2001) are the two most widely used ENMs. In both models, the coordinates of α-carbons, which can be obtained from experiments, are identified as the positions of nodes, and each residue pair with α-carbons located within a cutoff distance r_c is connected by a spring of uniform force constant γ. In accord with the original statistical thermodynamics theory of random polymer networks (Flory, Gordon et al. 1976), the GNM and ANM potentials for a protein of N residues are:

$$V_{GNM} = \frac{\gamma}{2}\left[\sum_{i=1}^{N-1}\sum_{j=i+1}^{N} \Gamma_{ij}\left(\boldsymbol{R_{ij}} - \boldsymbol{R_{ij}^0}\right) \bullet \left(\boldsymbol{R_{ij}} - \boldsymbol{R_{ij}^0}\right)\right] \quad (1)$$

$$V_{ANM} = \frac{\gamma}{2}\left[\sum_{i=1}^{N-1}\sum_{j=i+1}^{N} \Gamma_{ij}\left(R_{ij} - R_{ij}^0\right)^2\right] \quad (2)$$

where • designates the dot product, $\boldsymbol{R_{ij}}$ and $\boldsymbol{R_{ij}^0}$ are the instantaneous and native state distance vectors between residues i and j, $R_{ij}\ and\ R_{ij}^0$ are their magnitudes and Γ_{ij} is ijth element of the Kirchhoff matrix equal to -1, if $R_{ij} < r_c$, otherwise it equals to zero. Thus, the major difference between GNM and ANM is that GNM potential is contributed by both distance and orientation changes while ANM potential is only based on distance changes. Hinsen et al. was the first to propose a coarse-grained harmonic potential for all residue pairs, by using a distance dependent force constant (Hinsen 1998) while the use of uniform force constant accounts for specific and nonspecific interactions as the same. Modifications of ANM with more elaborate force constants have revealed a subtle improvement in the prediction accuracy (Yang, Song et al. 2009), such as negative exponents (Yang, Song et al. 2009) or an exponential decay function (Hinsen 1998). Recently, Bahar et al. suggested that the next level of optimization of ENM lies in the incorporation of secondary structure dependent force constant (Lezon and Bahar 2010).

2.1.2 ANM-based evaluation of global modes of motion

Previous studies have validated that the global modes of biomolecules are dominantly defined by the overall shape of the biomolecule or inter-residue contact distribution regardless of the detailed structure and energetics (Tirion 1996, Ma 2005). The most important point is that, in many studies, these global modes have been shown to be associated with functional motions (Bahar, Chennubhotla et al. 2007, Yang and Chng 2008), and thus it is essential to identify them computationally, and ANM is one of those methods to achieve this goal effectively (Eyal, Yang et al. 2006).

ANM modes are computed based on eigenvalue decomposition of the Hessian matrix (**H**). **H** is the matrix of the second derivatives of V_{ANM} with respect to residue position. Eigenvalue decomposition of **H** yields 3N-6 eigenvectors. For instance, the kth eigenvector, $\mathbf{u_k} = (u_{x1}, u_{y1}, u_{z1}, \ldots u_{zN})_k^T$, also called ANM mode k, describes the normalized displacements of N residues in the x, y and z directions as driven by mode k. It defines the normal coordinate along which the structure moves as residues moves along ANM mode k. Also, λ_k, the corresponding eigenvalue measures the frequency of that mode and also provides information on the shape of the protein subject to that V_{ANM} . The obtain the displacement of all residue positions along mode k, we use the equation below (Xu, Tobi et al. 2003) :

$$\Delta \boldsymbol{R} = \boldsymbol{R^k} - \boldsymbol{R^0} = \pm \boldsymbol{l} * \boldsymbol{\lambda_k^{-0.5}} * \boldsymbol{u_k} \qquad \textbf{(3)}$$

Where l is a constant and it is a product size scaling factor, Boltzmann constant (k_B) and absolute temperature (T). $\boldsymbol{R^0}$ is the initial conformation. With different values of l, we can generate an ensemble of conformations along mode k.

2.2 LEUCINE TRANSPORTER: A MODEL SYSTEM FOR EXPLORING SODIUM-COUPLED NEUROTRANSMITTER TRANSPORT

Neurotransmitter symporters are integral membrane proteins which are ion-coupled transporters: they can drive the uphill uptake of chemical transmitter from neural synapse and terminate neurotransmission mediated by dopamine, serotonin, noradrenaline, glycine and GABA(Krishnamurthy and Gouaux 2012). LeuT is a bacterial homologue the crystal structure of which has offered valuable insights into the mechanism of function of mammalian neurotransmitter transporters. So far, there are 50 available crystal structures of LeuT fold family members, in distinct conformations such as outward-open, inward-open, outward occluded, competitive and non-competitive bound states, which have revealed a mechanistic framework for the transport and transport inhibition of neurotransmitter. The paragraphs below describe the current understanding of mechanistic and pharmacological properties of these mammalian neurotransmitter sodium symporters (NSSs) gained from the structures of LeuT.

2.2.1 Structure of LeuT

LeuT is composed of 12 transmembrane helices. The first 10 helices are correlated by an inverted symmetry topology: helices 1 to 5 and helices 6 to 10 are related by a pseudo two-fold axis of symmetry (Yamashita, Singh et al. 2005) (Figure 1). This structure indicates a relationship with the molecular organization of solute carrier 6 (SLC6) transporters. Helices1 and

6 have discontinuous parts with loops connecting their portions ‘a’ and ‘b’. The regions where the helices are broken harbor the ions and substrate binding sites (Figure 1). The substrate, leucine, binds a binding pocket that is occluded from extracellular solvent upon closure of the gating residue F253 (on TM6a). The two sodium ion binding sites are located in the close

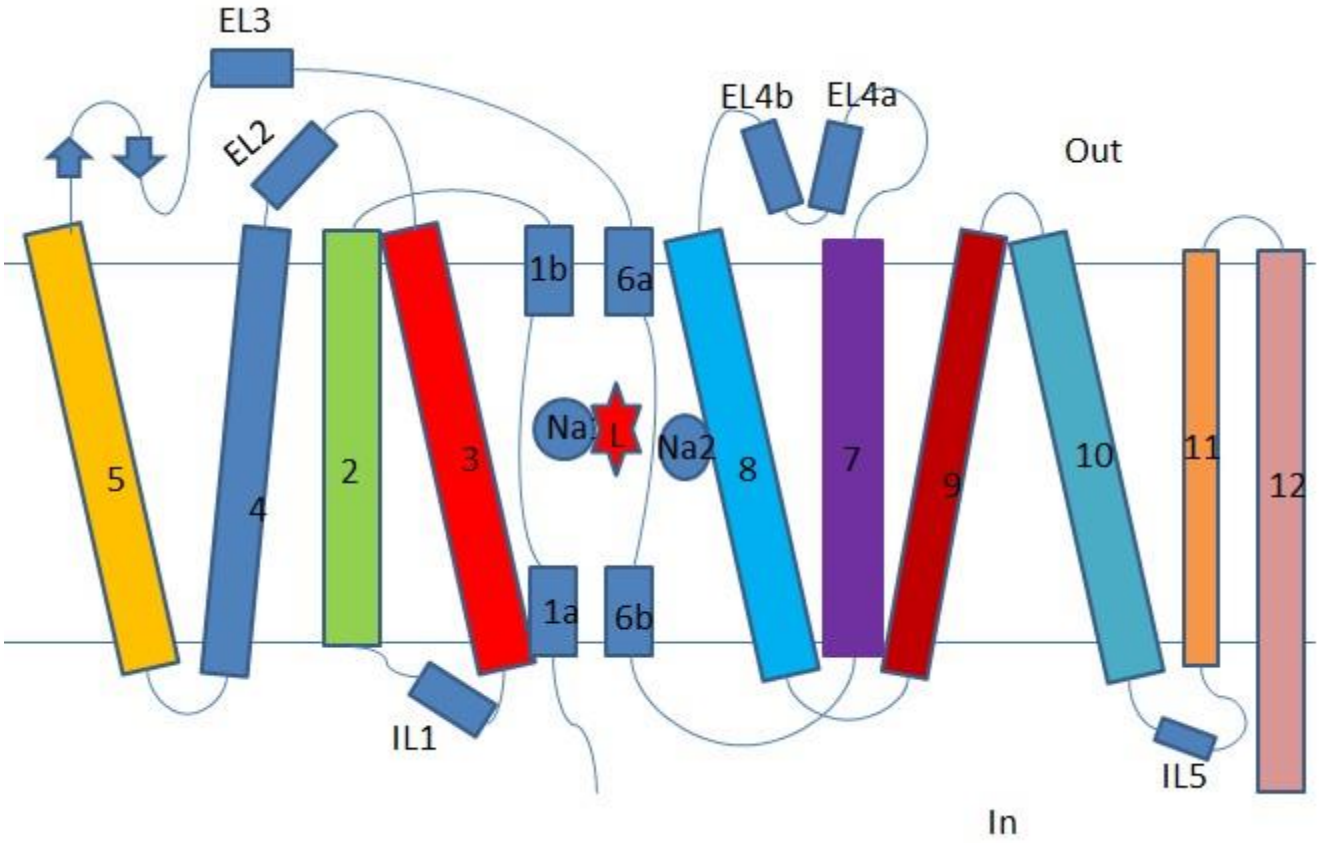

neighborhood of the substrate binding site (Yamashita, Singh et al. 2005).

Figure 1 Secondary structure of LeuT

The positions of leucines (L; *red star*) and two sodium ions (*blue ellipses*) are depicted in the topological diagram of the LeuT. The structure contains 12 transmembrane helices. EL2, EL3 and EL4a-b are extracellular loops. The diagram also shows the intracellular loops IL1 and IL5.

Though LeuT shares structural similarities with mammalian NSS family members, the amino acid transport by LeuT is not chloride dependent, which is different from NSS members that require both sodium and chloride for effective transport (Yamashita, Singh et al. 2005). Forrest et al. suggested the importance of LeuT for the identification of a potential chloride site through homology modeling and site-directed mutagenesis on mammalian serotonin transporter and stated that chloride binds in a pocket close to sodium site 1 (Na1) with residues in TM7 involved in anion coordination, and E290 in LeuT being a key site for chloride conductance (Forrest, Tavoulari et al. 2007). A recent report by Kantcheva et al. validated this site (Kantcheva, Quick et al. 2013).

2.2.2 Transport cycle and alternating access in LeuT

For a comprehensive understanding of LeuT transport cycle, structural data for the major LeuT intermediate states are required. The current available crystal structures are in the outward open, outward-occluded and inward-open states; and there is no available crystal structure for inward-occluded state. To offer a complete picture of the transport cycle, we generated the inward-occluded state structure obtained from MD simulation.

LeuT has a group of nearly invariant helices constructing the ‘scaffold’ domain (TM3, 4, 8 and 9) and a group of helices which undergo relatively large movement acting as the ‘core’ domain (TMs 1, 2, 6 and 7) (Yamashita, Singh et al. 2005, Forrest, Zhang et al. 2008). In order to stabilize the conformations of the outward-open and inward-open states (both are substrate-free) when obtaining their crystal structure, the Gouaux laboratory mutated specific residues and used specific antibodies (Krishnamurthy and Gouaux 2012).

Figure 2 illustrates the series of structures visited during the LeuT transport cycle, starting from the outward-open conformation (Figure 2A). TM1b and TM6a are released allowing them to move outward due to the mutation (Y108F) which weakens then substrate binding (Krishnamurthy and Gouaux 2012). We can see that the extracellular gate (labelled in blue circle) is open and the binding site for leucine is exposed for substrate binding. The intracellular gate is closed, which requires Na^+ binding to stabilize intracellular closed conformation, as confirmed by single- molecule FRET studies as well (Zhao, Terry et al. 2010).

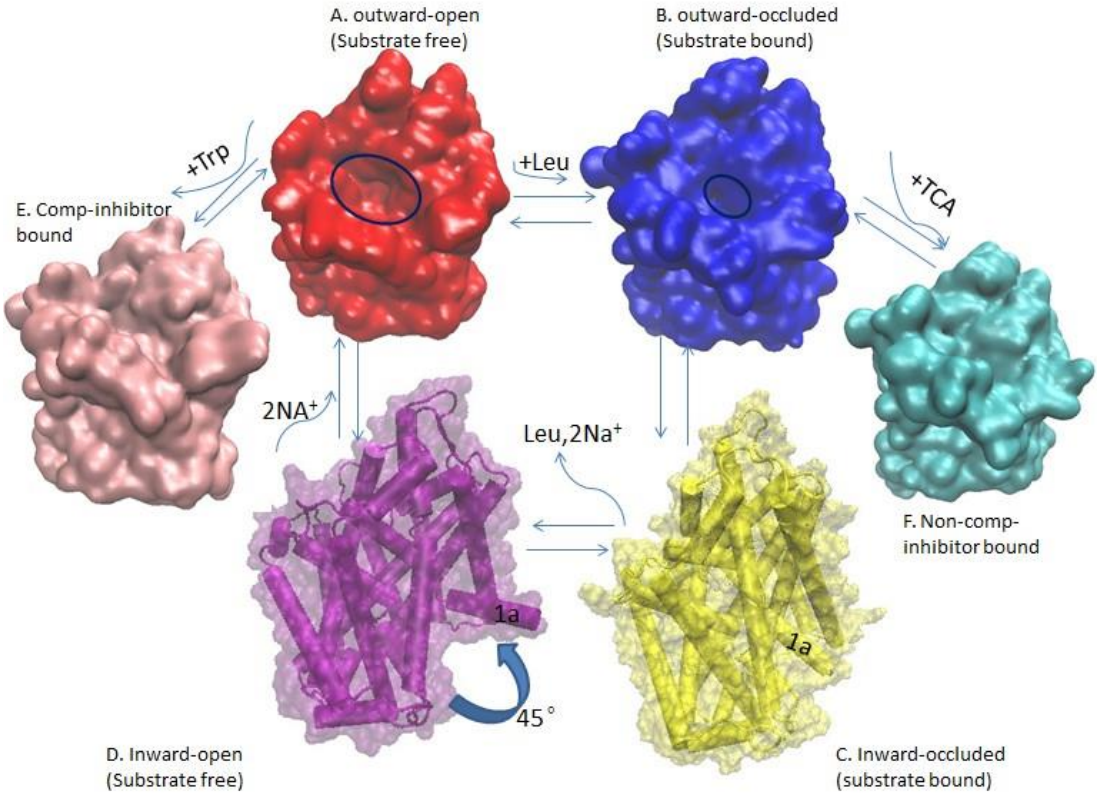

Figure 2 Transport cycle of LeuT.

A. outward-open (substrate-free) state (*red*, PDB ID: 3TT1), B. outward-occluded (substrate-bound) (*blue*, PDB ID: 2A65), C. inward-occluded (substrate bound) (*yellow*, note: this conformer is obtained from simulations as the structure is not experimentally available yet.) D. inward-open (substrate free) (*magenta*, PDB ID : 3TT3), E. Competitive-inhibitor Trp bound outward-open (*pink*, PDB ID : 3F3A), F. Non-competitive inhibitor TCA bound outward-occluded. (*cyan*, PDB ID :2Q6H)

Thus,the outward-open state is substrate-free but Na^+-bound. Once binding leucine, LeuT changes conformation into the outward-occluded conformation (Figure 2B) where the extracellular gate is closed. Then, the outward-occluded conformation transits to the inward-occluded state, the crystal structure of which is not available for far. Finally, the inward-occluded state opens its intracellular gate with leucine and Na^+ released, it reconfigures into the inward-open substrate-free state as a consequence of large hinge-like movements within the core domain relative to the scaffold domain, and shifts in extracellular loops (Krishnamurthy and Gouaux 2012). The most notable change includes TM1a tilting by 45 degree from its position in the closed state as shown in Figure 2D.

Generally, during the LeuT transport cycle, local hinge like bending of helices are coupled to the formation and disruption of substrate- and sodium-binding sites, which are translated by almost rigid-body motion of other helices and loops and thereby opening and closing the extracellular and intracellular gates (Krishnamurthy and Gouaux 2012).

Previous structural and biophysical studies supported the alternating access mechanism in neurotransmitter transporter (Forrest, Zhang et al. 2008). Accordingly, the membrane proteins' binding site is accessible to only one side of membrane upon opening and closing intracellular and extracellular gates, alternatively (Penmatsa and Gouaux 2014). Shimamura et al. found that in Mhp1, which is another LeuT-fold protein, outward-open and inward-open states are created by rigid helical movements, where four helices move against a rigid core to provide access to the substrate in either side of the transporter (Shimamura, Weyand et al. 2010). Also, Perez et al. showed that BetP transports the osmolyte betaine involving helical elements that works as a rigid-bodies coupled with small conformational changes (Perez, Koshy et al. 2012). In LeuT, TM1a moves as much as 45 degree (Figure 2D), but it has a minimal movement of 18 degree in

BetP (Perez, Koshy et al. 2012). To validate the large-scale changes in the position of TM1a in LeuT, single molecule FRET studies have been performed, which confirmed that displacements of TM1a are associated with the release of substrate (Zhao, Terry et al. 2011).

2.2.3 Pharmacological properties of LeuT

Neurotransmitter sodium-coupled symporters (NSSs) regulate endogenous neurotransmitter concentrations and are targets for a wide range of therapeutic agents including selective serotonin reuptake inhibitors (SSRIs), serotonin-noradrenaline reuptake inhibitors and tricyclic antidepressants (TCAs) (Wang, Goehring et al. 2013), which are used to treat depression, ADHD and fibromyalgia as a few examples. Therefore, LeuT has been used to examine the structure of the complexes NSSs form with antidepressant drugs. TCAs, such as clomipramine binds with weak affinity a site in the extracellular vestibule of LeuT (Singh, Yamashita et al. 2007), consistent with their observation that TCAs are non-competitive inhibitors of transport in LeuT (**Figure 2**F). In the presence of bound-TCA, LeuT is locked in an occluded state. Although TCAs and SSRIs are non-competitive inhibitors for LeuT-coupled transport, they do not necessarily represent how antidepressants act on mammalian NSSs. Many studies indicate that anti-depressants inhibit biogenic amine transport by competitive binding (Henry, Field et al. 2006, Andersen, Stuhr-Hansen et al. 2011).

To illustrate the mechanism of competitive inhibition, Singh et al. tested different amino acids and eventually found that tryptophan (Trp) inhibited LeuT transport competitively and stabilized LeuT in the outward-open state (Figure 2E), while other amino acids like Ala, Gly and Met stabilized an occluded state through competitive inhibition (Singh, Piscitelli et al. 2008). Furthermore, in order to make LeuT behave like the human biogenic amine transporters, the

Gouaux group mutated some key residues in LeuT, and TCAs and SSRIs were found to inhibit this specifically mutated LeuT competitively and trap it in the outward open state as what Trp does for LeuT (Wang, Goehring et al. 2013). Their studies define common and simple principles for the action of SSRIs and TCAs on human biogenic amine transporters. In addition, using LeuT as a molecular model, Kristensen et al. modified residues lining the binding pocket in TM1, 3, 6, 8 and 9 in the noradrenaline transporter (NET), and identified the highly binding affinity shift of NET from talopram to citalopram which is a highly specific and most selective SERT inhibitor (Andersen, Stuhr-Hansen et al. 2011). All those studies highlight the role that LeuT plays as a template to model the structures of human neurotransmitter transporters.

2.3 APPLICATION OF ENM TO LEUCINE TRANSPORTER

In this section, we apply the ANM to LeuT as a template model for NSSs. We compare the ANM predictions to the principal components of structural variation deduced from principal component analysis (PCA) of experimental data on LeuT fold family members. Also, we compare the conformation sampling ability between ANM predicted conformers and full atomic MD simulations of LeuT.

2.3.1 Metrics for comparing experimental data and ANM predictions

For a give protein, if we have two structures A and B, a metric for structural change is the 3N-dimensinal deformation vector $\mathbf{d_{AB}} = \mathbf{R^A} - \mathbf{R^B}$, where $\mathbf{R^A}$ and $\mathbf{R^B}$ are the respective vectors of the 3N coordinates of N residues for the structures. To eliminate translational and rotational differences, the two structures are optimally superimposed and then we use the coordinates of the α-carbons with respect to the superimposed reference frames to construct are $\mathbf{R^A}$ and $\mathbf{R^B}$. The correlation cosine between eigenvector $\mathbf{u_k}$ (evaluated for one of the conformers) and deformation vector $\mathbf{d_{AB}}$ measures the level of similarity between the direction of ANM mode k and the structural change $\mathbf{d_{AB}}$ experimentally observed between conformers A and B. It is interesting to assess whether the soft modes (k = 1, 2, 3 etc.) predicted for conformer A agree with $\mathbf{d_{AB}}$, which would mean that the intrinsic dynamics of the protein in state A favors its structural change into state B. This has been the case observed in many applications, suggesting that proteins have evolved to favor soft modes that enable functional changes in structure.

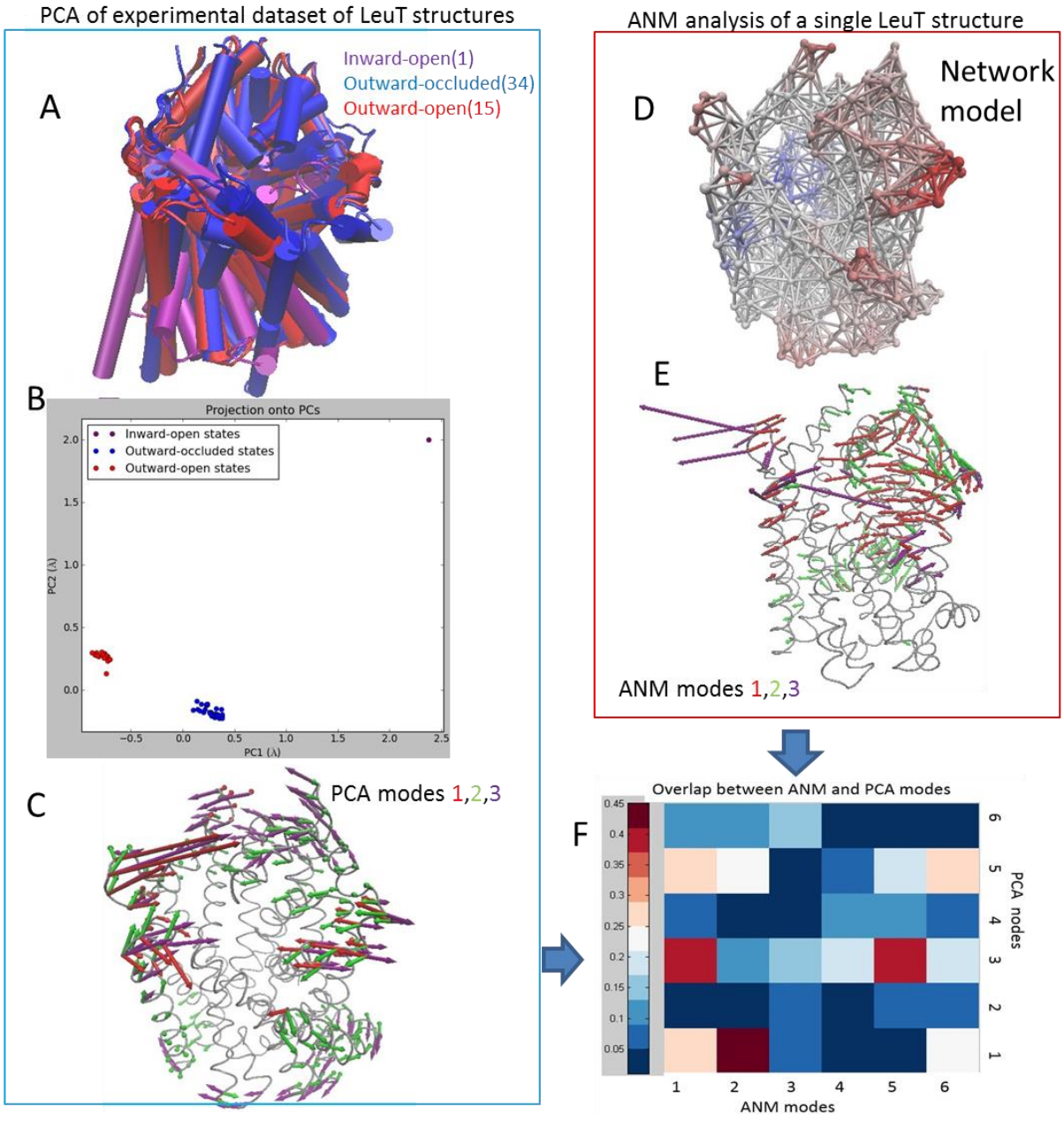

Figure 3 **Description of the method for comparing ANM-predicted modes with the principal structural variations observed in all available crystal structures with LeuT fold.**

(A) Superposition of the ensemble of 50 available crystal structures that are structurally homologous to LeuT. (**B**) Projection of the structures on the top 2 PCs. (C) Structural changes along the top three PCA modes (**D**) ANM representation of LeuT (**E**) Structural variations along the softest three ANM modes. (F) Overlap between top 6 ANM and PCA modes.

For a number of protein targets, there is a large ensemble of structures available in the Protein Data Bank (PDB). For LeuT fold family members, there are currently 50 crystal structures available in PDB (**Figure 3**A). Bakan and Bahar showed that a principal component analysis (PCA) of the structures can be performed to extract principal modes of structural changes based on experimental data, which, then, may be compared to the softest modes predicted by ANM (Bakan and Bahar 2009), as outlined in **Figure 3**. The PCA of the ensemble of experimentally resolved structures, requires the evaluation of a 3Nx3N covariance matrix, **C**, defined as

$$\mathbf{C} = \langle \Delta \boldsymbol{R}\, \Delta \boldsymbol{R}^{\boldsymbol{T}} \rangle = \frac{\mathbf{1}}{\boldsymbol{m}} \sum_{\boldsymbol{A}} (\Delta \boldsymbol{R}^{\boldsymbol{A}} \Delta \boldsymbol{R}^{(\boldsymbol{A})\boldsymbol{T}}),$$

where *m* is the number of structures in the ensemble and $\Delta \boldsymbol{R}^{\boldsymbol{A}}$ is the deviation of conformation A away from the ensemble average <**R**>. After eigenvalue decomposition of **C**, $\mathbf{C} = \sum_{\boldsymbol{n}=\mathbf{1}}^{\boldsymbol{m}} \boldsymbol{\sigma}_{\boldsymbol{n}} \boldsymbol{p}_{\boldsymbol{n}} \boldsymbol{p}_{\boldsymbol{n}}$ we get the principal components $\boldsymbol{p}_{\boldsymbol{n}}$ of structural variations (eigenvectors) and the corresponding variances (eigenvalues) σ_n. Among those eigenvalues, σ_1 is the largest variance and the corresponding principal vector $\boldsymbol{p}_{\mathbf{1}}$ describes the displacement along this largest variance mode, also called PCA1 or PC1. Obviously, $\boldsymbol{p}_{\mathbf{1}}$ contributes the most to the average root-mean-square deviations <RMSD> between structures.

The ensemble of structures can be projected onto those top PCs defined space. Thus, each structure **A** or **B** can be represented by a point in the space spanned by the PCs. The points in Figure 3B represent such an ensemble of structures (50 of them in the case of LeuT) mapped into the subspace spanned by PC1 and PC2. We can see that the three different states, outward-open (*red*; 15 structures), outward-occluded (*blue*; 34 structures) and inward-open (*purple*; 1

structure), are clearly separated into three distinctive clusters. Compared to PC2, there is a broader dispersion along PC1.

Conceptually, ANM modes are similar to PCA modes. ANM modes are based on the (theoretical) Hessian matrix, **H**, while PCA modes are based on the (experimental) covariance matrix **C**, and by definition, **C** is the inverse of Hessian. For PCA, the input is the ensemble of those experimentally resolved structures while in ANM, the native contact topology of a single known structure is the only input used to construct **H**. Thus, if the ensembles agrees completely with the ANM predicted displacement in structure, $\lambda_k = \frac{1}{\sigma_k}$, and $\boldsymbol{u}_k = \boldsymbol{p}_k$ for all k. However, this is not possible in reality because the experimentally resolved structures do not necessarily sample all accessible structures, and also ANM is a coarse-grained model which provides an estimate of the collective movements intrinsically defined by the protein structural topology. As a result, only the top-ranking modes (the largest variance PCs and softest or lowest frequency ANM modes) are taken into account and the overlap between them is examined. Figure 3F shows the overlap between the top 6 PCs and ANM modes. We can see that ANM mode 2 and PC1 exhibit a high overlap value. These two modes will be analyzed further in the following. This type of comparison enables us to identify the ANM and PCA modes that are the counterpart of each other, confirmed both experimentally and computationally, thus providing robust information on the collective change in structure accessible to the examined family of proteins.

2.3.2 Comparison of ANM soft modes with PC modes derived from experiments

In previous session, we identified that PC1 and ANM2 show the highest overlap. We projected the ensemble of LeuT structures onto those two directions for further analysis. The residue motions represented by PC1 (*red arrow*) and ANM2 (*green arrow*) are shown in Figure 4C and individual fluctuations for those two models can be viewed in Figure 4A as well. The reference ANM structure is the first resolved LeuT crystal structure (2A65) and it is in leucine-bound outward-occluded state. Both PC1 and ANM2 capture the dramatic movement of TM1b and TM6a. These two helical segments form the flexible core domain, and in consistency with the studies performed by Gouaux et al. TM1b,TM2 and TM6a shift away from leucine-bound outward-occlued state to leucine-free outward-open state (Krishnamurthy and Gouaux 2012). In addition, the extracellular and cytoplasmic entries, has been suggested by Gouaux et al., to expand upon movement of surface-exposed elements, including intracellular loop1 (IL1), extracellular loop 2 (EL2) and extracellular loop 4 (EL4) (Yamashita, Singh et al. 2005). Indeed, previous work showed that both EL2 and EL4 participate in the conformational changes during neurotransmitter transport by NET and SERT (Stephan, Chen et al. 1997, Smicun, Campbell et al. 1999). Both PC1 and ANM2 capture the movement of EL2, and PC1 further captures EL4 displacement which is the largest movement along PC1.

Then, the level of correlation between the projections of the structures onto these two collective displacement directions was examined. As shown in Figure 4B, the structures perfectly align along these two axes (correlation coefficient of 0.99), indicating the equivalence of the predicted ANM2 and experimentally observed (PC1) global modes. The figure also shows that the structures resolved to date are essentially conformers with different levels of deformation along this combined PC1/PC2 axis, apart from minor local fluctuations.

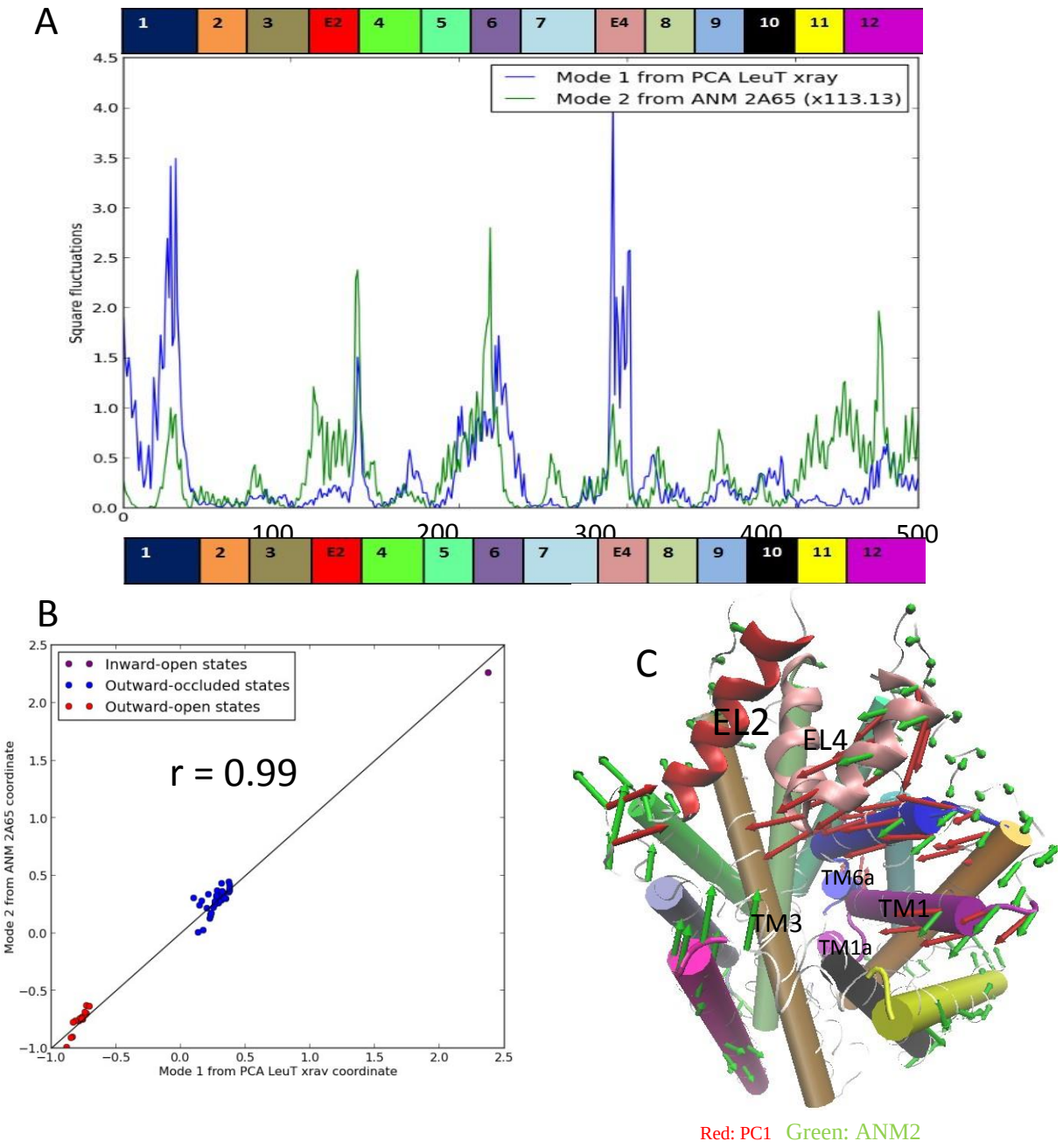

Figure 4 **Results for LeuT.**

(A) Comparison of the weighted sum of square displacements along PC1 with this predicted along ANM2 mode. (**B**) Projection of the 50 crystal structures of LeuT onto PC1 and ANM2. (C) Structural variations along PC1 and ANM2.

2.3.3 Comparison of ANM-predicted conformers with the conformations sampled in MD simulations

We examined the correlation between ANM2 mode and PC1 derived from MD trajectories generated for LeuT. These simulations permitted us to sample all the possible states visited during the LeuT cycle (Figure 2). As shown in Figure 5A, the ANM2 mode and PC1 have a high correlation of 0.96. In addition, we compared MD simulations' conformers with experimentally resolved structures, and the correlation between ANM2 and PC1 was still high. Their correlation dropped a little to 0.91 (Figure 5B).

Then, we tested the sampling ability of MD simulations, in comparison to the predictions of ANM. First we compared how the 1st essential mode obtained from simulations compare with ANM mode 2 (Figure 5A), which led to a good correlation (of 0.96). We then projected ANM predicted conformations (*green dots*) and MD simulation snapshots (*yellow dots*) onto the subspace spanned by the top two PCs, PC1 and PC2, derived from experimentally resolved structures. The ANM sampled conformations showed close overlap with the experimentally resolved structures especially in the outward-open occluded states (Figure 5C) while MD simulation conformations tend to drift away from experimental structures though some of them were close to the outward-facing open structures (Figure 5D).

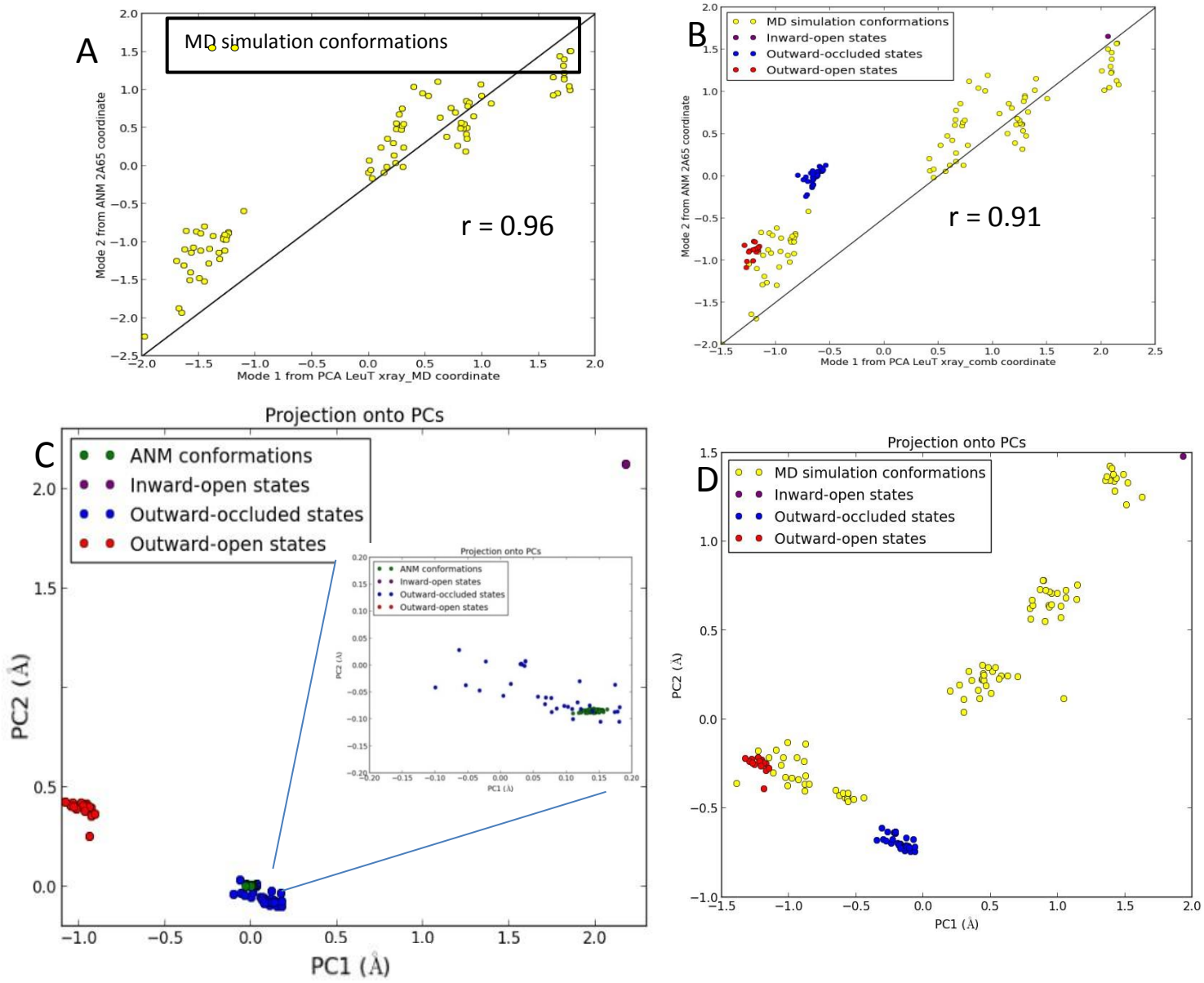

Figure 5 **Comparison of the conformational space sampled by MD simulations with the principal subspaces inferred from experiments and ANM theory.**

(A) Projection of MD snapshots onto ANM2 and the 1st essential mode derived from MD. (**B**) Projection MD simulation conformations and experimental structures onto PC1 and ANM2. (C) Projection of ANM predicted conformations on top two PCs derived from experiments. (D) projection of MD simulation conformations on top two PCs

2.4 CONCLUSION AND FUTURE WORK

From our results, we can see that both PCA modes and ANM modes capture the conformational flexibility of LeuT, consistent with experimental studies. Also, there is strong correlation (0.99) between ANM2 and PC1 based on the experimental structures (Figure **4**C). In addition, the correlation is still high, though dropped slightly, based on MD conformations (0.96) (Figure **5**A) and mixed conformations (MD conformations and experimental structures)(0.91) (Figure **5**B). In a similar study involving HIV 1 protease, Yang et al. also reported the close similarity between the motions predicted by ENMs and those computed by the PCA of experimental structures only, PCA of MD simulation snapshots, and PCA of NMR ensembles (Yang, Song et al. 2008).

ANM-sampled conformations overlap with experimental structures around the outward-occluded state. This might because we only sampled 70 ANM prediction conformations for the top 3 ANM modes, starting from an outward-facing occluded conformation. MD sampled conformations tend to drift away from the experimental structures, though some of them cluster around the outward-open state experimental structure. It remains to be verified if the new cluster of conformations in Figure 5D is complementary to the experimental structures and provide an adequate representation of those unavailable (or not resolved) to date.

In the future, we may use of ENMs to generate conformational ensembles for docking, as suggested by many studies (Cavasotto, Kovacs et al. 2005, Sperandio, Mouawad et al. 2010). Also, a systematic study of the dynamics of families of proteins can be performed to help us understand the relation between sequence evolution, structure selection and functional promiscuity. Bahar et al. have already performed a systematic analysis for structurally resolved

and sequentially homologous proteins and made accessible the corresponding software, Prody (Bakan, Meireles et al. 2011).

ANM results are dependent on the overall architecture/fold of the structure. They do not incorporate the effects of specific interactions or detailed atomic coordinates. They do not offer information on local changes in structure and interactions. Also, sequence information is not included in ANM. In addition, inadequate description of non-linear effects and solvent effect etc. limits the applications of ENMs. In cases where such local detailed interactions are of interest, MD simulations can be utilized. Such simulations become particularly useful in druggability assessments where the specific interactions between the protein and the ligand on a local scale become important. We will introduce MD simulation and their use in druggability assessment in the next chapter.

3.0 DRUGGABILITY ASSESSMENT: APLLICATION TO IONOTROPIC GLUTAMATE RECEPTORS (IGLUR) N-TERMINAL DOMAIN AND LIGAND-BINDING DOMAIN

Druggability assessment of a target protein has become an area of interest toward hit-to-lead optimization in recent years (Keller, Pichota et al. 2006). Here, we define focus on computational assessment of druggability which is an estimation of binding sites and binding affinities of a potential drug acting on a certain protein target with the help of MD simulations (Bakan, Nevins et al. 2012). Recent genome analysis revealed that 10% of human genome is druggable and 50% of those druggable proteins are correlated to disease-causing genes (Hopkins and Groom 2002). Thus, early assessment of druggability may play an important role in drug discovery in saving the cost due to the failure at the later toxicity/efficacy test stage.

Both NMR screening of libraries of small molecules (Hajduk, Huth et al. 2005) and multiple crystallography where small molecule form complex a with the target protein (Allen, Bellamacina et al. 1996) have proven useful in making those assessment experimentally. Hajduk et al showed the correspondence between the sites experimentally observed to bind large fractions of fragments (or drug-like molecules) available in solutions and the sites known to have high ligand-binding affinity (Hajduk, Huth et al. 2005). Based on those observations, they suggested a metric, druggability index to compute the druggability of target proteins and built a model to distinguish druggable and non-druggable sites with a reasonable accuracy rate.

However, the experimental methods are expensive. Recently, the computational screening of a library of fragment-like molecules and organic probe molecules against known binding sites indicated that computational methods can distinguish druggable and non-druggable targets successfully (Huang and Jacobson 2010). Due to dynamics of protein, some allosteric sites and druggable pockets can be captured by MD simulations, even though they cannot be identified by examination of the crystal structures (Ivetac and Andrew McCammon 2010).

In addition, methods for incorporating water and organic probes into MD simulations have been developed by Guvench and Mackerell (Guvench and MacKerell Jr 2009). Further, Bakan et al. recently developed a similar method but with an optimized probe set. This set is drawn from small organic fragments overrepresented in FDA drugs, which have diverse physicochemical properties (Bakan, Nevins et al. 2012). They showed that MD simulation-based druggability assessment can capture and predict ligand-binding sites or even the allosteric sites for a number of targets. The method thus enables us to investigate the binding landscape of iGluR N-terminal domains (NTDs), especially those of AMPARs and NMDARs.

3.1 OUTLINE OF METHODS

MD simulations were performed using the simulation package NAMD (Phillips, Braun et al. 2005) with the CHARMM (Brooks, Brooks et al. 2009) force field. The detailed protocol is described by Bakan et al., 2012, (Bakan, Nevins et al. 2012). Smulations were conducted for 40 - 60 ns (See Appendix A for details). Due to the fast diffusion of small probes, this time scale can successfully explore the entire surface of the target protein and identify most probable binding pockets (Bakan, Nevins et al. 2012).

The free energy in this method is estimated based on the assumption that the probe molecules follow a Boltzmann distribution and thereby allow us to convert probability distributions into binding free energies. A grid-based method is used and the binding free energy at each grid i is evaluated as $\Delta G^{i}_{probebinding}$ = -RT $ln(n_i/n_0)$. Here, n_i/n_0 is the ratio of the observed density of probes n_i to the expected density $n_{0,}$ R is the gas constant and T is the absolute temperature (K). Binding events are accounted for by considering probe molecules as independent particles. Interaction spots are identified by removing the voxels that overlap with the lower energy voxels. Then, usually 6 or 8 proximal (located within 5.5 to 6.5 Å) spots are merged to predict a so-called *maximal affinity*. Interaction spots (28 to 32 heavy atoms) are then clustered and merged to locate each binding site. The interaction spots are supposed to be potential druggable sites provided that the corresponding maximal affinity is 10uM (which corresponds to a binding free energy of -6.86 kcal/mol). The maximal affinity is calculated based on the premise that the free energies of different binding spots are additive. Thus, the maximal affinity is estimated by the sum of free energies of interaction spots in that region for each site.

Once all the different sites are assessed, the program ranks all the possible druggable sites in terms of their binding free energy from the lowest to the highest.

All the probes in this chapter are shown as spheres and reported by their center of mass. They are color-coded based on the fragment name shown in Appendix A. The probes included in our simulations are isopropylamine (IPAM), acetate (ACET), acetamide (ACAM), imidazole (IMID), isopropanol (IPRO), isobutene (IBUT) and benzene (BENZ).

3.2 STRUCTURAL FEATURES OF IGLUR N-TERMINAL DOMAINS

Ionotropic glutamate receptors (iGluRs) consist of a family of glutamate-gated cation channels that regulate the majority of neurotransmission in the central nervous system. The alterations in iGluRs are associated with severe acute and chronic neurodegenerative diseases. The iGluR family consists of three subfamilies: α-amino-3-hydroxy-5methyl-4-isozazolepropionic acid receptors (AMPARs), kainite receptors (KRs) and N-methyl-D-aspartate receptors (NMDARs). Those subfamilies share an architecture of three major parts (shown in Figure 6): an extracellular domain (ECD), a transmembrane domain (TMD) and an intracellular carboxyl-terminal domain (Traynelis, Wollmuth et al. 2010). The ECD consists of a distal N-terminal domain (NTD) and ligand-binding domain (LBD).

Figure 6 displays the full length structure of GluA2 AMPAR resolved by Gouaux and collaborators (Sobolevsky, Rosconi et al. 2009). Both NTDs and LBDs share the clamshell-like bilobate fold features which belong to the periplasmic binding protein (PBP)-like family (Quiocho and Ledvina 1996). The function of the LBD is well-studied and characterized; L-glutamate docking to the cleft of upper lobe (UL) and lower lobe (LL) leads to the closure of cleft, which triggers channel activation through allosteric transition by TMD (Armstrong and Gouaux 2000). The function of the NTDs remains to be further studied. In NMDARs, the NTDs play a key role in signaling as a allosteric modulator of channel opening probability (Gielen, Retchless et al. 2009). And this role resulted in a surge in the development of NMDAR modulators /drugs. However, the allosteric modulation of NTDs in non-NMDARs is still not well understood and is still under debate.

In addition, NMDARs contain Zn^{2+} binding sites and an ifenprodil molecule was found to bind to NMDARs which was proposed to stabilize the closed-cleft conformation of the NTDs

(Karakas, Simorowski et al. 2009, Traynelis, Wollmuth et al. 2010). However, for AMPARs and KRs, no ions or small molecules are known to bind. In this chapter we mainly explore the potential druggable sites on the NTDs of AMPARs and NMDARs.

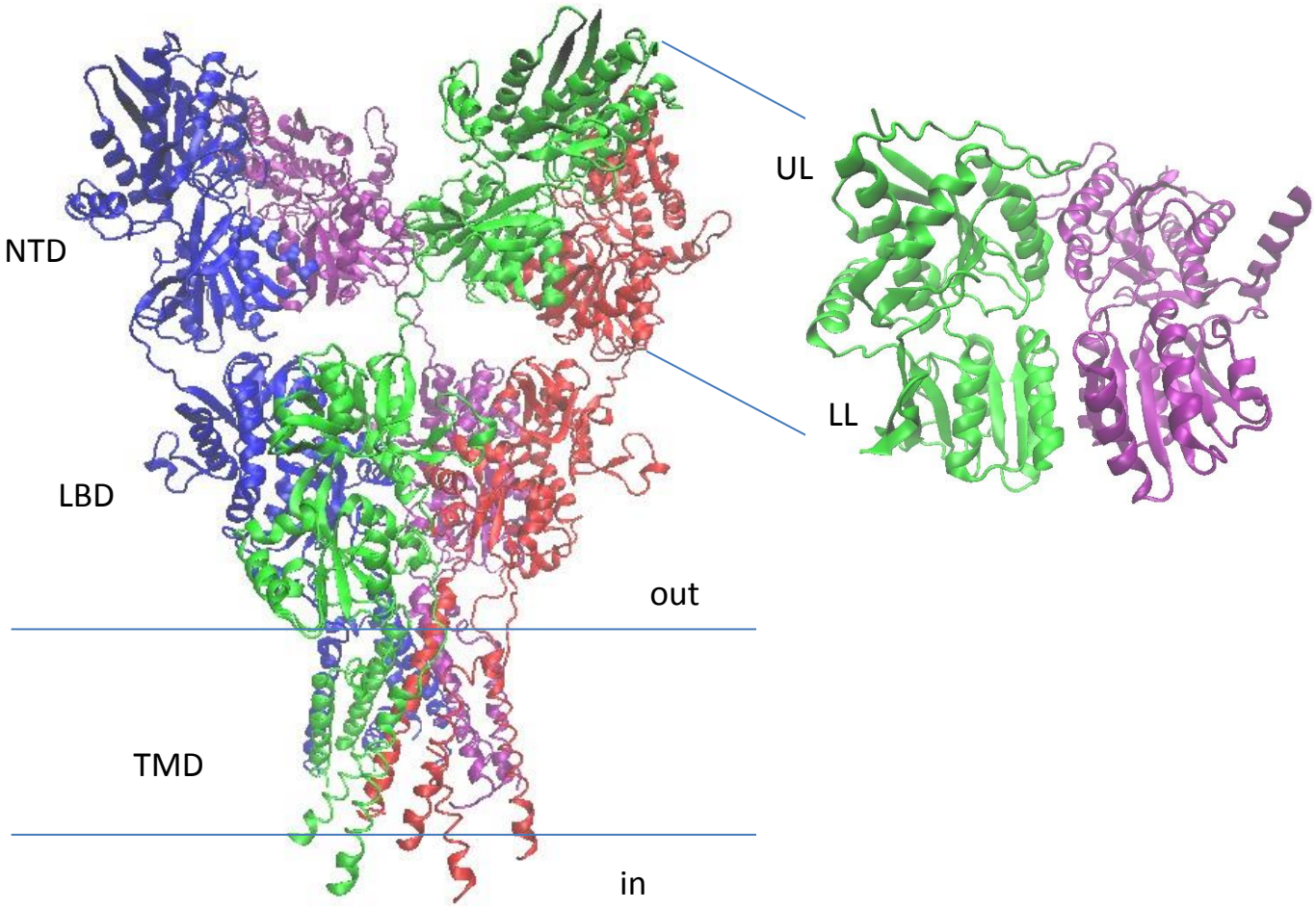

Figure 6 Complete structure of GluA2 *(left)* (except for the C-terminal domain) and the structure of the NTD dimer of GluA2 *(right)*

GluA2 is one of the subtypes of AMPAR. This complete GluA2 crystal structure (except for the C-terminal domain) was obtained by Soblevsky et al. (Sobolevsky, Rosconi et al. 2009)

3.3 LIGAND-BINDING SITES ON IGLUR LBD

As introduced previously, the LBD of iGluRs is a bilobate structure similar to the bacterial PBP proteins, which bind ligands in the cleft due to evolutionary optimization (Sukumaran, Rossmann et al. 2011). The ion channel opening is initiated by the binding of glutamate in the LBD cleft (Armstrong and Gouaux 2000). We benchmark the druggability assessment method first to see how well this property of the LBD can be reproduced. We perform simulations using the GluR2 AMPAR LBD because this domain has a lot of crystal structure bound with either agonist or antagonist and it is a good model for analysis (Pøhlsgaard, Frydenvang et al. 2011).

In AMPARs, receptor desensitization is initiated by reorganization of the dimer interface. Though the exact mechanism is not clear yet, there is a large number of crystal structures of LBDs with certain mutations which give us a few insight on the structural changes relevant to receptor desensitization. It was reported by Sun et al. that cyclothiazide can stabilize the dimer interface through positive allosteric modulation (Sun, Olson et al. 2002). AMPAR currents can be enhanced by those positive modulator through its decreasing effect on receptor desensitization. In Figure 7, we show that our probes capture the binding sites of cyclothiazide at the interface of LBD and the locations of the probe molecules overlap with those binding sites. Particularly, a high affinity binding site consisting of 6 hotspots, all of which composed of ACAMs (*yellow spheres*) is identified, which closely overlaps owith the upper site for cyclothiazide (*shown in stick representation*) allosteric modulator binding. This site yielded a drug-like affinity of 0.413μM or a binding free energy of -8.76 kcal/mol. Thus, we can see that the probes adopt a binding pattern similar to those experimentally detected for positive modulators of AMPAR LBD.

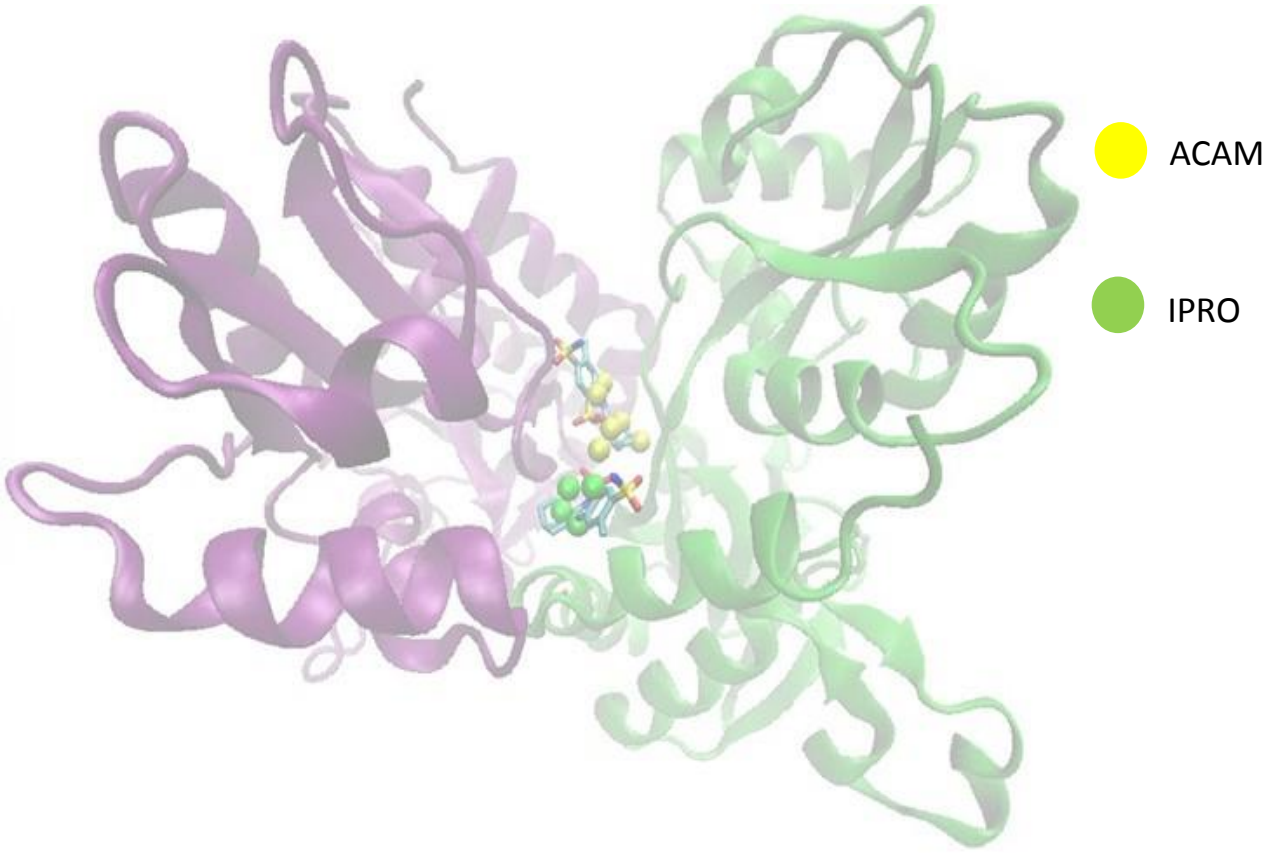

Figure 7 **Probes that capture the known drug-binding sites in the LBD dimer of GluA2.**

The structure of GluA2 NTD dimer in the presence of two cyclothiazide molecules (PDB ID: 1LBC) is shown. Cyclothiazide is a known positive allosteric modulator at GluA2 LBD. GluA2 binds two cyclothiazides (shown by CPK *stick representation*) at the interface between the monomers of the LBD dimers. Probe molecules shown by *spheres* (coinciding with their mass center) exhibit a high propensity to populate this site.

3.4 DRUG-LIKE PROBE CLUSTERS CAPTURING DIMER INTERFACE FROM NTD MONOMER SIMULATION

There are 9 distinct subtypes of iGluR NTDs crystal structures available. We have performed 40ns druggability simulation for 7 subtypes in monomeric forms in the presence of drug fragments (probes) and water. The most interesting result is the identification of monomer-monomer interfacial regions captured by our probes (Table 1 and Figure 8).

Residues that participate in the formation of NTDs UL and LL dimer interface are obtained from crystal contacts experimentally (Jin, Singh et al. 2009, Karakas, Simorowski et al. 2009, Kumar and Mayer 2010, Guorui, Yinong et al. 2011). However, for the NMDARs, no distinct LL interface is identified for NMDAR homo/hetero dimers, only UL results are reported.

The high-affinity binding sites (clusters of 6 or 7 probes) which contain more than 2 probes within 5Å of the interfacial UL and HL regions are reported, which are proposed to be the potential drug-like binding sites. Those probes that bind the interfacial regions are called 'interfacial probes'.

Figure 8A shows that the druggability simulations accurately capture the high-affinity binding sites at the monomer-monomer UL and LL interfaces of GluA3 NTD (shown as spheres). At the UL interface (Figure 8B, the magnification of the UL interface), there are 7 probes with total affinity of 18.31nM. Six of the probes are within 5 Å of the interfacial residues (shown in *purple sticks*) and 4 of them are within 4 Å; whereas for the LL interface (Figure 8C), 3 out of 7 probes bind the interfacial region. Both sites bind isopropanols (IPROs).

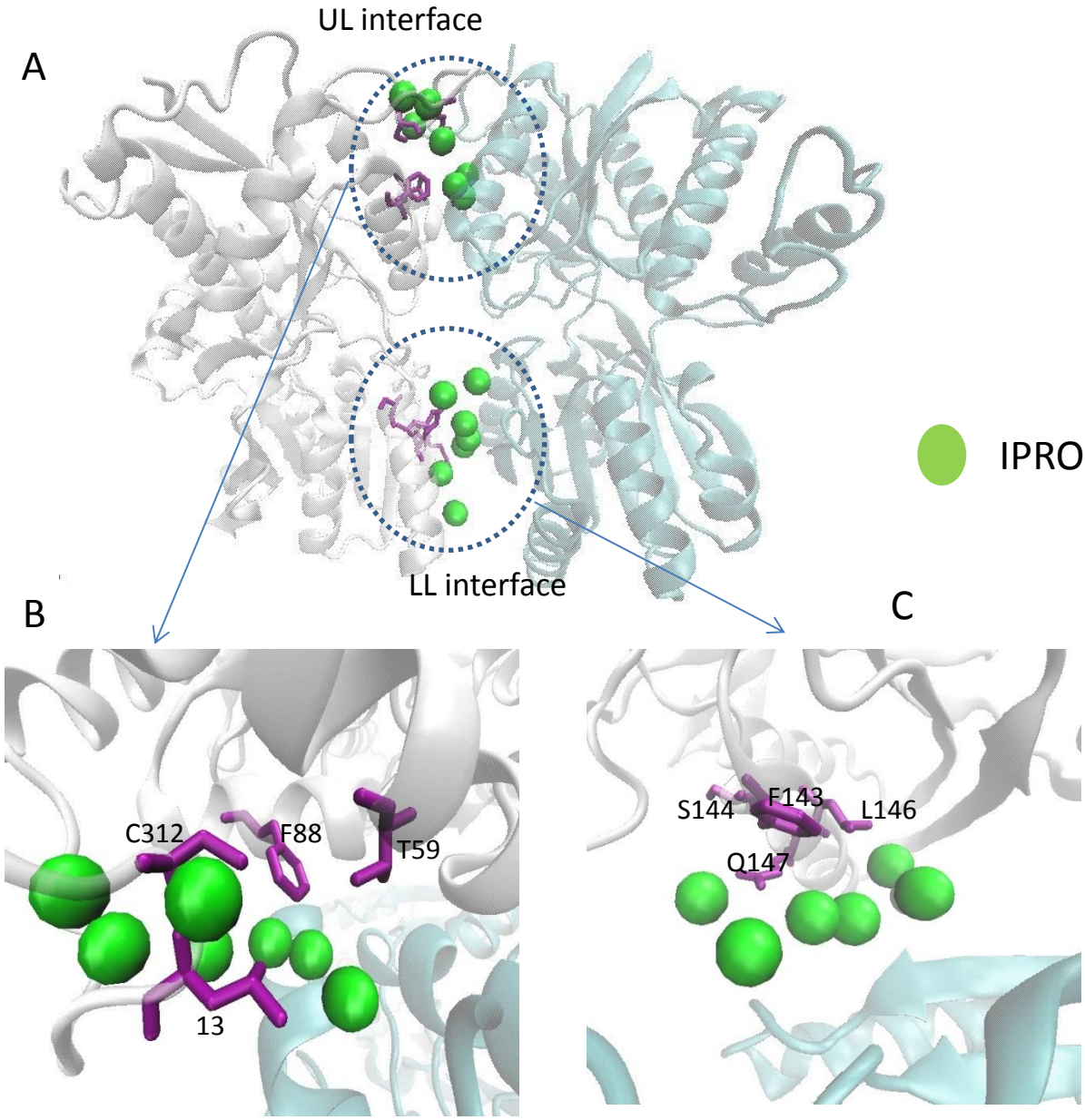

Figure 8 Interlobe (UL-UL and LL-LL) interface regions at the NTD dimer of GluA3, identified by druggability simulation to have a high propensity for binding small molecules.

(A) GluA3 monomer NTD (PDB ID: 3O21) chain C used in simulations is shown in *white* and the other chain (chain D) is shown in *light blue*. The residues that line the interface are shown in *purple sticks*. The interfacial region preferentially binds IPRO probes, which are shown in *green spheres.*

(B) Magnification of UL-UL interface. (C) Magnification of LL-LL interface.

For all iGluRs NTDs which have known UL and LL interfacial regions, except for GluA2 and GluK2, high-affinity sites for interfacial probes were identified. We can see that non-polar hydrophobic molecules, such as isopropanol (IRPO) and isobutane (IBUT), are the two dominating probes at those binding sites. The binding sites that contain 6 interfacial probes out of 7 are labelled in *red* (Table 1).

GluK3 has the largest number of interfacial probes at both the UL and LL interfaces, which indicates that it has a higher probability to form interfacial interactions or to stabilize a dimeric form. We also concluded that among AMPARs and NMDARs, GluA3 and GluN2B were more likely to form interfaces in terms of the number of interfacial probes in the binding sites. Generally, for all subtypes, the UL interfacial residues are captured by high affinity binding probe clusters, which indicates that the ULs are more likely to form interfaces compared to the LLs.

We note that this method helps identify protein-protein interfaces consistent with experiments and it has future implications on the identification of other unknown protein-protein interfaces. In the next session, we will further discuss the druggability simulations performed for the NTD dimers of iGluRs.

Table 1 High affinity binding sites on iGluR monomers

The table reports the high affinity binding sites which contain more than 2 hot spots within 5Å from the UL or LL interface. For NMDARs, there were no LL interface binding probes. Thus only UL interface results are reported for NMDARs.

iGluRs	UL interface result for NTD monomer simulation			
	No. of interfacial probes	Probe composition	Binding free energy (kcal/mol)	Affinity (nM)
GluA1	2	6 IBUT, 1 IPRO	-11.71	2.90
GluA2	6	7 IBUT	-10.98	9.90
GluA3	6	7 IPRO	-10.61	18.31
GluK2	4	2 IBUT, 5 IPRO	-10.10	43.60
GluK3	6	6 IBUT, 1 IPRO	-12.19	1.29
NR1	3	5 IBUT, 2 IPRO	-12.08	1.55
NR2B	4	6 BENZ, 1 IPRO	-10.72	15.36

iGluRs	LL interface result from NTD monomer simulation			
	No. of interfacial probes	Probe composition	Binding Free energy (kcal/mol)	Affinity (nM)
GluA1	2	4 IPRO, 3 IBUT	-11.53	3.96
GluA2	-	-	-	-
GluA3	3	7 IPRO	-11.56	3.72
GluK2	-	-	-	-
GluK3	6	4 IPRO, 3 IBUT	-10.89	11.59

(Note: Probe abbreviations: isopropanol (IPRO), isopropyl amine (IPAM), Benzene (BENZ), and isobutane (IBUT))

3.5 DRUGGABILITY ASSESSMENT OF IGLUR NTD DIMER

In this section, we proceed to evaluate the druggable sites in AMPARs and NMDARs. Among AMPARs, as we saw in previous section, GluA3 has a relatively larger interface accessible to probe molecules. We picked up GluA3 for NTD dimer simulations. For NMDARs, we used the GluN1-GluN2B heterodimer NTD structure complexed with ifenprodil. Ifenprodil is a well-known small molecule used to treat neurological diseases. It specifically inhibits the GluN1 and GluN2B subunits of NMDAR (Karakas, Simorowski et al. 2011).

3.5.1 Druggability assessment of GluA3 NTD dimer

In the druggability simulation of GluA3 NTD dimer, two potential drug-binding sites were identified, located at the UL and LL interfaces, respectively (Figure 9). Residues within 4.5 Å of the probe clusters were considered to interact with the probes. Residues on α3,α2 and L1 flap, which are key conserved UL interfacial residues were found to interact with the probes at the UL interface (Table 2). The UL probes clustered all at close proximity of the corresponding residues that formed the binding pocket that contribute majorly to the binding affinity (Figure 10A). Examination of the LL site (Figure 10C), on the other hand, showed that all 7 probes identified to bind most frequently the interface make close contacts with key residues on α5, α6 and β7. Particularly, one IPRO was observed to consistently make close contacts (within 4 Å) with R163.

The LL interface is largely polar. Especially R163 and R184 project towards together interface to generate positive electrostatic potential and the charge repulsion presumably contributes to the greater separation if the lobes compared to other AMPARs NTD subtypes (Jin, Singh et al. 2009). Thus, the IPRO here, which interacts with R163, prevents the same charge repulsion and helps stabilize the NTD LL interface in a tightly packed conformation. In addition, two other hydrophobic probes (IPROs) interact with M150 to contribute to the binding affinity as well. Another potential drug binding site is the binding pocket formed by M150 by two α5 (Figure 10).

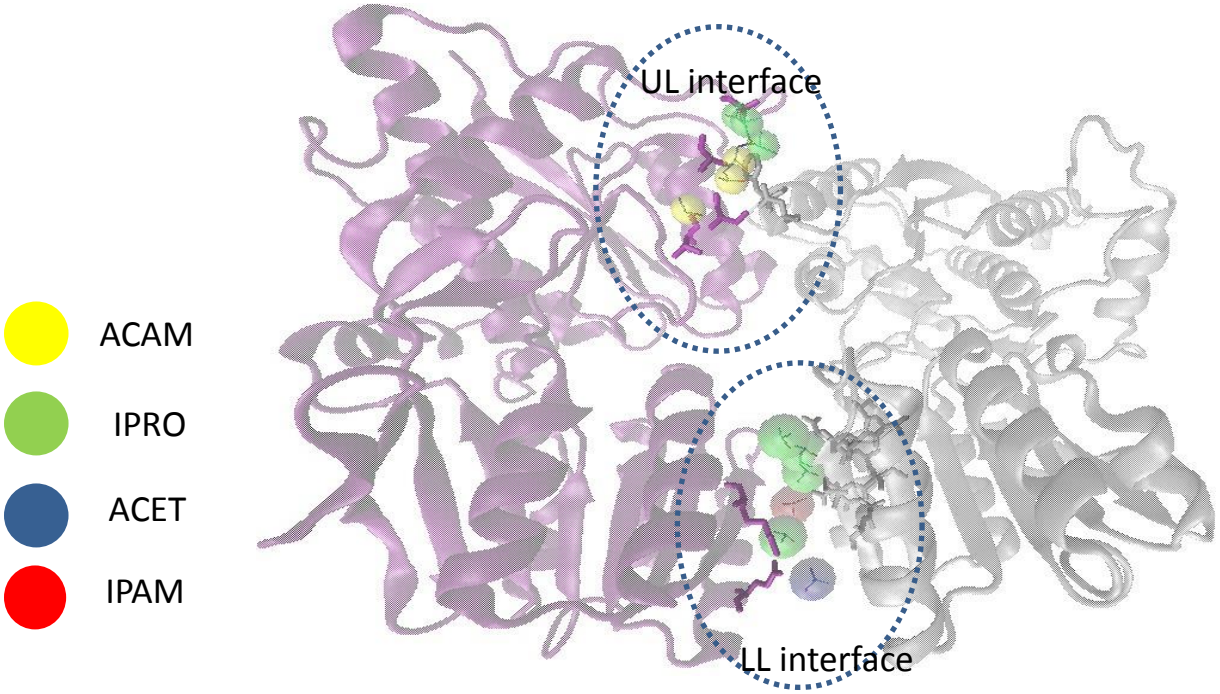

Figure 9 Potential drug binding sites deduced from GluA3 NTD dimer simulations

Two binding sites are shown, at the UL and LL interfaces of the GluA3 NTD dimer. The residues located within 4.5 Å interatomic distance from the probes are shown in sticks. Probe molecules are shown in spheres.

Table 2 Druggability of GluA3 NTD dimer

Probe cluster (binding sites)	Interacting residues	Binding free energy(kcal/mol)	Affinity	Probe cluster compositions	Charge
UL interface	α3: T86, S87, A91 α2 : N54, F56 L1 flap: A317	-8.21	1.04uM	3 ACAM 3 IPRO	-0.04e
LL interface (sol 1)	α5: L146 to A152 α6: E180 β7 : R163	-12.19	1.31nM	5 IPRO 1 ACTT 1 IPAM	1e
LL interface (sol 2)	M150 on two α5	-12.25	1.17nM	5 IPRO 2 IPAM	2e

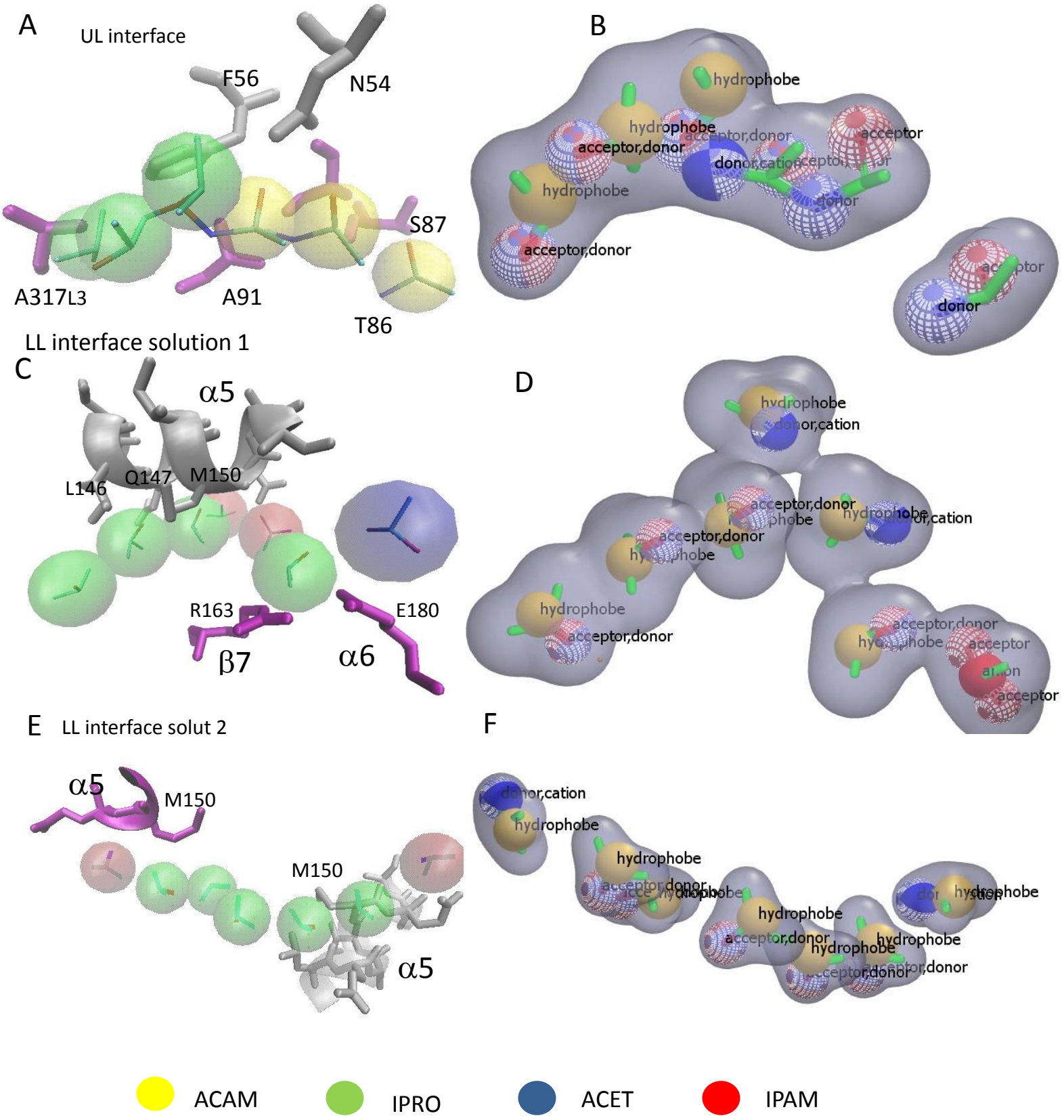

Figure 10 Binding sites at GluA3 NTD dimer interface and corresponding PMs.

(A) Magnification of probe-binding site at the UL interface and (B) its corresponding PM (shown using OpenEye)

(C) Magnification of probe-binding site at the LL interface and (D) its corresponding PM (shown using OpenEye)

(D) Magnification of probe-binding site at the LL interface and (D) its corresponding PM (shown using OpenEye)

3.5.2 Druggability assessment of GluN1-GluN2B NTD dimer

In previous studies for NMDARs, the allosteric drug-binding site at NTD was usually located at the interface between two NTD subunits (Karakas, Simorowski et al. 2011). In druggability simulation of GluN1-GluN2B NTD dimer, three potential drug-binding sites are captured by the probe clusters (Figure 11 and Table 3). The first two sites are located at the NTD hetero-dimer interface, and the third is located between α7, β2 and loop1 and is presumed to be the possible allosteric regulation site in GluN2B.

At the UL interface, the key residues belonging to L1 flap, α3 and α6 were found to be in close contact (within 4.5 Å) with site 1 probe clusters (Figure 12A). Particularly, residue T103 interacting with an IPRO probe, on a loop extended from β3, has been identified as a key residue for both ifenprodil- and zinc-binding (Rachline, Perin-Dureau et al. 2005), which maintains the architecture of the zinc-binding pocket and the GluN2B NTD clamshell structure as a whole (Karakas, Simorowski et al. 2009).

Site 2 is located in the LL interface. Therein residues in α5, participating in the interface region, were observed interact with the probe cluster (Figure 12C). In addition, one of the probes is close to K131 on a loop which may play a role upon drug binding on the NMDARs (Karakas, Simorowski et al. 2011).

In addition to those binding sites located in the UL or LL interface regions, we also identified a third binding site which binds in a pocket formed by loop, an α helix and a β sheet. This site exhibits a binding affinity of 0.152uM and is proposed to be an allosteric binding site yet to be experimentally validated.

The PMs for the above three sites are shown in Figure 12BDF. These will be used for virtual screening for further analysis.

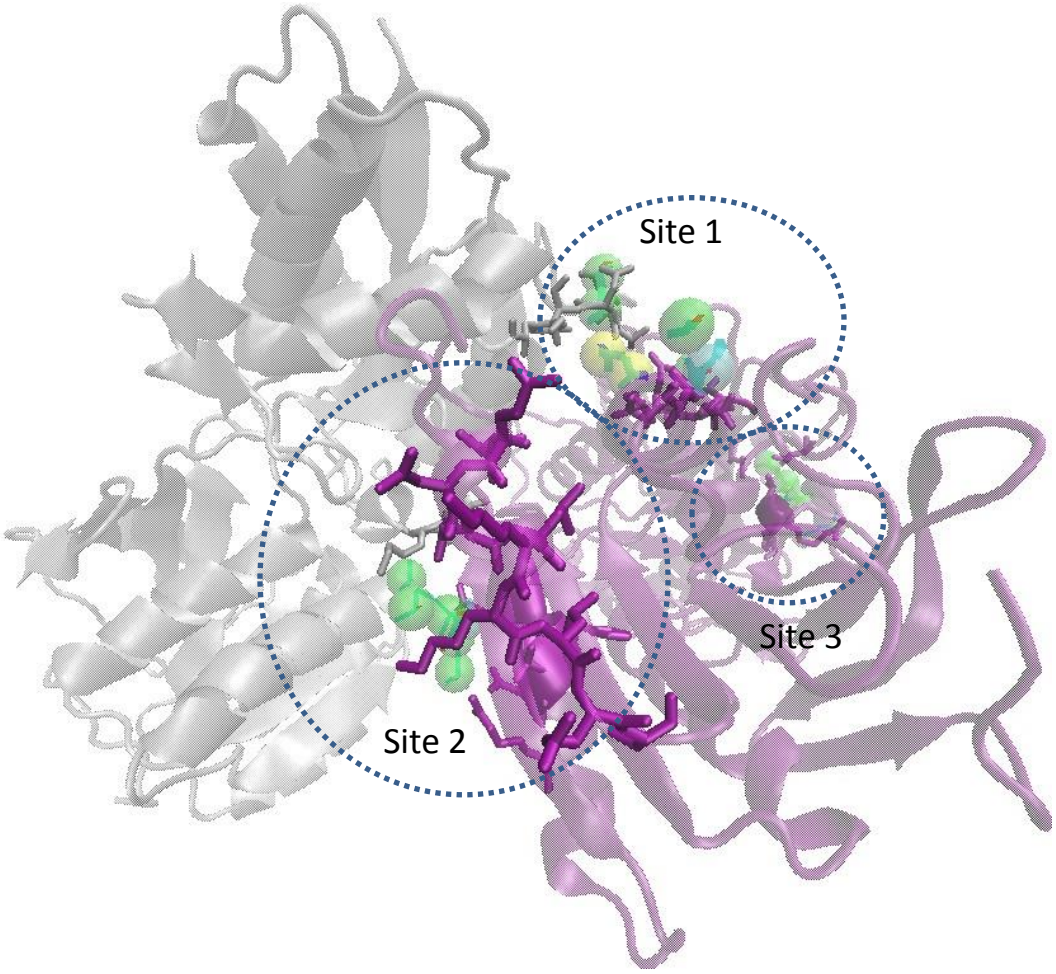

Figure 11 Potential drug-binding sites captured by GluN1-GluN2B dimer druggability simulation

The residues within 4.5 Å of the binding sites probes are shown in sticks. Probe molecules are shown in spheres. GluN1 NTD is colored *silver* and GluN2B NTD, *purple*.

Table 3 Druggability of GluN1-GluN2B NTD dimer

Probe cluster (binding sites)	Interacting residues	Binding free energy (kcal/mol)	Affinity	Probe cluster compositions	Charge
Site 1	GluN1 NTD: L1 flap: from N311 to I314 α3: Y114 GluN2B NTD: α6 : E235, T238 Loop: T103	-9.50	0.12uM	5 IPRO 1 IPAM I BENZ	-1.90e
Site 2	GluN1 NTD: Loop: K131 GluN2B NTD α5: Q180 to N184, R187	-7.43	3.83M	5 IPRO 1 BENZ	0.15e
Site 3	α7 helix: V293, R294 β2 sheet: V68 Loop1: F59	-9.35	0.152uM	4 IPRO 2 ACTT 1 IBUT	-1.45e

(Probe abbreviations: isopropanol (IPRO), isopropyl amine (IPAM), Benzene (BENZ), acetate (ACTT), acetamide (ACAM) and isobutene (IBUT))

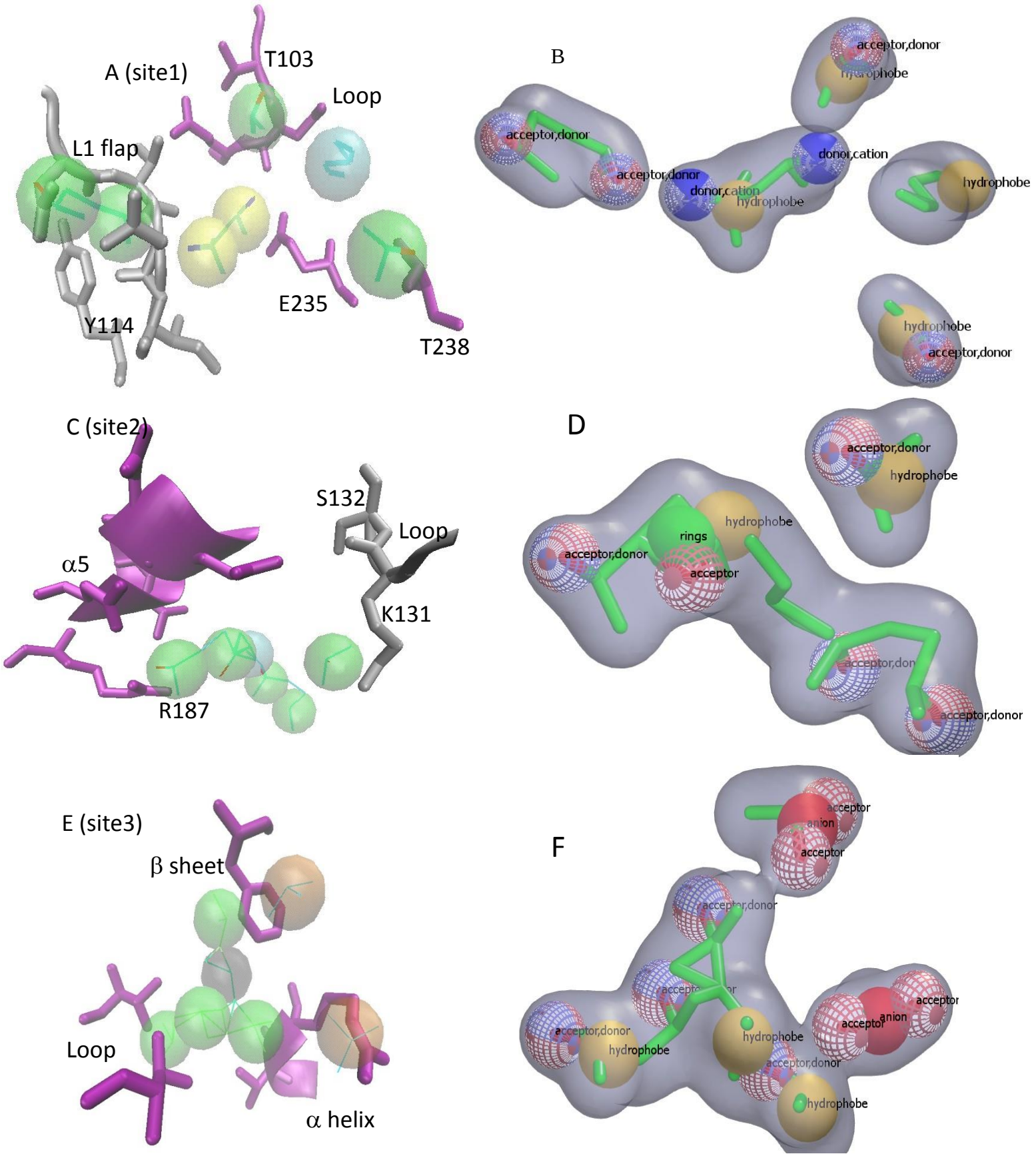

Figure 12 Binding sites at GluN1-GluN2B NTD dimer and corresponding PMs

(A) Magnification of Site 1 and its PM (B). Magnification of Site 1 and its PM. (C) Magnification of Site 2 and its PM (D). (E) Magnification of Site 3 and its PM (F).

3.6 CONCLUSION

In this chapter, we assessed the druggabilities of iGluRs NTD monomers and dimers. To detect high affinity binding sites, only those drug-like probe clusters (6 to 7 probes) were reported as potential drug-binding sites. At the beginning, we benchmarked this method by investigating the well-characterized ligand binding sites of GluA2 LBD dimer. And we found that our probe cluster captured the known drug binding site and some probes overlapped with the residues in the known drug.

Then, we further explored the potential binding sites of iGluR NTD monomers. Drug probes identified residues involved in the interfacial region for each NTD subtype and the corresponding high affinity binding sites were reported as well. This suggests that we can use this method to accurately predict proten-protein interaction interfaces. Among the iGluRs, GluA3 showed the most accessible interfacial region for binding probes, due to the high flexibility of GluA3 (Dutta, Shrivastava et al. 2012). The identified high affinity binding sites in the interface region suggest likelihood of drug binding site at the interface of GluA3 NTD.

Finally, we explored the druggable sites in the GluA3 NTD dimer and GluN1-GluN2B NTD dimer. The simulation of GluA3 dimer provided an interesting result: we found two high affinity binding sites at the interfacial regions and some key interfacial residues were found to be in close contact with our probes, which further strengthen our hypothesis that there exists sites that may potentially bind drugs at the LL GluA3 NTD interface. We characterized the pharmacophore features of the high affinity site found by probe clusters. The PM can be employed as a template for virtual screening of compounds (from known libraries of chemical compounds) to identify potential molecules conforming to the PMs. And those hits can be further optimized with higher efficacy to GluA3 and eventually be tested experimentally.

This study offers a new insight into the identification of allosteric regulatory binding sites in GluA3 NTD where few drugs have been found to bind to it yet. For NMDARs, the druggability analysis of GluN1-GluN2B NTD dimer also identified possible drug binding sites at the interface region though there are fewer interacting interfacial residues in the binding pocket compared to GluA3. Additionally, we identified another binding site, though not close to interface region located in a pocket formed by helices and loop. PMs have been built for those sites as well and we will use them for further virtual screening.

4.0 PREDICTING DRUG-TARGET INTERACTIONS USING PROBABILISTIC MATRIX FACTORIZATION

Quantitative analysis of known drug-target interactions emerged in recent years as a useful approach for drug repurposing and assessing side effects. In the present study, we present a method that uses Probabilistic Matrix Factorization (PMF) for this purpose, which is particularly useful for analyzing large interaction networks. DrugBank drugs clustered based on PMF latent variables show phenotypic similarity even in the absence of 3D shape similarity. Benchmarking computations show that the method outperforms those recently introduced provided that the input dataset of known interactions is sufficiently large - which is the case for enzymes and ion channels, but not for GPCRs and nuclear receptors. Runs performed on DrugBank after hiding 70% of known interactions show that, on average, 88 of the top 100 predictions hit the hidden interactions. *De novo* predictions permit us to identify new potential interactions. Drug-target pairs implicated in neurobiological disorders are overrepresented among *de novo* predictions.

4.1 ANALYSIS OF DRUG-TARGET INTERACTION NETWORK

Drug discovery and development became increasingly challenging in recent years, evidenced by the estimated cost of around $1.8 billion for the development of a novel molecular entity with suitable pharmacological properties (Paul, Mytelka et al. 2010). This cost increase partly originates from the failure of many drug candidates in Phase II or III clinical trials due to their toxicity or lack of efficacy (Berg, Rogers et al. 2010). The efficiency of drug discovery and development might be improved by adopting a systemic approach that takes into consideration the interaction of existing drugs and candidate compounds with the entire network of target proteins and other biomolecules in a cell (Csermely, Korcsmáros et al. 2013). Indeed, the "one gene, one drug, one disease" paradigm is widely recognized to fail in describing experimental observations (Hopkins, Mason et al. 2006). Many drugs act on multiple targets, and many targets are themselves involved in multiple pathways. For example, β-lactam antibiotics and most antipsychotic drugs exert their effect through interactions with multiple proteins (Sorger, Allerheiligen et al. 2011). Biological networks are highly robust to single-gene knockouts, as recently shown for yeast where 80% of the gene knockouts did not affect cell survival (Hillenmeyer, Fung et al. 2008). Similarly, 81% of the 1,500 genes knocked out in mice did not cause embryonic lethality, further corroborating the robustness of biological networks against single target perturbagens (Zambrowicz and Sands 2004). These results suggest that quantitative systems pharmacology strategies that take account of target (and drug) promiscuities can present attractive alternative routes to drug discovery.

Recent years have seen many network-based models adopted to reduce the complexity of, and efficiently explore, drug-target interaction systems (Berger and Iyengar 2009). In particular, the

development of computational methods that can efficiently assess potential new interactions became an important goal. In this regard, the important role that machine learning approaches such as Active Learning (AL) can play has been recently been highlighted (Murphy 2011). Computational approaches used to predict unknown drug-target interactions can be divided into roughly four categories: chemical-similarity-based methods (Keiser, Roth et al. 2007), target-similarity-based methods (Li, An et al. 2011), integrative (both target- and chemical-similarity-based) methods (Yamanishi, Araki et al. 2008), holistic approaches (Gottlieb, Stein et al. 2011, Sirota, Dudley et al. 2011). The first two posit that if two entities are chemically or structurally similar they will share interactions. The integrative approaches combine the chemical- and target-similarity methods. While the intuition behind these approaches is very reasonable, their performance has been observed to be tied to the underlying similarity computation method. We also note that the utility of different methods may depend on the size of the dataset being analyzed, e.g., computing chemical-chemical and target-target similarity matrices can be problematic for large databases like STITCH (Kuhn, Szklarczyk et al. 2012) (that contains information on the interactions between more than 2.6 million proteins and 300,000 chemicals). To overcome these limitations, holistic methods have been introduced, which utilize a number of different data sources such as gene expression perturbation (Dudley, Sirota et al. 2011) or high-throughput screening (Cheng, Li et al. 2011).

In this study, we propose a novel approach by using a collaborative filtering algorithm to predict interactions without reliance on chemical/target similarity or external data collection. We validate the utility of Probabilistic Matrix Factorization (PMF) for predicting unknown drug-target interactions with the help of a detailed investigation of its performance. The method is

shown to group drugs according to their therapeutic effects, irrespective of their 3-dimensional (3D) shape similarity. Benchmarking computations show that the method outperforms recent methods (Yamanishi, Araki et al. 2008, Yamanishi, Kotera et al. 2010, Gönen 2012)when applied to large datasets of protein-drug associations, such as those of enzyme- and ion channel-drug pairs; whereas it performance falls short of these methods' with decreasing size of the examined dataset (e.g. GPCR- and nuclear receptor-drug datasets). The ability of the method to efficiently analyze, and make inferences from, large datasets of protein-drug interactions suggests that with growing sizes of those datasets, the utility (and accuracy) of the method will further improve.

Application of the same benchmarking procedure to DrugBank (Knox, Law et al. 2011) confirms its ability to disclose hidden data: 88 out of top 100 predictions (or 587 out of 1,000) are found to hit known (but hidden) interactions, when only 30% of the entire data is used for training. Finally, when the method is trained on the entire dataset of drug-target interactions compiled in DrugBank, *de novo* predictions for drug repurposing can be made along with the corresponding confidence levels. Top predictions include many drugs indicated for neurodegenerative diseases or neurobiological disorders, including drug-target pairs apparently supported by previous experiments (not reported in DrugBank), e.g., ergotamine–serotonin receptor 1A ($5HT_{1A}$) (Tfelt-Hansen, Saxena et al. 2000), amoxapine–5-HT_{2A} (Pälvimäki, Majasuo et al. 1996), verapamil–calmodulin (Epstein, Fiss et al. 1982).

In conclusion, the newly introduced computational method provides an efficient approach for identifying potential drug-target association between chemicals and targets, and formulating

new hypotheses for repurposable drugs or side effects, thus complementing those deduced from chemical-chemical or target-target similarities.

4.2 OVERVIEW OF METHODS

The drug-target interaction network is a bipartite graph with two types of nodes; drugs, and targets. Each edge represents an interaction between a drug and a target. The drug-target interaction identification problem is to determine the missing edges that are likely to exist given all nodes and some of the edges in the network.

4.2.1 Dataset

We used DrugBank (version of September 20, 2011) as database (Knox, Law et al. 2011). All drugs annotated therein as approved, along with their annotated targets, are included in our dataset (i.e., we excluded compounds annotated as withdrawn or nutraceutical), resulting in N = 1,413 drugs and M = 1,050 targets with 4,731 interactions among them. The interaction network displays small-world characteristics: many nodes have low degree and a few, very high degree, as illustrated in the panels b and c of Figure S1, in line with previous studies on drug-target networks (Yıldırım, Goh et al. 2007). On average, there are 3.35 interactions per drug, and 4.50 interactions per target.

4.2.2 Probabilistic Matrix Factorization (PMF)

PMF is a member of the Collaborative Filtering family of Machine Learning algorithms that decomposes the connectivity matrix, $\mathbf{R}_{N \times M}$, of a bipartite graph of N drugs and M targets as a product of two matrices of latent variables (LVs) (Salakhutdinov and Mnih 2008). $\mathbf{R}_{N \times M}$ is defined as:

$$R_{ij} = \begin{cases} 1 \text{ if drug } i \text{ interacts with target } j \\ 0 \text{ otherwise} \end{cases} \quad (1)$$

The matrix $\mathbf{R}_{N \times M}$ is modeled as the product of two matrices $\mathbf{U}^{T}_{N \times D}$ and $\mathbf{V}_{D \times M}$, that express each drug/target in terms of a set of D LVs. Our objective is to find the best approximation for LVs, while avoiding over-fitting. The predicted N x M is then expressed as:

$$\hat{\mathbf{R}}_{N \times M} = \mathbf{U}^{T}_{N \times D} \mathbf{V}_{D \times M} \quad (2)$$

where U^T and V are composed of N rows u_i^T and M columns v_j, respectively, each being D-dimensional. The PMF adopts a probabilistic linear model with Gaussian noise to model the interaction. Therefore, the conditional probability over observed interactions is represented as

$$p(\mathbf{R} \mid \mathbf{U}, \mathbf{V}, \sigma^2) = \prod_{i=1}^{N} \prod_{j=1}^{M} \left[f(R_{ij} \mid \mathbf{u}_i^T \mathbf{v}_j, \sigma^2) \right]^{I_{ij}} \quad (3)$$

where f((x | u,σ^2) is the Gaussianly distributed probability density function for x, with mean u and variance σ^2, and I_{ij} is the indicator function equal to 1 if the entry R_{ij} is known, and 0 otherwise. Therefore, p(R | U, V, σ^2) gives us a probabilistic representation of the connectivity matrix, R (Mnih and Salakhutdinov 2007). Using zero-mean, spherical Gaussian priors on LVs, we can write

$$p(\mathbf{U} \mid \sigma_U^2) = \prod_{i=1}^{N} f(\mathbf{u}_i \mid \mathbf{0}, \sigma_U^2 \mathbf{I}) \tag{4}$$

and

$$p(\mathbf{V} \mid \sigma_V^2) = \prod_{j=1}^{M} f(\mathbf{v}_j \mid 0, \sigma_V^2 \mathbf{I}) \tag{5}$$

Which lead to the log-likelihood of U and V given by

$$\ln(p(\mathbf{U}, \mathbf{V} \mid \mathbf{R}, \sigma^2, \sigma_U^2, \sigma_V^2)) = -\frac{1}{2\sigma^2} \sum_{i=1}^{N} \sum_{j=1}^{M} I_{ij} (R_{ij} - \mathbf{u}_i^T \mathbf{v}_j)^2 - \frac{1}{2\sigma_U^2} \sum_{i=1}^{N} \mathbf{u}_i^T \mathbf{u}_i - \frac{1}{2\sigma_V^2} \sum_{j=1}^{M} \mathbf{v}_j^T \mathbf{v}_j + C \tag{6}$$

Here C is a term that does not depend on LVs; the first term on the right-hand side is the squared error function to be minimized; and the two summations over the square magnitudes of $\mathbf{u_i}$ and $\mathbf{v_j}$ are regularization terms that favor simpler solutions and penalize over-fitting. The above log-likelihood directly follows from the Bayes' rule where R stands for data, and U and V represent the model (see Supplementary Material for details). To learn an optimal model means to find the U and V matrices, or the D-dimensional LV vectors, $\mathbf{u_i}$ ($1 \leqslant i \leqslant N$) and $\mathbf{v_j}$ ($1 \leqslant j \leqslant M$)), that maximize the log-likelihood function.

The PMF method yields the optimal $\mathbf{u_i}$ and $\mathbf{v_j}$ vectors corresponding to each drug, $\mathbf{d_i}$, and each target $\mathbf{t_j}$, respectively. The basic idea is that the model is forced towards making a 'no-

interaction' prediction by the regularization – i.e. there is a penalty associated with any non-zero value in the LV matrices. However, there is also a penalty for failing to capture known interactions– i.e., if the dot product of the LV vectors corresponding to an interacting drug-target pair is close to zero. Therefore the learning of a model means to optimally balance out two objectives: developing a sufficiently complex model to describe the known interactions, but not overly complex to end up in over-fitting. In this study, we use gradient descent for optimization. The adoption of higher D values usually yields more accurate results, although beyond a certain limit the increase in complexity and decrease in efficiency may not warrant the marginal improvement, if any, in prediction accuracy. D = 50 is adopted here as an optimal dimensionality for prediction runs. The method is highly efficient: a 50-dimensional model is trained on the entire DrugBank in approximately 2 seconds using a 2.00 GHz AMD Opteron processor. Moreover, the computing time to learn a PMF model scales linearly with the number of interactions, and as such, the method can be advantageously used for much larger datasets.

4.2.3 Active Learning (AL) using PMF

The AL strategy adopted in the present study is, in part, motivated by the success reported by Warmuth et al (Warmuth, Liao et al. 2003). who demonstrated that hit maximization is a viable AL strategy applicable to predicting drug-target interactions. The AL strategy adopted here also prioritizes the discovery of unknown interactions. Our method differs in that we aim at capturing the interactions between all drugs and targets, as opposed to predicting activity against a single target.

The procedure is the following: We begin with the set of N drugs and M targets, and known associations. The purpose is to identify new associations. For each candidate interaction, say the possible interaction between $\mathbf{d_i}$ and $\mathbf{t_j}$, we compute the model's estimate, (Eq 3). The dot product $\mathbf{u_i}^{\mathbf{T}}\mathbf{v_j}$ serves as a weight $\boldsymbol{\omega_{ij}}$ for the edge/connector between $\mathbf{d_i}$ and $\mathbf{t_j}$. Clearly, $\boldsymbol{\omega_{ij}}$, or the likelihood of association between $\mathbf{d_i}$ and $\mathbf{t_j}$, is high when $\mathbf{u_i}$ and $\mathbf{v_j}$ have both large values of the same sign at the same dimension(s). For example, a relatively large weight may originate from the 2nd component of both $\mathbf{u_i}$ and $\mathbf{v_j}$, which means that the predicted association is mainly due to latent variable 2. We evaluated the statistical weights $\boldsymbol{\omega_{ij}}(\mathbf{d_i}, \mathbf{t_j})$ for the N x M pairs of drug-targets for two purposes: (i) benchmarking the methodology via an iterative AL scheme, and (ii) making *de novo* predictions. In the former case, the method is benchmarked by hiding 70% of known interactions and examining whether the top-ranking prediction is a 'hit', i.e., whether it corresponds to a known (but hidden) interaction. The outcome from this test is fed back to the model, to repeat the calculation for the next prediction. Therefore, the AL model is updated at each iteration using the newly acquired 'hit' or 'miss' data until a predetermined number (m) of predictions are made. The passive learner (PL) makes the m predictions simultaneously without updating its model.

In the case of *de novo* predictions, all DrugBank data were used as input. *De novo* predictions also lend themselves to an AL scheme provided that the top-ranking prediction is experimentally tested and then the new hit or miss data are incorporated in the model to perform a new prediction, and so on, until the experimentation budget is exhausted.

4.3 PMF CLUSTERS DRUGS WITH THERAPEUTIC SIMILARITIES, IRRESPECTIVE OF THEIR CHEMICAL-STRUCTURAL SIMILARITIES

To assess whether the LVs provide us with a pharmacologically meaningful metric, we examined the clustering of drugs in the D-dimensional space of the latent vectors. The clustering was performed for D = 30 - the value that gave the lowest Akaike information criterion I (Akaike 1974), using as basis the drug-drug distance $L_1(d_i, d_j) = \Sigma_k |u_{ik} - u_{jk}|$ where u_{ik} designates the kth component of $\mathbf{u_i}$, and the summation is performed over D components.

Inasmuch as our method evaluates drugs based on their interaction profiles with targets, which in turn refer to specific therapeutic or phenotypic actions, the similarity of a pair of drugs should be high when their therapeutic effects are comparable and vice versa. Thus, the method will tend to cluster drugs that exhibit similar patterns of interactions (with target proteins), which we term as functionally similar drugs.

The heat map in Figure 13 displays the resulting organization of drugs in 30 clusters (indicated by different colors and indices along the axes). The dark regions on the map indicate high functional similarity. The dark blocks along the diagonal show that most clusters include highly similar members, except for two (clusters 29 and 30), which apparently combine the outliers.

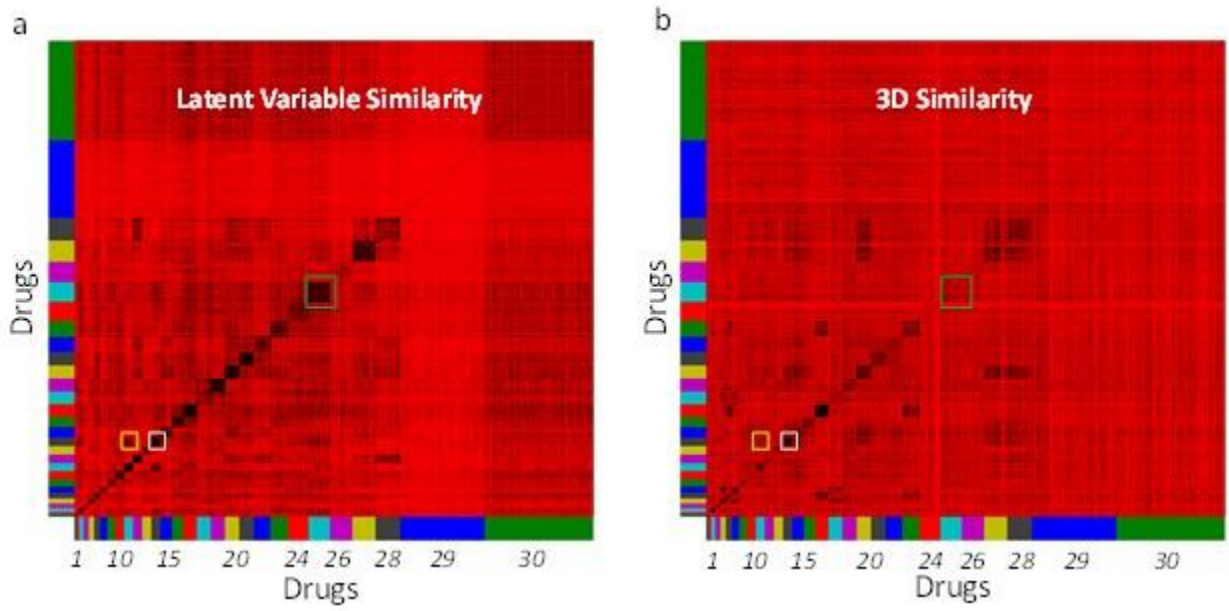

Figure 13 . Comparison of pairwise similarities of drugs

Comparison of pairwise similarities of drugs, based on their (a) therapeutic targets compiled in DrugBank and (b) 3D structure. Panel a displays the 30 clusters of drugs deduced from the PMF of 1,413 approved drugs and corresponding 1,050 targets compiled in DrugBank. By definition, drugs belonging to a given cluster share similar interaction patterns with respect to targets. Panel b displays their 3D similarities, with the drugs being ordered as in panel a. Dark regions indicate high similarity based on LVs (panel a) or 3D similarities (panel b). Comparison of the panels shows that close proximity in LV space (which indicates functional similarity) does not necessarily imply 3D-structure similarity. LV distances were distributed in the range [0, 1]; with the distribution of values also skewed in different ways. To render the two sets comparable, we performed rank normalization on both the LV similarities and 3D similarities. Selected boxes are enlarged in Figure 13 (white) and 4 (yellow).

Given that (promiscuous) proteins present more than one site for ligand-binding, different functionalities may be modulated by chemical-structurally different drugs, depending on the

binding site on the target (e.g. catalysis, substrate recognition, or allosteric signaling). Furthermore, a shared phenotype may arise from the targeting of different proteins along a given pathway. In order to make a better assessment of the properties of drugs grouped in those clusters, we examined their 3D structural similarities. High similarities would suggest that they bind similar epitopes, if not similar (or identical) structural domains or proteins. If, on the contrary, they are structurally dissimilar, this might indicate a different site on the same protein, or a different target on the same pathway, or other indirect effect due to drug-target network connectivity.

The extent of 3D structure similarity between pairs of drugs was computed using the OpenEye Scientific software (http://www.eyesopen.com/). 3D similarity was reported to be a better predictor than 2D methods for off-target interactions, and to perform equally well in on-target interactions (Yera, Cleves et al. 2011), although 3D methods may suffer from more noise due to the conformational flexibility of the small molecule. We generated for each drug all possible stereoisomers using OpenEye FLIPPER (Hawkins, Skillman et al. 2010), and up to 200 conformers per stereoisomer using OpenEye OMEGA (Hawkins, Skillman et al. 2010). All combinations of conformers accessible to the examined pair of drugs were examined using OpenEye Shape (Swann, Brown et al. 2011) toolkit; and the best matching pair was adopted to assign a 3D similarity score. This computationally expensive task led to the heat map presented in panel b of Figure 13. The drugs (along the axes) are ordered as in panel a to enable visual comparison.

The comparison of Figure 13 shows that some clusters of functionally similar drugs (panel a) also exhibit some 3D similarities (panel b), whereas others display little structural similarity. We examined more closely the individual clusters to see if shared therapeutic functions were captured even when 3D similarities were absent. Figure 14 illustrates the results for cluster 14. This cluster essentially consists of anti-anxiety drugs, the majority of which are both functionally (panel b) and structurally (panel c) similar. However, the cluster also includes a structurally dissimilar drug, ethchlorvynol (panel a), which shares the same type of phenotypic action (as a sedative) as the majority of the cluster membership (mostly targeting GABA receptors). The present approach thus detects chemically or structurally distinctive drugs that share common activities, which would have been missed by methods based on ligand fingerprint similarities.

Another interesting observation concerns the cross-correlations between different clusters (i.e. the off-diagonal regions of the heat maps). We note for example that cluster 11 also contains a set of sedatives. LVs are able to capture the commonality between the clusters 11 and 14 as may be seen by the strong signal (*dark region*) at the off-diagonal region enlarged in Figure 15b. The 3D similarity, on the other hand, cannot recognize the functional similarity and potential interference/side effects between these drugs in these two clusters (Figure 15c). The LVs thus provide information on drug groups that potentially share pathways or exhibit similar activity patterns despite their distinct physicochemical properties.

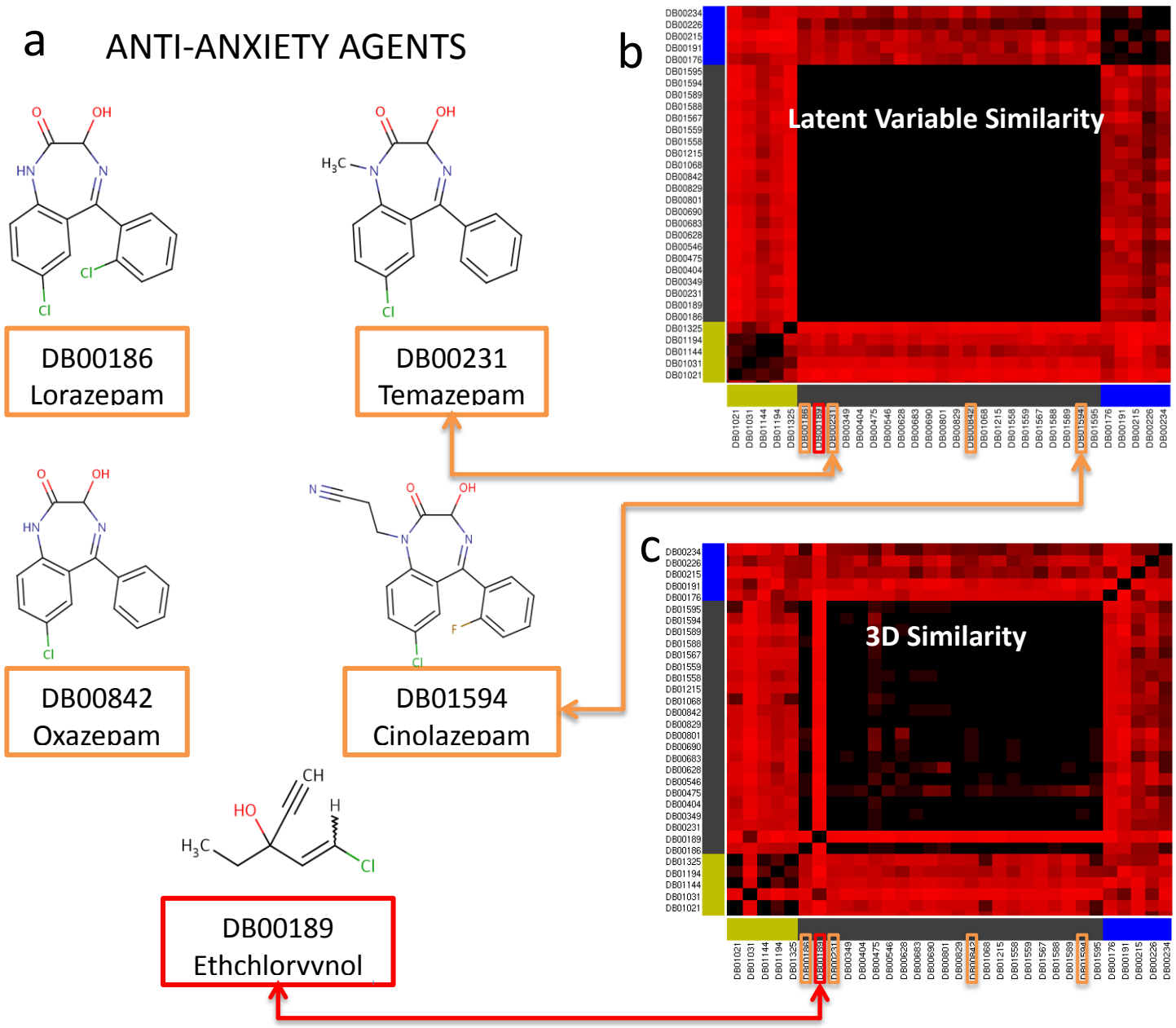

Figure 14 Latent variables can capture therapeutic action similarities when 3D similarity metrics cannot.

Closer examination of the similarities between the members of the cluster 14 in Figure 13 (enclosed in white boxes in Figure 13, enlarged in panels b and c here) shows that the cluster contains a series of anti-anxiety drugs. A few members of this cluster (indicated by orange boxes along the abscissa of panels b and c) are displayed in panel a, to illustrate their shared structural features, also indicated by the panel c that reflects their 3D similarities. The same cluster however contains ethchlorvynol, also used as a sedative, which would have been missed if we had used exclusively used 3D similarity to identify functionally similar drugs.

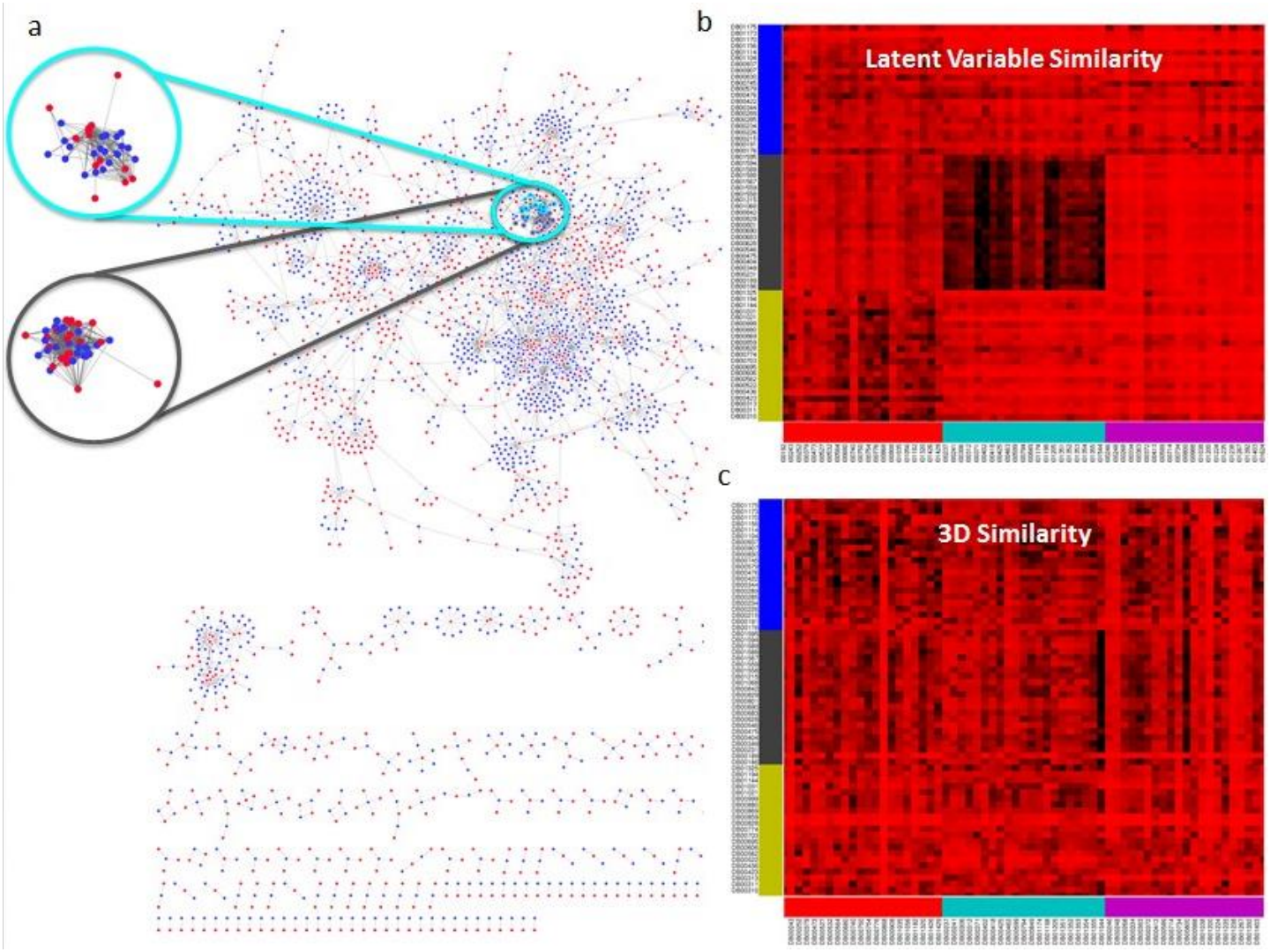

Figure 15 Strong cross-correlations between different clusters of drugs are consistent with their similar therapeutic functions

Cluster 11, color-coded cyan, is essentially composed of hypnotics and sedatives. Cluster 14 (dark gray) contains anti-anxiety drugs. The drugs in these two clusters are located very closely on the drug-target interaction network, as shown in panel a, consistent with their similar actions. The LV-derived heat maps capture the functional similarity between these two clusters (as indicated by strong signals, or the dark region, in panel b); the maps based on 3D similarity (panel c) do not. In panel a drugs are shown in blue, protein targets in red. Most drugs and targets are part of a single connected component. Data are retrieved from DrugBank. Cytoscape is used for visualization(Smoot, Ono et al. 2011).

4.4 BENCHMARKING COMPUTATIONS SUPPORT THE UTILITY OF THE METHOD FOR ANALYZING LARGE DATASETS

To evaluate the performance of the method in comparison to previous work, we considered three important studies in this area, one recently published by Gonen (Gönen 2012) and two by Yamanishi et al. (Yamanishi, Araki et al. 2008, Yamanishi, Kotera et al. 2010). Gonen used a Kernel-based matrix factorization (KBMF) with chemical and genomic similarities to predict multiple targets. Yamanishi et al., on the other hand, integrated chemical, genomic and pharmacological data to map all drugs and targets to the same unified feature space where each protein-compound pair closer than a predefined threshold was predicted to interact. Our approach differs from both studies, in that PMF assumes an independent LV for each row and column with Gaussian priors; whereas KBMF employs LVs spanning all rows and columns with Gaussian process priors, and Yamanishi et al project drugs and targets into a pharmacological space based on the eigenvalue decomposition of the graph-based similarity matrix.

The benchmarking procedure that we adopted is a five-fold cross-validation of drugs on four target classes: Enzymes, Ion channels, G-protein coupled receptors (GPCRs) and Nuclear Receptors. In order to achieve comparable results, we used the same protocol as that adopted earlier, i.e., we divided our dataset into five subsets, and each was used as a test set, and the others, as training sets. Due to the randomness involved in the selection of subsets, we repeated the cross-validation experiments 100 times with randomly selected subsets and evaluated the average AUC (area under the receiver operating curve) for each subset. The first four rows in Table 4 compare the results (columns 6-10) for the four classes, and the 5th row lists the average performances weighted by the size of the interaction space. Our method performs best when applied to large datasets (e.g. enzymes and ion channels); whereas Gonen's performs best in the

case of GPCRs, and Yamanishi et al.(2010) exhibits the highest performance for nuclear receptors, where the present method yields a relatively low (0.642) AUC value. Examination of the statistical significance of our results indicates that the mean AUC values obtained for all four sets are highly robust. Their covariance vary from 2% (Enzymes and Ion Channels) to 11% (Nuclear Receptors). Finally, the application of the same benchmarking protocol to DrugBank yielded an accuracy rate of 79.4 ± 0.01% (Table 4), supporting the utility of the method when applied to large datasets.

Table 4 Properties of the space of proteins-drugs, and performance of present method in comparison to others

Target type	# of known inter-actions	# of drugs (*N*)	# of targets (*M*)	Size of interaction space (*N*×*M*)	Percent occupancy of the space	Yamanishi (pred pharmacol effects)		Gonen	Present method
						2008[(a)]	*2010*[(a)]	*2012*[(a)]	(D = 50)
Enzymes	1,515	212	478	101,336	1.50%	0.821	0.845	0.832	0.861 ± 0.02
Ion Channels	776	99	146	14,454	5.37%	0.692	0.731	0.799	0.904 ± 0.02
GPCRs	314	105	84	8,820	3.56%	0.811	0.812	0.857	0.771 ± 0.04
Nuclear	44	27	22	594	7.41%	0.814	0.830	0.824	0.650 ± 0.11
All[(b)]	2,649	443	730	-	-	0.782	0.80	0.825	0.859 ± 0.03
DrugBank	4,731	1,413	1,050	1,483,650	0.32%	-	-	-	0.794 ± 0.01

(a)The last four columns present the comparison with Yamanishi's and Gonen's results for the same dataset.

(b) weighted-average mean and covariances, evaluated using the number of interactions as weights

In principle, it might be intrinsically harder to make accurate predictions for larger datasets as the size of the potential interaction space N×M grows quadratically when the number of drugs and targets grow linearly, particularly if the number of known interactions is small. The occupancy of the N×M interaction matrix is only 1.5% in the Enzyme class, which could make it difficult to learn an informative model. The present PMF technique, however, successfully learned an informative model and handled the complexity of interactions in this space of interactions, apparently due to the availability of a sufficiently large (absolute) number of known interactions.

Ion Channel-drug class has the second largest number of known interactions among the four. Although the size of interaction space is one order of magnitude smaller than Enzyme class, there are 776 known interactions leading to a percent occupancy of 5.37% of all possible ion channel-drug associations. The success of our method in this case may be attributed to both the relatively large number of known interactions and the rich annotation of that class of interactions.

The two other classes, GPCRs and nuclear receptors, are significantly smaller in terms of their interaction space and/or occupancy of that space. Nuclear receptors comprise only 27 drugs and 22 targets, and 44 interactions. A method that relies solely on connectivity, like ours, cannot presumably formulate an informative model when the set of 'edges' to construct the network connectivity matrix is incomplete. In those cases, the data that come from other sources, e.g. chemical similarity and genomic patterns amend this lack of information. Consequently, methods that incorporate such features (Yamanishi, Kotera et al. 2010, Gönen 2012) outperform ours.

To put the results into perspective, we indicated by a vertical dashed line in each panel the fraction of data (80%) used in previous studies (Yamanishi, Kotera et al. 2010, Gönen 2012)for training purposes. Consistent with the above findings, Ion Channels yield the best result: previous AUC values (Gönen 2012) (of 0.799; Table 4) are matched with about only 35% of the data. On the Enzyme group, we match the performance of Yamanishi et al. (Yamanishi, Kotera et al. 2010)(AUC of 0.845) with roughly 70% of the data used for training. GPCRs and Nuclear Receptors yield AUC values lower than those previously attained, irrespective of the fraction of hidden interactions.

In summary, the method is particularly suitable for screening and inferring repurposable drugs or potential side effects from large datasets where computational assessment of structure similarity kernels become prohibitively expensive. In cases where the dataset of known interactions is too small, on the other hand, 2D or 3D similarity metrics provide more accurate assessments.

4.5 THE ABSOLUTE NUMBER OF KNOWN INTERACTIONS OVERRIDES THE SCARCITY OF THE DATA IN DETERMINING THE ACCURACY RATE OF PMF ACTIVE LEARNER

As a more stringent test, 3,318 (70%) of the known 4,731 interactions in DrugBank were randomly hidden, reducing the average number of interactions per drug from 3.35 to 1. The resulting 'incomplete' interaction matrix was then used to predict the hidden interactions, one at a time (rank-ordered by statistical weights $\omega_{ij}(d_i, t_j)$) as described in the Methods. The outcome was checked in a simulated experiment to assess whether the predicted interaction is a true positive (TP) or a false positive (FP). If the prediction is an existing, but hidden, interaction, the result is considered a TP (or hit), otherwise a FP (or miss). Then the model is updated in line with our AL scheme, and this loop is repeated until the completion of m = 1,000 predictions. At that point, the simulation is halted and the overall performance of the model, or the hit ratio, is evaluated. Note that this method gives us a lower bound for hit ratio because the predictions are labeled as hits only if they are annotated in DrugBank, although they can be true but not yet observed experimentally or annotated in DrugBank.

The results are presented in Figure 16. The figure displays the number of hits as a function of the number of predictions, obtained with three approaches: active learning (*dark blue curves*), passive learning (*dark red curves*) and random (*green*). The approach is able to achieve, on average, 587 hits out of 1,000 predictions via AL, 407 hits, via PL; and the corresponding variances (indicated by the dashed curves) are 35 and 46, respectively. Compared to the random probability of 2.23 hits per 1,000 predictions, the AL result is a 263-fold improvement over random. The improvement of AL over PL is 1.44 fold. The AL improvement over random was

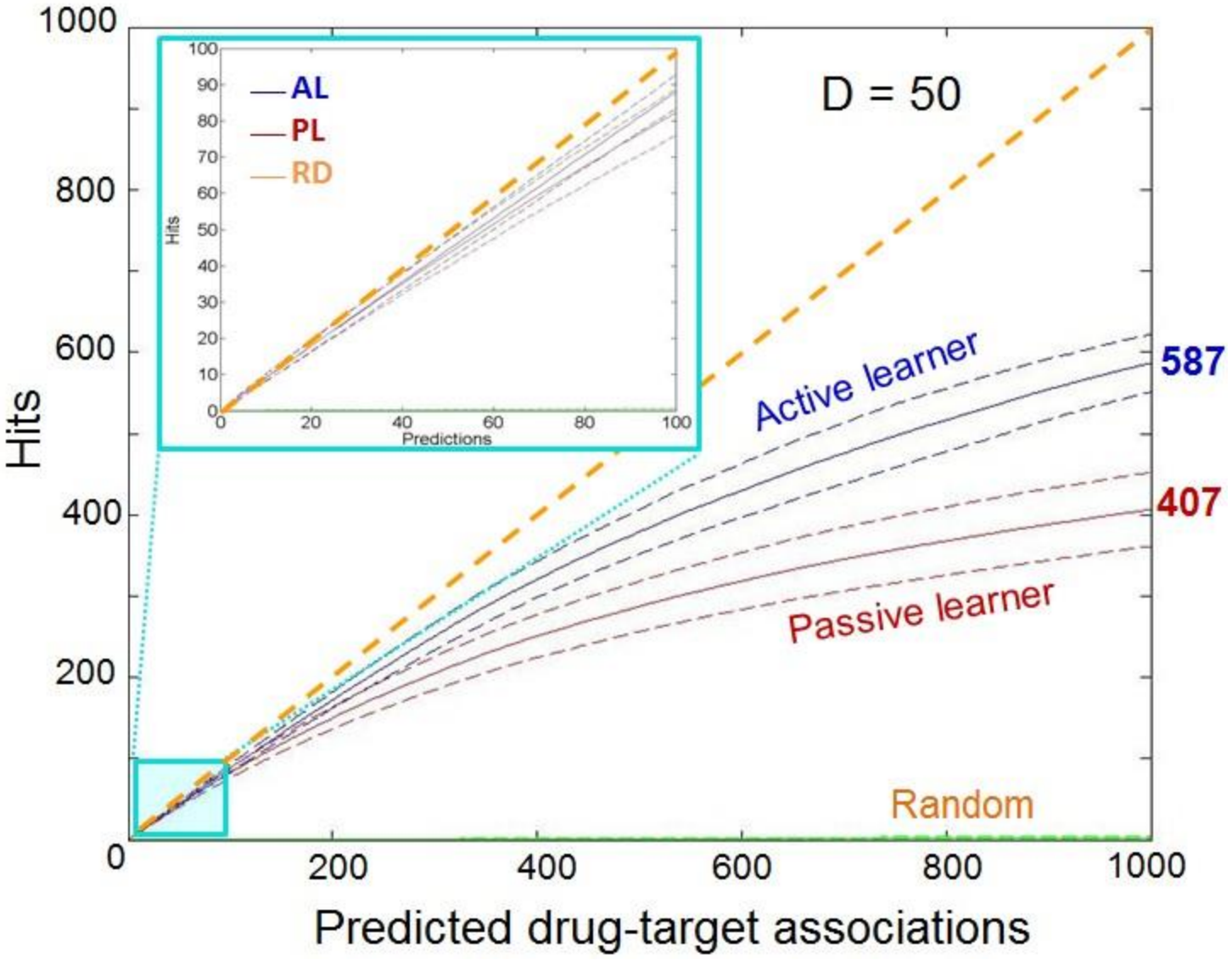

Figure 16 Ability of PMF to recapitulate hidden drug-target interactions.

The number of drug-target interactions per drug was reduced from 3.35 (average) to 1 by hiding 70% of known interactions, selected randomly. Simulations were repeated n = 96 times for each of the $1 < m < 1{,}000$ predictions (abscissa) and the number of hits (correctly identified hidden interactions) is plotted for each run, along the ordinate. The dark blue and dark red solid curves refer to the average performance obtained by active learning and passive learning protocols, respectively, using D = 50, $\varepsilon = 3$, $\lambda = 0.01$, and u = 0.9 in the adopted PMF algorithm. Dashed curves show the corresponding variances (by one standard deviation) above and below the mean value. The green curves (practically overlapping with the abscissa) refer to results from random predictions. The inset shows a close-up of the first 100 predictions. AL reaches an accuracy rate (hit ratio) of 88.0 ± 4.7% and 58.7± 3.5 % in the respective cases of m = 100 and 1,000 predictions.

reported to be up to 3.19-fold in a previous SVM-based study for predicting the activity of 1,316 drugs against a single target.38 The same study also reported 1.59-fold improvement between passive and active learners. Closer examination of the results from the top 100 predictions (enlarged in the inset) further shows that hit ratios of 88.0 ± 4.7% and 82.2 ± 6.4% are obtained by the respective AL and PL protocols.

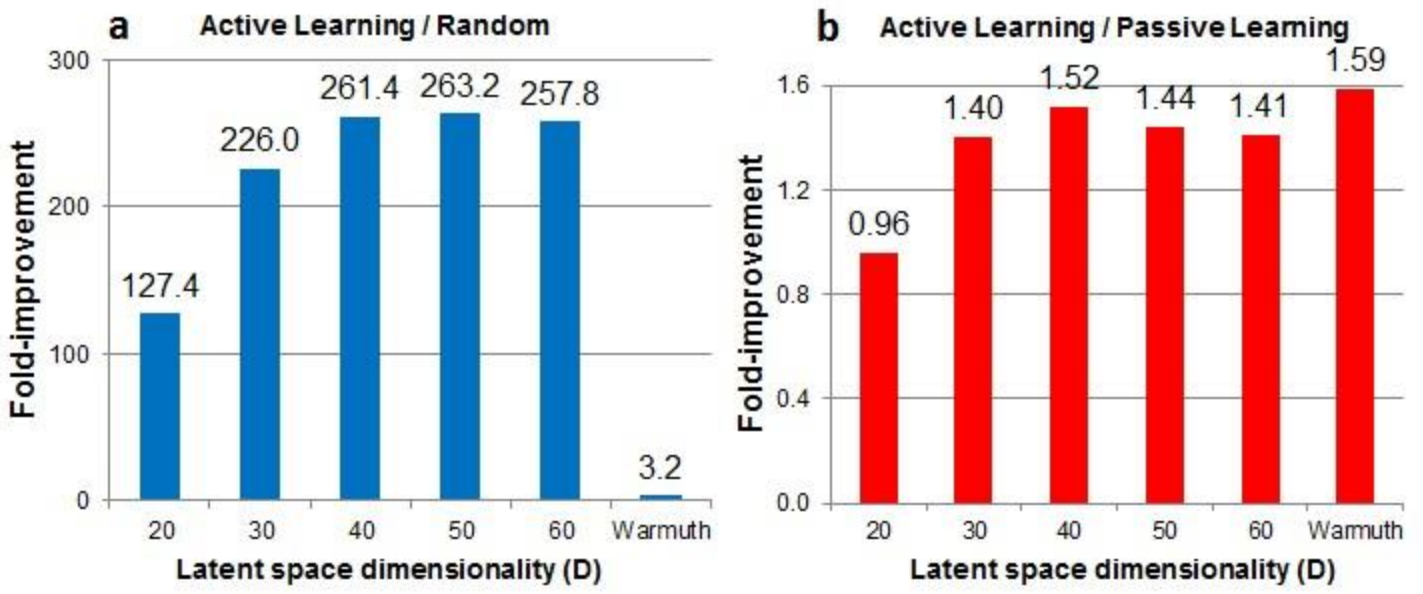

Figure 17 Improvement in prediction accuracy by active learning (AL) over random (panel a) and over passive learning (PL) (panel b), as a function of the latent space dimensionality

Fold-improvement is based on hit ratios obtained at the end of 1,000 predictions, using same parameters as Figure 16. The AL performance levels off at about D = 50 in panel a. The last bar in each panel refers to the work of Warmuth et al. (2003).

The results are obtained with D = 50, which yields optimal results, as can be seen from Figure 17 display the dependence of the results on D, in support of the choice of D = 50.

These results permit us to draw two conclusions. First, a hit ratio of 88% is attainable in the top 100 predictions (and 59% in top 1,000) upon adopting a PMF-based AL strategy for identifying hidden/unknown interactions in a sparse (0.32% occupancy) dataset of about 1.5 million potential interactions. Second, the AL method outperforms random by two orders of magnitude and PL by a ratio of 1.5 approximately, in support of AL strategy for predicting new interactions.

4.6 *DE NOVO* PREDICTIONS OF DRUG-TARGET INTERACTIONS

We used our method to predict new (potential) drug-target interactions after training our model on the latest available version of DrugBank (Sept 10, 2013) comprised of 5,041 interactions between 1,502 approved drugs and 1,138 targets. The highest confidence pairs obtained for twenty distinct drugs are presented in Table 5.

Table 5 *De novo* predictions, rank-ordered based on confidence

Drug	Target	Support from previous experiments (ref)
Ergotamine	serotonin receptor 1A (5-HT_{1A}[a])	direct(Tfelt-Hansen, Saxena et al. 2000)
Amoxapine	serotonin receptor 2A (5-HT_{2A})	direct(Pälvimäki, Majasuo et al. 1996)
Minaprine	histamine receptor H_1	-
Trimipramine	α_{2A} adrenergic receptor	indirect[b]
Amitriptyline	serotonin receptor 2C (5-HT_{2c})	indirect[b]
Tramadol	serotonin receptor 2C (5-HT_{2c})	indirect[b]
Clozapine	D(1B) dopamine receptor	indirect[b]
Doxepin	D(1A) dopamine receptor	indirect[b]
Nicardipine	histamine receptor H_1	-
Flunitrazepam	GABA[a]α_1	indirect[b]
Paliperidone	serotonin receptor 7 (5-HT_7)	direct(Kast 2010)
Iloperidone	α_{2B} adrenergic receptor	indirect[b]
Propericiazine	α_{1A} adrenergic receptor (ADRA1A[a])	indirect[b]
Asenapine	α_{1B} adrenergic receptor	indirect[b]
Verapamil	calmodulin	direct (Petersen and Mørk 1996)
Meperidine	Na[a] channel 10, type α	direct (Wagner, Eaton et al. 1999)
Cinnarizine	calmodulin	direct(ZIMMER and HOFMANN 1987)
Paroxetine (paxil)	histamine receptor H_1	direct(Fava 1999)
Orphenadrine	DAT[a]	indirect[c]
Citalopram	Na[a]-dependent NET[a]	indirect(Petersen and Mørk 1996)

(a)Abbreviations: GABA: γ-aminobutyric-acid receptor; 5-HT: 5-hydroxytryptamine (or serotonin) receptor. NET: norepinephrine (or noradrenaline) transporter; ADRA1A: adrenoreceptor α1 A; DAT: dopamine transporter.

(b)The cases listed as 'indirect' refer to interactions of the drugs with different subtypes of the identified target

(c) orphenadrine inhibits norepinephrine reuptake thus potentiating the effect of norepinephrine There are several drugs acting as norepinephrine-dopamine reuptake inhibitors, and ophenadrine might exhibit same behavior.

The pairs therein were observed to lie frequently among the top-ranking 10 pairs (in the space of $N \times M = 1.7x10^6$ potential interactions), deduced from 10^4 independent runs initiated with different random numbers.

We note that the list of *de novo* predictions in Table 5 is dominated by drugs used for neurological or psychiatric disorders, consistent with the known pharmacological promiscuity of this of drugs. The last column 2 lists the experimental support from the literature, if any, for the possible interaction of the drug-target pair in each row. Among pairs supported by previous experiments, we note ergotamine–serotonin receptor 1A (5HT1A) (Tfelt-Hansen, Saxena et al. 2000), amoxapine–5-HT_{2A} (Pälvimäki, Majasuo et al. 1996), verapamil–calmodulin (Epstein, Fiss et al. 1982), paliperidone–5-HTc (Kast 2010), meperidine–sodium channels (Wagner, Eaton et al. 1999), cinnarizine–calmodulin (ZIMMER and HOFMANN 1987). We also note that chronic treatment with paroxetine has been recently reported to increase the mRNA levels of histamine receptor H1, indicating an association between paroxetine and Histamine receptor H1 (Rahmadi, Narita et al. 2011). Although paroxetine is a potent serotonin reuptake inhibitor, its weight gain side effect has been attributed to its medication action on histamine receptors(Fava 1999).

Many others (indicated as 'indirect') are interactions known to occur either with subtypes of the listed targets or proteins implicated in the same phenotype (e.g., citalopram induces norepinephrine receptor hypoactivity (Petersen and Mørk 1996), which may relate to

norepinephrine transport by NET). Yet, the validity of these predictions need to be established by experiments.

4.7 DISCUSSION

Over the last couple of years, there have been a number of computational studies performed to identify targets of existing drugs and drug candidates other than those originally known/proposed to be targeted. A pioneering study is that of Roth, Shoichet and coworkers (Keiser, Roth et al. 2007, Keiser, Setola et al. 2009) based on compound chemical similarities. Dudley et al focused on inverse correlations between gene expression profiles in the presence of a drug and in a disease state (Dudley, Sirota et al. 2011). Yamanishi and his colleagues represented drugs and targets in an integrated 'pharmacological space' (Yamanishi, Araki et al. 2008, Yamanishi, Kotera et al. 2010).Gonen used a KBMF method where chemical and genomic similarities were integrated (Gönen 2012).We proposed a PMF-based AL methodology that can be advantageously used for large datasets.

The applicability of the method to large datasets is worth further attention, given that we will increasingly have access to bigger data (e.g. STITCH Database (Kuhn, Szklarczyk et al. 2012)), which will be exploited for repurposable drug identification. The software developed here, made accessible in http://www.csb.pitt.edu/Faculty/bahar/files/, is readily scalable. For very large datasets, which typically have more known interactions, the PMF is able to construct a better model using the plethora of available data; whereas when the number of known interactions is limited, the use of chemical and genomic kernels allows KBMF to outperform PMF. The application of KBMF to large datasets may, however, become challenging, For

example, STITCH contains on the order of 106 proteins and 105 compounds, implying that 1012 sequence and 1010 chemical similarity comparisons are needed to make predictions. However, the PMF method is independent of chemical, structural or other similarity metrics, and its computation time scales linearly with the number of known interactions; and it proves to perform well on large datasets. The datasets reporting drug-target interactions are constantly improving in quality and quantity, and therefore expected to give even better results when analyzed by an efficient tool. Finally, the extension of the method to analyzing big data (with millions of nodes) is foreseeable in the near future. The recently introduced GraphChi tool (Kyrola, Blelloch et al. 2012) can be used for optimized and parallelized model learning for further performance improvements.

The fact that the PMF is independent of 2D/3D shape comparison methods commonly employed in drug-target pair inferences implies that the derived LVs capture similarities based on the interaction patterns of drugs at the cellular level, even if their molecular structures are dissimilar (see Figure 13 and Figure 14). As such, the method may be advantageously used for lead hopping, thus complementing those (e.g. SVM classification algorithms) used in conjunction with 2D or 3D pharmacophoric fingerprints (see Saeh et al. (Saeh, Lyne et al. 2005)). Inasmuch as the currently proposed method does not require structural data for proteins but knowledge of drug-target interactions, it can be advantageously applied to membrane proteins (major drug targets) for which structural data still remain sparse. It can also be used to make predictions across major drug or target classification boundaries. One implication is that the *de novo* predictions are not restricted to major drug or target classification boundaries.

A major utility of the developed tool is the ability to deliver testable hypotheses with regard to repurposable drugs, thus significantly reducing the search space for identifying potent

applications of existing drugs (that proved to meet ADMET requirements). The number of experiments that can be efficiently conducted is usually limited, e.g. of the order of 102 if not 101 for high-confidence assays as opposed to the complete space of ~1.5 million combinations for the dataset used in this study. The fact that the top-ranking predictions exhibit a hit ratio of 59% (for the top 1,000 predictions; or 88% for top 100 predictions) suggest that *de novo* predictions made by the presently introduced method of approach applied to increasingly large datasets are likely to provide useful guidance for experimentally testing, streamlining or prioritizing existing or investigational drugs or new compounds. Another important by-product is the probabilistic assessments on potential side effects, a topic that will become increasingly important with advances in personalized medicine.

5.0 CONCLUSION AND FUTURE WORK

In this thesis, we have performed analysis of several neuron-signaling membrane proteins: LeuT and iGluR family, using both computational molecular and systems-level approaches: ENM analysis, all-atom MD simulations based druggability assessment as well as probabilistic matrix factorization (PMF) in analysis of drug-target interaction network.

Using NMA-ENM, we gained a better understanding of the conformation sampling ability of ANM in LeuT. The advantage of this approach is that it can help us to extend the conformational space accessible to LeuT based on a single structure among the available LeuT crystal structures and it is fast without depending on the availability of numerous representative structures (that are needed for PCA analysis, for instance.) The consistency between ENM-predicted motion and the dominate motion computed by PCA of experimental structures enables us to use ENM to decipher a pathway of communication via residues identified from the intrinsic topology of the protein. The most cooperative motion identified by the native topology network models is highly correlated with the potential structural changes in different forms.

The flexibility of proteins and ligands has been widely recognized important for identifying binding sites in proteins. MD simulation of proteins in the presence of small organic molecules and water, which takes entropy and enthalpy into account, enables us to capture those allosteric binding sites which is hard to be captured by experimental approaches due to protein flexibility. Using this druggability assessment method, we described a landscape of binding sites

for iGluR NTDs monomers and dimers. Particularly, we have identified binding sites at the UL and LL interfaces of GluA3 NTD dimer and GluN1-GluN2B NMDA heterodimer. PMs have been built for those potential binding sites captured by probe clusters in the previous GluA3 NTD dimers and GluN1-GluN2B NTD dimers druggability simulation.

Based on those pharmocophore models, virtual screenings have been done to find potential hit compounds for NMDAR (GluN1-GluN2B) and AMAPR (GluA3). As shown in **Table 6**, no literature evidence have been found to offer hint about whether the predicted drugs bind to our targets. However, for Marimastat, which is predicted by NMDAR PM, as a top-ranking drug predicted by PMF for AMPAR. Also, Arbutamine which targets β-adrenergic receptors is captured by both NMDAR and AMPAR PMs, which might suggest it is likely to bind the iGluRs.

Table 6 Drugs predicted using pharmacophore models

Targets	Position of the binding sites	Drugs	Supporting evidence
NMDAR(GluN1-GluN2B)	Site 1 (UL interface)	Arbutamine	-
	Site 2(LL interface)	Adenosine	-
	Site 3(helices and loops interface)	Marimastat	Indirect (Captured by PMF)
AMPAR(GluA3)	UL interface	Carteolol	-
	LL interface	Arbutamine	-

De novo prediction of the above two targets via PMF has been performed as well. **Table 7** lists the top-ranking 10 drugs based on confidence levels. For NMDAR (GluN1), among the top 10 drugs, 3 have direct literature support for their binding to the target (highlighted in *red*) and 6 hae indirect support either binding to subtypes of GluN1 or reveal some binding profiles indicating it might bind to the target from previous experiments. Also, among those 10 drugs, all,

except Felbamate andMemantine, are antagonists of sodium-dependent noradrenaline transporter and sodium-dependent serotonin transporter. Therefore, they have been employed as antidepressant drugs or neuropathic pain analgesia. Chlorpheniramine and Atomoxetine can target dopamine transporter as well.

Table 7 Top-ranking 10 drugs predicted by PMF for NMDA GluN1 and GluN2B subunits

Target	Top10 predicted Drugs	Supporting evidence from DrugBank or Literature
NMDAR (GluN1)	**Tramadol**	Indirecta (GluN3A)
	Tapentadol	Indirect(Schäfer 2009, Vadivelu, Mitra et al. 2010)
	Chlorpheniramine	Indirect(Díaz-Trelles, Novelli et al. 2000)
	Felbamate	Indirecta(GluN2B, GluN2A GluN3A)
	Atomoxetine	Direct(Ludolph, Udvardi et al. 2010)
	Levomilnacipran	Direct(Shuto, Takada et al. 1995)
	Desvenlafaxine	Indirect(Raabe and Gentile 2008)
	Cocaine	-
	Dextromethorphan	Indirecta(GluN3A)
	Memantine	Direct(Kotermanski, Wood et al. 2009)
NMDAR (GluN2B)	Tramadol	Indirecta (GluN3A)
	Orphenadrine	Indirecta(GluN1, GluN2D, GluN3A, GluN3B)
	Ketamine	Indirect (GluN3A)
	Amantadine	Indirecta(GluN3A)
	Mirtazapine	Direct(Bienkowski, Krzascik et al. 2001)
	Halothane	Indirecta (GluN3A, GluN3B, GluN2A)
	Amisulpride	-
	Thiothixene	-
	Dopamine	-
	Sulpride	-
AMPAR (GluA3 subunit)	Marimastat	Indirect(Captured by NMDA PM)
	Zonisamide	Indirect(Sarid-Segal, Knapp et al. 2009)
	Dalfampridine	-
	Miconazole	-
	Halothane	Indirecta (GluN3A, GluN3B, GluN2A)
	Antithymocyte globulin	-
	Bosutinib	-

	Amiloride	-
	L-Carnitine	Indirect(Castorina, Maria Ambrosini et al. 1993, Zanelli, Solenski et al. 2005)
	Drotrecogin alfa	-

Note: a.The cases listed as 'indirect' refer to interactions of the drugs with different subtypes of the identified target from DrugBank.

For NMDAR (GluN2B), among the top 10 drugs, only the first 6 drugs have either direct or indirect supporting evidence. Tramadol ranks first in both GluN1 and GluN2B, and it has been found to directly interact with GluN3A. The top 10 drugs for AMPAR (GluA3) have much less supporting evidence and most of the predicted drugs are ion channel blockers. This is due to those AMPARs, especially GluA3, which have much fewer known existing drugs binding to them compared to NMDARs. And in the dataset we used for *de novo* prediction, there is only one known interaction which is between GluA3 and lithium. Lack of known interactions affects PMF performance as discussed in chapter4. Interestingly, Marimastat ranking first among PMF *de novo* predictions made for AMPAR, is also captured by NMDAR PM based on druggability simulations.

In summary, the results from the application of PMF and druggability simulations based PM may be advantageously combined to obtain consensus hit compounds. PMF outperforms the latter in terms of new drug-target associations prediction. However, there is still overlap between those two models like drug Marimastat. The PMF method relies on the existing known interaction information for that specific target.

Thus, in the presence of knowledge in ligand-binding profile, PMF emerges as a powerful approach for predicting repurposable drugs. On the other hand, for exploring potential binding site on those targets, especially when there are fewer data on drugs, druggability simulations provides valuable testable hypotheses.

APPENDIX A

DETAILS OF DRUGGABILITY SIMULATION

System			PDB ID	Time (ns)	Probe composition
NTD monomers	AMPA	GluA1	3SAJ	40	50%IPRO,10%ACAM,10%IBUT,10%IMID,10%ACTT,10%IPAM
		GluA2	3HSY	40	50%IPRO,10%ACAM,10%IBUT,10%IMID,10%ACTT,10%IPAM
		GluA3	3O21	40	70%IPRO,10%ACAM,10%ACTT,10%IPAM
	Kainate	GluK2	3H6G	40	50%IPRO,10%ACAM,10%IBUT,10%IMID,10%ACTT,10%IPAM
		GluK3	3OLZ	40	50%IPRO,10%ACAM,10%IBUT,10%IMID,10%ACTT,10%IPAM
	NMDA	NR1	3Q41	40	50%IPRO,10%ACAM,10%IBUT,10%IMID,10%ACTT,10%IPAM
		NR2B	3JPY	40	20%IPRO,10%ACAM,10%IBUT,10%IMID,10%ACTT,40%BENZ
NTD dimers	AMPA	GluA3	3O21	40	40%IPRO,10%ACAM,15%IBUT,15%ACTT,15%IPAM,5%BENZ
	NMDA	N1-N2B	3QEL	40	30%IPRO,10%ACAM,10%IBUT,10%IMID,10%ACTT,10%IPAM,20 % BENZ

BIBLIOGRAPHY

Abrams, C. F. and E. Vanden-Eijnden (2010). "Large-scale conformational sampling of proteins using temperature-accelerated molecular dynamics." Proceedings of the National Academy of Sciences **107**(11): 4961-4966.

Acharya, C., A. Coop, J. E. Polli and A. D. Mackerell, Jr. (2011). "Recent advances in ligand-based drug design: relevance and utility of the conformationally sampled pharmacophore approach." Curr Comput Aided Drug Des **7**(1): 10-22.

Akaike, H. (1974). "A new look at the statistical model identification." Automatic Control, IEEE Transactions on **19**(6): 716-723.

Allen, K. N., C. R. Bellamacina, X. Ding, C. J. Jeffery, C. Mattos, G. A. Petsko and D. Ringe (1996). "An experimental approach to mapping the binding surfaces of crystalline proteins." The Journal of Physical Chemistry **100**(7): 2605-2611.

Andersen, J., N. Stuhr-Hansen, L. Zachariassen, S. Toubro, S. M. Hansen, J. N. Eildal, A. D. Bond, K. P. Bøgesø, B. Bang-Andersen and A. S. Kristensen (2011). "Molecular determinants for selective recognition of antidepressants in the human serotonin and norepinephrine transporters." Proceedings of the National Academy of Sciences **108**(29): 12137-12142.

Armstrong, N. and E. Gouaux (2000). "Mechanisms for activation and antagonism of an AMPA-sensitive glutamate receptor: crystal structures of the GluR2 ligand binding core." Neuron **28**(1): 165-181.

Atilgan, A., S. Durell, R. Jernigan, M. Demirel, O. Keskin and I. Bahar (2001). "Anisotropy of fluctuation dynamics of proteins with an elastic network model." Biophysical journal **80**(1): 505-515.

Bahar, I., A. R. Atilgan and B. Erman (1997). "Direct evaluation of thermal fluctuations in proteins using a single-parameter harmonic potential." Fold Des **2**(3): 173-181.

Bahar, I., A. R. Atilgan and B. Erman (1997). "Direct evaluation of thermal fluctuations in proteins using a single-parameter harmonic potential." Folding and Design **2**(3): 173-181.

Bahar, I., C. Chennubhotla and D. Tobi (2007). "Intrinsic dynamics of enzymes in the unbound state and relation to allosteric regulation." Current opinion in structural biology **17**(6): 633-640.

Bahar, I., T. R. Lezon, A. Bakan and I. H. Shrivastava (2009). "Normal mode analysis of biomolecular structures: functional mechanisms of membrane proteins." Chemical reviews **110**(3): 1463-1497.

Bahar, I., T. R. Lezon, A. Bakan and I. H. Shrivastava (2010). "Normal mode analysis of biomolecular structures: functional mechanisms of membrane proteins." Chem Rev **110**(3): 1463-1497.

Bahar, I., T. R. Lezon, L. W. Yang and E. Eyal (2010). "Global dynamics of proteins: bridging between structure and function." Annu Rev Biophys **39**: 23-42.

Bajorath, J. (2008). "Computational analysis of ligand relationships within target families." Curr Opin Chem Biol **12**(3): 352-358.

Bakan, A. and I. Bahar (2009). "The intrinsic dynamics of enzymes plays a dominant role in determining the structural changes induced upon inhibitor binding." Proceedings of the National Academy of Sciences **106**(34): 14349-14354.

Bakan, A., L. M. Meireles and I. Bahar (2011). "ProDy: protein dynamics inferred from theory and experiments." Bioinformatics **27**(11): 1575-1577.

Bakan, A., N. Nevins, A. S. Lakdawala and I. Bahar (2012). "Druggability assessment of allosteric proteins by dynamics simulations in the presence of probe molecules." Journal of chemical theory and computation **8**(7): 2435-2447.

Basak, S. C. (2012). "Chemobioinformatics: the advancing frontier of computer-aided drug design in the post-genomic era." Curr Comput Aided Drug Des **8**(1): 1-2.

Berg, J., M. Rogers and P. Lyster (2010). "Systems biology and pharmacology." Clinical Pharmacology & Therapeutics **88**(1): 17-19.

Berger, S. I. and R. Iyengar (2009). "Network analyses in systems pharmacology." Bioinformatics **25**(19): 2466-2472.

Bienkowski, P., P. Krzascik, E. Koros, W. Kostowski, A. Scinska and W. Danysz (2001). "Effects of a novel uncompetitive NMDA receptor antagonist, MRZ 2/579 on ethanol self-administration and ethanol withdrawal seizures in the rat." European journal of pharmacology **413**(1): 81-89.

Brooks, B. R., C. L. Brooks, A. D. MacKerell, L. Nilsson, R. J. Petrella, B. Roux, Y. Won, G. Archontis, C. Bartels and S. Boresch (2009). "CHARMM: the biomolecular simulation program." Journal of computational chemistry **30**(10): 1545-1614.

Brvar, M., A. Perdih, M. Oblak, L. P. Mašič and T. Solmajer (2010). "In silico discovery of 2-amino-4-(2, 4-dihydroxyphenyl) thiazoles as novel inhibitors of DNA gyrase B." Bioorganic & medicinal chemistry letters **20**(3): 958-962.

Campillos, M., M. Kuhn, A. C. Gavin, L. J. Jensen and P. Bork (2008). "Drug target identification using side-effect similarity." Science **321**(5886): 263-266.

Castorina, M., A. Maria Ambrosini, A. Giuliani, L. Pacifici, M. Teresa Ramacci and L. Angelucci (1993). "A cluster analysis study of acetyl-L-carnitine effect on NMDA receptors in aging." Experimental gerontology **28**(6): 537-548.

Cavasotto, C. N., J. A. Kovacs and R. A. Abagyan (2005). "Representing receptor flexibility in ligand docking through relevant normal modes." Journal of the American Chemical Society **127**(26): 9632-9640.

Chang, R. L., L. Xie, L. Xie, P. E. Bourne and B. O. Palsson (2010). "Drug off-target effects predicted using structural analysis in the context of a metabolic network model." PLoS Comput Biol **6**(9): e1000938.

Chen, L., J. Lu, J. Zhang, K. R. Feng, M. Y. Zheng and Y. D. Cai (2013). "Predicting chemical toxicity effects based on chemical-chemical interactions." PLoS One **8**(2): e56517.

Chen, L., J. K. Morrow, H. T. Tran, S. S. Phatak, L. Du-Cuny and S. Zhang (2012). "From laptop to benchtop to bedside: structure-based drug design on protein targets." Curr Pharm Des **18**(9): 1217-1239.

Cheng, F., C. Liu, J. Jiang, W. Lu, W. Li, G. Liu, W. Zhou, J. Huang and Y. Tang (2012). "Prediction of drug-target interactions and drug repositioning via network-based inference." PLoS Comput Biol **8**(5): e1002503.

Cheng, T., Q. Li, Y. Wang and S. H. Bryant (2011). "Identifying compound-target associations by combining bioactivity profile similarity search and public databases mining." Journal of chemical information and modeling **51**(9): 2440-2448.

Csermely, P., T. Korcsmáros, H. J. Kiss, G. London and R. Nussinov (2013). "Structure and dynamics of molecular networks: A novel paradigm of drug discovery: A comprehensive review." Pharmacology & therapeutics **138**(3): 333-408.

Díaz-Trelles, R., A. Novelli, J. A. Vega, A. Marini and M. T. Fernández-Sánchez (2000). "Antihistamine terfenadine potentiates NMDA receptor-mediated calcium influx, oxygen radical formation, and neuronal death." Brain research **880**(1): 17-27.

Doruker, P., A. R. Atilgan and I. Bahar (2000). "Dynamics of proteins predicted by molecular dynamics simulations and analytical approaches: Application to α - amylase inhibitor." Proteins: Structure, Function, and Bioinformatics **40**(3): 512-524.

Dudley, J. T., M. Sirota, M. Shenoy, R. K. Pai, S. Roedder, A. P. Chiang, A. A. Morgan, M. M. Sarwal, P. J. Pasricha and A. J. Butte (2011). "Computational repositioning of the anticonvulsant topiramate for inflammatory bowel disease." Science translational medicine **3**(96): 96ra76-96ra76.

Dutta, A., I. H. Shrivastava, M. Sukumaran, I. H. Greger and I. Bahar (2012). "Comparative dynamics of NMDA-and AMPA-glutamate receptor N-terminal domains." Structure **20**(11): 1838-1849.

Enyedy, I. J. and W. J. Egan (2008). "Can we use docking and scoring for hit-to-lead optimization?" J Comput Aided Mol Des **22**(3-4): 161-168.

Epstein, P. M., K. Fiss, R. Hachisu and D. M. Andrenyak (1982). "Interaction of calcium antagonists with cyclic AMP phosphodiesterases and calmodulin." Biochemical and biophysical research communications **105**(3): 1142-1149.

Eyal, E., L.-W. Yang and I. Bahar (2006). "Anisotropic network model: systematic evaluation and a new web interface." Bioinformatics **22**(21): 2619-2627.

Fava, M. (1999). "Weight gain and antidepressants." The Journal of clinical psychiatry **61**: 37-41.

Fitzgerald, J. B., B. Schoeberl, U. B. Nielsen and P. K. Sorger (2006). "Systems biology and combination therapy in the quest for clinical efficacy." Nat Chem Biol **2**(9): 458-466.

Floquet, N., J. D. Marechal, M. A. Badet-Denisot, C. H. Robert, M. Dauchez and D. Perahia (2006). "Normal mode analysis as a prerequisite for drug design: application to matrix metalloproteinases inhibitors." FEBS Lett **580**(22): 5130-5136.

Flory, P. J., M. Gordon and N. G. McCrum (1976). "Statistical Thermodynamics of Random Networks [and Discussion]." Proceedings of the Royal Society of London. A. Mathematical and Physical Sciences **351**(1666): 351-380.

Forrest, L. R., S. Tavoulari, Y.-W. Zhang, G. Rudnick and B. Honig (2007). "Identification of a chloride ion binding site in Na+/Cl−-dependent transporters." Proceedings of the National Academy of Sciences **104**(31): 12761-12766.

Forrest, L. R., Y.-W. Zhang, M. T. Jacobs, J. Gesmonde, L. Xie, B. H. Honig and G. Rudnick (2008). "Mechanism for alternating access in neurotransmitter transporters." Proceedings of the National Academy of Sciences **105**(30): 10338-10343.

Gielen, M., B. S. Retchless, L. Mony, J. W. Johnson and P. Paoletti (2009). "Mechanism of differential control of NMDA receptor activity by NR2 subunits." Nature **459**(7247): 703-707.

Gönen, M. (2012). "Predicting drug–target interactions from chemical and genomic kernels using Bayesian matrix factorization." Bioinformatics **28**(18): 2304-2310.

Gottlieb, A., G. Y. Stein, E. Ruppin and R. Sharan (2011). "PREDICT: a method for inferring novel drug indications with application to personalized medicine." Molecular systems biology **7**(1).

Gottlieb, A., G. Y. Stein, E. Ruppin and R. Sharan (2011). "PREDICT: a method for inferring novel drug indications with application to personalized medicine." Mol Syst Biol **7**: 496.

Grubmüller, H. (1995). "Predicting slow structural transitions in macromolecular systems: conformational flooding." Physical Review E **52**(3): 2893.

Guorui, Y., Z. Yinong, G. Shenyan, Z. Jie, X. Huaxi, I. M. Irimpan and J. Rongsheng (2011). "Crystal structure of the glutamate receptor GluA1 N-terminal domain." Biochemical Journal **438**(2): 255-263.

Guvench, O. and A. D. MacKerell Jr (2009). "Computational fragment-based binding site identification by ligand competitive saturation." PLoS computational biology **5**(7): e1000435.

Hajduk, P. J., J. R. Huth and S. W. Fesik (2005). "Druggability indices for protein targets derived from NMR-based screening data." Journal of medicinal chemistry **48**(7): 2518-2525.

Haliloglu, T., I. Bahar and B. Erman (1997). "Gaussian dynamics of folded proteins." Physical review letters **79**(16): 3090.

Hawkins, P. C., A. G. Skillman, G. L. Warren, B. A. Ellingson and M. T. Stahl (2010). "Conformer generation with OMEGA: algorithm and validation using high quality structures from the Protein Databank and Cambridge Structural Database." Journal of chemical information and modeling **50**(4): 572-584.

Henry, L. K., J. R. Field, E. M. Adkins, M. L. Parnas, R. A. Vaughan, M.-F. Zou, A. H. Newman and R. D. Blakely (2006). "Tyr-95 and Ile-172 in transmembrane segments 1 and 3 of human serotonin transporters interact to establish high affinity recognition of antidepressants." Journal of Biological Chemistry **281**(4): 2012-2023.

Hillenmeyer, M. E., E. Fung, J. Wildenhain, S. E. Pierce, S. Hoon, W. Lee, M. Proctor, R. P. S. Onge, M. Tyers and D. Koller (2008). "The chemical genomic portrait of yeast: uncovering a phenotype for all genes." Science **320**(5874): 362-365.

Hinsen, K. (1998). "Analysis of domain motions by approximate normal mode calculations." Proteins Structure Function and Genetics **33**(3): 417-429.

Hopkins, A. L. (2007). "Network pharmacology." Nat Biotech **25**(10): 1110-1111.

Hopkins, A. L. (2008). "Network pharmacology: the next paradigm in drug discovery." Nat Chem Biol **4**(11): 682-690.

Hopkins, A. L. and C. R. Groom (2002). "The druggable genome." Nature reviews Drug discovery **1**(9): 727-730.

Hopkins, A. L., J. S. Mason and J. P. Overington (2006). "Can we rationally design promiscuous drugs?" Current opinion in structural biology **16**(1): 127-136.

Horvath, D. (1997). "A virtual screening approach applied to the search for trypanothione reductase inhibitors." J Med Chem **40**(15): 2412-2423.

Huang, N. and M. P. Jacobson (2010). "Binding-site assessment by virtual fragment screening." PloS one **5**(4): e10109.

Huber, T. and W. F. van Gunsteren (1998). "SWARM-MD: Searching conformational space by cooperative molecular dynamics." The Journal of Physical Chemistry A **102**(29): 5937-5943.

Iadevaia, S., Y. Lu, F. C. Morales, G. B. Mills and P. T. Ram (2010). "Identification of optimal drug combinations targeting cellular networks: integrating phospho-proteomics and computational network analysis." Cancer Res **70**(17): 6704-6714.

Iorio, F., R. Bosotti, E. Scacheri, V. Belcastro, P. Mithbaokar, R. Ferriero, L. Murino, R. Tagliaferri, N. Brunetti-Pierri, A. Isacchi and D. di Bernardo (2010). "Discovery of drug mode of action and drug repositioning from transcriptional responses." Proc Natl Acad Sci U S A **107**(33): 14621-14626.

Iskar, M., G. Zeller, P. Blattmann, M. Campillos, M. Kuhn, K. H. Kaminska, H. Runz, A. C. Gavin, R. Pepperkok, V. van Noort and P. Bork (2013). "Characterization of drug-induced transcriptional modules: towards drug repositioning and functional understanding." Mol Syst Biol **9**: 662.

Ivetac, A. and J. Andrew McCammon (2010). "Mapping the Druggable Allosteric Space of G‐Protein Coupled Receptors: a Fragment‐Based Molecular Dynamics Approach." Chemical biology & drug design **76**(3): 201-217.

Jia, J., F. Zhu, X. Ma, Z. W. Cao, Y. X. Li and Y. Z. Chen (2009). "Mechanisms of drug combinations: interaction and network perspectives." Nat Rev Drug Discov **8**(2): 111-128.

Jin, G., C. Fu, H. Zhao, K. Cui, J. Chang and S. T. Wong (2012). "A novel method of transcriptional response analysis to facilitate drug repositioning for cancer therapy." Cancer Res **72**(1): 33-44.

Jin, R., S. K. Singh, S. Gu, H. Furukawa, A. I. Sobolevsky, J. Zhou, Y. Jin and E. Gouaux (2009). "Crystal structure and association behaviour of the GluR2 amino‐terminal domain." The EMBO journal **28**(12): 1812-1823.

Joffe, E. (1991). "Complication during root canal therapy following accidental extrusion of sodium hypochlorite through the apical foramen." Gen Dent **39**(6): 460-461.

Kantcheva, A. K., M. Quick, L. Shi, A.-M. L. Winther, S. Stolzenberg, H. Weinstein, J. A. Javitch and P. Nissen (2013). "Chloride binding site of neurotransmitter sodium symporters." Proceedings of the National Academy of Sciences **110**(21): 8489-8494.

Karakas, E., N. Simorowski and H. Furukawa (2009). "Structure of the zinc‐bound amino‐terminal domain of the NMDA receptor NR2B subunit." The EMBO journal **28**(24): 3910-3920.

Karakas, E., N. Simorowski and H. Furukawa (2011). "Subunit arrangement and phenylethanolamine binding in GluN1/GluN2B NMDA receptors." Nature **475**(7355): 249-253.

Kast, R. (2010). "Glioblastoma chemotherapy adjunct via potent serotonin receptor‐7 inhibition using currently marketed high‐affinity antipsychotic medicines." British journal of pharmacology **161**(3): 481-487.

Keiser, M. J., B. L. Roth, B. N. Armbruster, P. Ernsberger, J. J. Irwin and B. K. Shoichet (2007). "Relating protein pharmacology by ligand chemistry." Nature biotechnology **25**(2): 197-206.

Keiser, M. J., B. L. Roth, B. N. Armbruster, P. Ernsberger, J. J. Irwin and B. K. Shoichet (2007). "Relating protein pharmacology by ligand chemistry." Nat Biotechnol **25**(2): 197-206.

Keiser, M. J., V. Setola, J. J. Irwin, C. Laggner, A. I. Abbas, S. J. Hufeisen, N. H. Jensen, M. B. Kuijer, R. C. Matos and T. B. Tran (2009). "Predicting new molecular targets for known drugs." Nature **462**(7270): 175-181.

Keiser, M. J., V. Setola, J. J. Irwin, C. Laggner, A. I. Abbas, S. J. Hufeisen, N. H. Jensen, M. B. Kuijer, R. C. Matos, T. B. Tran, R. Whaley, R. A. Glennon, J. Hert, K. L. Thomas, D. D. Edwards, B. K. Shoichet and B. L. Roth (2009). "Predicting new molecular targets for known drugs." Nature **462**(7270): 175-181.

Keller, T. H., A. Pichota and Z. Yin (2006). "A practical view of 'druggability'." Current opinion in chemical biology **10**(4): 357-361.

Knox, C., V. Law, T. Jewison, P. Liu, S. Ly, A. Frolkis, A. Pon, K. Banco, C. Mak and V. Neveu (2011). "DrugBank 3.0: a comprehensive resource for 'omics' research on drugs." Nucleic acids research **39**(suppl 1): D1035-D1041.

Kotermanski, S. E., J. T. Wood and J. W. Johnson (2009). "Memantine binding to a superficial site on NMDA receptors contributes to partial trapping." The Journal of physiology **587**(19): 4589-4604.

Krejsa, C. M., D. Horvath, S. L. Rogalski, J. E. Penzotti, B. Mao, F. Barbosa and J. C. Migeon (2003). "Predicting ADME properties and side effects: the BioPrint approach." Curr Opin Drug Discov Devel **6**(4): 470-480.

Krishnamurthy, H. and E. Gouaux (2012). "X-ray structures of LeuT in substrate-free outward-open and apo inward-open states." Nature **481**(7382): 469-474.

Kuhn, M., M. Al Banchaabouchi, M. Campillos, L. J. Jensen, C. Gross, A. C. Gavin and P. Bork (2013). "Systematic identification of proteins that elicit drug side effects." Mol Syst Biol **9**: 663.

Kuhn, M., D. Szklarczyk, A. Franceschini, C. von Mering, L. J. Jensen and P. Bork (2012). "STITCH 3: zooming in on protein–chemical interactions." Nucleic acids research **40**(D1): D876-D880.

Kumar, J. and M. L. Mayer (2010). "Crystal structures of the glutamate receptor ion channel GluK3 and GluK5 amino-terminal domains." Journal of molecular biology **404**(4): 680-696.

Kwong, L. N., J. C. Costello, H. Liu, S. Jiang, T. L. Helms, A. E. Langsdorf, D. Jakubosky, G. Genovese, F. L. Muller, J. H. Jeong, R. P. Bender, G. C. Chu, K. T. Flaherty, J. A. Wargo, J. J. Collins and L. Chin (2012). "Oncogenic NRAS signaling differentially regulates survival and proliferation in melanoma." Nat Med **18**(10): 1503-1510.

Kyrola, A., G. E. Blelloch and C. Guestrin (2012). GraphChi: Large-Scale Graph Computation on Just a PC. OSDI.

Lee, M. J., A. S. Ye, A. K. Gardino, A. M. Heijink, P. K. Sorger, G. MacBeath and M. B. Yaffe (2012). "Sequential application of anticancer drugs enhances cell death by rewiring apoptotic signaling networks." Cell **149**(4): 780-794.

Lehar, J., A. S. Krueger, W. Avery, A. M. Heilbut, L. M. Johansen, E. R. Price, R. J. Rickles, G. F. Short, 3rd, J. E. Staunton, X. Jin, M. S. Lee, G. R. Zimmermann and A. A. Borisy (2009). "Synergistic drug combinations tend to improve therapeutically relevant selectivity." Nat Biotechnol **27**(7): 659-666.

Lezon, T. R. and I. Bahar (2010). "Using entropy maximization to understand the determinants of structural dynamics beyond native contact topology." PLoS computational biology **6**(6): e1000816.

Li, J., X. Zhu and J. Y. Chen (2009). "Building disease-specific drug-protein connectivity maps from molecular interaction networks and PubMed abstracts." PLoS Comput Biol **5**(7): e1000450.

Li, Y. Y., J. An and S. J. Jones (2011). "A computational approach to finding novel targets for existing drugs." PLoS computational biology **7**(9): e1002139.

Lindorff-Larsen, K., S. Piana, R. O. Dror and D. E. Shaw (2011). "How fast-folding proteins fold." Science **334**(6055): 517-520.

Lounkine, E., M. J. Keiser, S. Whitebread, D. Mikhailov, J. Hamon, J. L. Jenkins, P. Lavan, E. Weber, A. K. Doak, S. Cote, B. K. Shoichet and L. Urban (2012). "Large-scale prediction and testing of drug activity on side-effect targets." Nature **486**(7403): 361-367.

Ludolph, A. G., P. T. Udvardi, U. Schaz, C. Henes, O. Adolph, H. U. Weigt, J. M. Fegert, T. M. Boeckers and K. J. Föhr (2010). "Atomoxetine acts as an NMDA receptor blocker in clinically relevant concentrations." British journal of pharmacology **160**(2): 283-291.

Ma, J. (2005). "Usefulness and limitations of normal mode analysis in modeling dynamics of biomolecular complexes." Structure **13**(3): 373-380.

Miller, J. R., S. Dunham, I. Mochalkin, C. Banotai, M. Bowman, S. Buist, B. Dunkle, D. Hanna, H. J. Harwood, M. D. Huband, A. Karnovsky, M. Kuhn, C. Limberakis, J. Y. Liu, S. Mehrens, W. T. Mueller, L. Narasimhan, A. Ogden, J. Ohren, J. V. Prasad, J. A. Shelly, L. Skerlos, M. Sulavik, V. H. Thomas, S. VanderRoest, L. Wang, Z. Wang, A. Whitton, T. Zhu and C. K. Stover (2009). "A class of selective antibacterials derived from a protein kinase inhibitor pharmacophore." Proc Natl Acad Sci U S A **106**(6): 1737-1742.

Mnih, A. and R. Salakhutdinov (2007). Probabilistic matrix factorization. Advances in neural information processing systems.

Moses, H., 3rd, E. R. Dorsey, D. H. Matheson and S. O. Thier (2005). "Financial anatomy of biomedical research." JAMA **294**(11): 1333-1342.

Murphy, R. F. (2011). "An active role for machine learning in drug development." Nature chemical biology **7**(6): 327-330.

Murphy, R. F. (2011). "An active role for machine learning in drug development." Nat Chem Biol **7**(6): 327-330.

Myers, S. and A. Baker (2001). "Drug discovery--an operating model for a new era." Nat Biotechnol **19**(8): 727-730.

Newman, D. J. (2008). "Natural products as leads to potential drugs: an old process or the new hope for drug discovery?" J Med Chem **51**(9): 2589-2599.

Oprea, T. I. and J. Mestres (2012). "Drug repurposing: far beyond new targets for old drugs." AAPS J **14**(4): 759-763.

Oprea, T. I., A. Tropsha, J. L. Faulon and M. D. Rintoul (2007). "Systems chemical biology." Nat Chem Biol **3**(8): 447-450.

Ou-Yang, S. S., J. Y. Lu, X. Q. Kong, Z. J. Liang, C. Luo and H. Jiang (2012). "Computational drug discovery." Acta Pharmacol Sin **33**(9): 1131-1140.

Pälvimäki, E.-P., H. Majasuo, A. Laakso, M. Kuoppamäki, E. Syvälahti, B. Roth and J. Hietala (1996). "Interactions of selective serotonin reuptake inhibitors with the serotonin 5-HT2c receptor." Psychopharmacology **126**(3): 234-240.

Paolini, G. V., R. H. Shapland, W. P. van Hoorn, J. S. Mason and A. L. Hopkins (2006). "Global mapping of pharmacological space." Nat Biotechnol **24**(7): 805-815.

Paul, S. M., D. S. Mytelka, C. T. Dunwiddie, C. C. Persinger, B. H. Munos, S. R. Lindborg and A. L. Schacht (2010). "How to improve R&D productivity: the pharmaceutical industry's grand challenge." Nature reviews Drug discovery **9**(3): 203-214.

Penmatsa, A. and E. Gouaux (2014). "How LeuT shapes our understanding of the mechanisms of sodium‐coupled neurotransmitter transporters." The Journal of physiology **592**(5): 863-869.

Perez, C., C. Koshy, Ö. Yildiz and C. Ziegler (2012). "Alternating-access mechanism in conformationally asymmetric trimers of the betaine transporter BetP." Nature **490**(7418): 126-130.

Petersen, B. and A. Mørk (1996). "Chronic treatment with citalopram induces noradrenaline receptor hypoactivity. A microdialysis study." European journal of pharmacology **300**(1): 67-70.

Phillips, J. C., R. Braun, W. Wang, J. Gumbart, E. Tajkhorshid, E. Villa, C. Chipot, R. D. Skeel, L. Kale and K. Schulten (2005). "Scalable molecular dynamics with NAMD." Journal of computational chemistry **26**(16): 1781-1802.

Pøhlsgaard, J., K. Frydenvang, U. Madsen and J. S. Kastrup (2011). "Lessons from more than 80 structures of the GluA2 ligand-binding domain in complex with agonists, antagonists and allosteric modulators." Neuropharmacology **60**(1): 135-150.

Quiocho, F. A. and P. S. Ledvina (1996). "Atomic structure and specificity of bacterial periplasmic receptors for active transport and chemotaxis: variation of common themes." Molecular microbiology **20**(1): 17-25.

Raabe, R. and L. Gentile (2008). "Antidepressant interactions with the NMDA NR1-1b subunit." Journal of Biophysics **2008**.

Rachline, J., F. Perin-Dureau, A. Le Goff, J. Neyton and P. Paoletti (2005). "The micromolar zinc-binding domain on the NMDA receptor subunit NR2B." The Journal of neuroscience **25**(2): 308-317.

Rahmadi, M., M. Narita, A. Yamashita, S. Imai, N. Kuzumaki and T. Suzuki (2011). "Sleep disturbance associated with an enhanced orexinergic system induced by chronic treatment with paroxetine and milnacipran." Synapse **65**(7): 652-657.

Reddy, A. S. and S. Zhang (2013). "Polypharmacology: drug discovery for the future." Expert Rev Clin Pharmacol **6**(1): 41-47.

Ripphausen, P., B. Nisius, L. Peltason and J. Bajorath (2010). "Quo vadis, virtual screening? A comprehensive survey of prospective applications." J Med Chem **53**(24): 8461-8467.

Saeh, J. C., P. D. Lyne, B. K. Takasaki and D. A. Cosgrove (2005). "Lead hopping using SVM and 3D pharmacophore fingerprints." Journal of chemical information and modeling **45**(4): 1122-1133.

Salakhutdinov, R. and A. Mnih (2008). Bayesian probabilistic matrix factorization using Markov chain Monte Carlo. Proceedings of the 25th international conference on Machine learning, ACM.

Sarid-Segal, O., C. M. Knapp, W. Burch, M. A. Richardson, S. Bahtia, K. DeQuattro, M. Afshar, C. Richambault, L. Sickels and E. Devine (2009). "The anticonvulsant zonisamide reduces ethanol self-administration by risky drinkers." The American journal of drug and alcohol abuse **35**(5): 316-319.

Schäfer, M. (2009). "Novel concepts for analgesia in severe pain—current strategies and future innovations." European Journal of Pain Supplements **3**(S1): 6-10.

Schames, J. R., R. H. Henchman, J. S. Siegel, C. A. Sotriffer, H. Ni and J. A. McCammon (2004). "Discovery of a novel binding trench in HIV integrase." Journal of medicinal chemistry **47**(8): 1879-1881.

Schlitter, J., M. Engels and P. Kruger (1994). "Targeted molecular dynamics: a new approach for searching pathways of conformational transitions." J Mol Graph **12**(2): 84-89.

Shan, Y., E. T. Kim, M. P. Eastwood, R. O. Dror, M. A. Seeliger and D. E. Shaw (2011). "How does a drug molecule find its target binding site?" Journal of the American Chemical Society **133**(24): 9181-9183.

Shaw, D. E., M. M. Deneroff, R. O. Dror, J. S. Kuskin, R. H. Larson, J. K. Salmon, C. Young, B. Batson, K. J. Bowers and J. C. Chao (2008). "Anton, a special-purpose machine for molecular dynamics simulation." Communications of the ACM **51**(7): 91-97.

Shekhar, C. (2008). "In silico pharmacology: computer-aided methods could transform drug development." Chem Biol **15**(5): 413-414.

Shimamura, T., S. Weyand, O. Beckstein, N. G. Rutherford, J. M. Hadden, D. Sharples, M. S. Sansom, S. Iwata, P. J. Henderson and A. D. Cameron (2010). "Molecular basis of alternating access membrane transport by the sodium-hydantoin transporter Mhp1." Science **328**(5977): 470-473.

Shuto, S., H. Takada, D. Mochizuki, R. Tsujita, Y. Hase, S. Ono, N. Shibuya and A. Matsuda (1995). "(.+-.)-(Z)-2-(Aminomethyl)-1-phenylcyclopropanecarboxamide Derivatives as a New Prototype of NMDA Receptor Antagonists." Journal of medicinal chemistry **38**(15): 2964-2968.

Siegel, M. G. and M. Vieth (2007). "Drugs in other drugs: a new look at drugs as fragments." Drug Discov Today **12**(1-2): 71-79.

Singh, S. K., C. L. Piscitelli, A. Yamashita and E. Gouaux (2008). "A competitive inhibitor traps LeuT in an open-to-out conformation." Science **322**(5908): 1655-1661.

Singh, S. K., A. Yamashita and E. Gouaux (2007). "Antidepressant binding site in a bacterial homologue of neurotransmitter transporters." Nature **448**(7156): 952-956.

Sirota, M., J. T. Dudley, J. Kim, A. P. Chiang, A. A. Morgan, A. Sweet-Cordero, J. Sage and A. J. Butte (2011). "Discovery and preclinical validation of drug indications using compendia of public gene expression data." Sci Transl Med **3**(96): 96ra77.

Sirota, M., J. T. Dudley, J. Kim, A. P. Chiang, A. A. Morgan, A. Sweet-Cordero, J. Sage and A. J. Butte (2011). "Discovery and preclinical validation of drug indications using compendia of public gene expression data." Science translational medicine **3**(96): 96ra77-96ra77.

Sliwoski, G., S. Kothiwale, J. Meiler and E. W. Lowe, Jr. (2014). "Computational methods in drug discovery." Pharmacol Rev **66**(1): 334-395.

Smicun, Y., S. D. Campbell, M. A. Chen, H. Gu and G. Rudnick (1999). "The role of external loop regions in serotonin transport Loop scanning mutagenesis of the serotonin transporter external domain." Journal of Biological Chemistry **274**(51): 36058-36064.

Smoot, M. E., K. Ono, J. Ruscheinski, P.-L. Wang and T. Ideker (2011). "Cytoscape 2.8: new features for data integration and network visualization." Bioinformatics **27**(3): 431-432.

Sobolevsky, A. I., M. P. Rosconi and E. Gouaux (2009). "X-ray structure, symmetry and mechanism of an AMPA-subtype glutamate receptor." Nature **462**(7274): 745-756.

Song, C. M., S. J. Lim and J. C. Tong (2009). "Recent advances in computer-aided drug design." Brief Bioinform **10**(5): 579-591.

Sorger, P. K., S. R. Allerheiligen, D. R. Abernethy, R. B. Altman, K. L. Brouwer, A. Califano, D. Z. D'Argenio, R. Iyengar, W. J. Jusko and R. Lalonde (2011). Quantitative and systems pharmacology in the post-genomic era: new approaches to discovering drugs and understanding therapeutic mechanisms. An NIH white paper by the QSP workshop group, NIH Bethesda.

Sperandio, O., L. Mouawad, E. Pinto, B. O. Villoutreix, D. Perahia and M. A. Miteva (2010). "How to choose relevant multiple receptor conformations for virtual screening: a test case of Cdk2 and normal mode analysis." European Biophysics Journal **39**(9): 1365-1372.

Stephan, M. M., M. A. Chen, K. M. Penado and G. Rudnick (1997). "An extracellular loop region of the serotonin transporter may be involved in the translocation mechanism." Biochemistry **36**(6): 1322-1328.

Sugita, Y. and Y. Okamoto (1999). "Replica-exchange molecular dynamics method for protein folding." Chemical Physics Letters **314**(1): 141-151.

Sukumaran, M., M. Rossmann, I. Shrivastava, A. Dutta, I. Bahar and I. H. Greger (2011). "Dynamics and allosteric potential of the AMPA receptor N ‐ terminal domain." The EMBO journal **30**(5): 972-982.

Summa, V., A. Petrocchi, F. Bonelli, B. Crescenzi, M. Donghi, M. Ferrara, F. Fiore, C. Gardelli, O. Gonzalez Paz and D. J. Hazuda (2008). "Discovery of raltegravir, a potent, selective orally bioavailable HIV-integrase inhibitor for the treatment of HIV-AIDS infection." Journal of medicinal chemistry **51**(18): 5843-5855.

Sun, Y., R. Olson, M. Horning, N. Armstrong, M. Mayer and E. Gouaux (2002). "Mechanism of glutamate receptor desensitization." Nature **417**(6886): 245-253.

Swann, S. L., S. P. Brown, S. W. Muchmore, H. Patel, P. Merta, J. Locklear and P. J. Hajduk (2011). "A unified, probabilistic framework for structure-and ligand-based virtual screening." Journal of medicinal chemistry **54**(5): 1223-1232.

Takarabe, M., M. Kotera, Y. Nishimura, S. Goto and Y. Yamanishi (2012). "Drug target prediction using adverse event report systems: a pharmacogenomic approach." Bioinformatics **28**(18): i611-i618.

Tfelt-Hansen, P., P. Saxena, C. Dahlöf, J. Pascual, M. Lainez, P. Henry, H.-C. Diener, J. Schoenen, M. Ferrari and P. Goadsby (2000). "Ergotamine in the acute treatment of migraine A review and European consensus." Brain **123**(1): 9-18.

Tirion, M. M. (1996). "Large amplitude elastic motions in proteins from a single-parameter, atomic analysis." Physical review letters **77**(9): 1905.

Traynelis, S. F., L. P. Wollmuth, C. J. McBain, F. S. Menniti, K. M. Vance, K. K. Ogden, K. B. Hansen, H. Yuan, S. J. Myers and R. Dingledine (2010). "Glutamate receptor ion channels: structure, regulation, and function." Pharmacological reviews **62**(3): 405-496.

Vadivelu, N., S. Mitra and D. Narayan (2010). "Recent advances in postoperative pain management." The Yale journal of biology and medicine **83**(1): 11.

van Gunsteren, W. F. and H. J. Berendsen (1990). "Computer simulation of molecular dynamics: Methodology, applications, and perspectives in chemistry." Angewandte Chemie International Edition in English **29**(9): 992-1023.

Wagner, B. K., T. Kitami, T. J. Gilbert, D. Peck, A. Ramanathan, S. L. Schreiber, T. R. Golub and V. K. Mootha (2008). "Large-scale chemical dissection of mitochondrial function." Nat Biotechnol **26**(3): 343-351.

Wagner, L. E., M. Eaton, S. S. Sabnis and K. J. Gingrich (1999). "Meperidine and Lidocaine Block of Recombinant Voltage‐Dependent Na+ Channels: Evidence that Meperidine is a Local Anesthetic." Anesthesiology **91**(5): 1481.

Walsh, C. T. and M. A. Fischbach (2009). "Repurposing libraries of eukaryotic protein kinase inhibitors for antibiotic discovery." Proc Natl Acad Sci U S A **106**(6): 1689-1690.

Wang, H., A. Goehring, K. H. Wang, A. Penmatsa, R. Ressler and E. Gouaux (2013). "Structural basis for action by diverse antidepressants on biogenic amine transporters." Nature **503**(7474): 141-145.

Wang, R., L. Liu, L. Lai and Y. Tang (1998). "SCORE: A new empirical method for estimating the binding affinity of a protein-ligand complex." Molecular modeling annual **4**(12): 379-394.

Warmuth, M. K., J. Liao, G. Rätsch, M. Mathieson, S. Putta and C. Lemmen (2003). "Active learning with support vector machines in the drug discovery process." Journal of Chemical Information and Computer Sciences **43**(2): 667-673.

Wolber, G. and T. Langer (2005). "LigandScout: 3-D pharmacophores derived from protein-bound ligands and their use as virtual screening filters." Journal of chemical information and modeling **45**(1): 160-169.

Xu, C., D. Tobi and I. Bahar (2003). "Allosteric changes in protein structure computed by a simple mechanical model: hemoglobin T↔ R2 transition." Journal of molecular biology **333**(1): 153-168.

Yamanishi, Y., M. Araki, A. Gutteridge, W. Honda and M. Kanehisa (2008). "Prediction of drug–target interaction networks from the integration of chemical and genomic spaces." Bioinformatics **24**(13): i232-i240.

Yamanishi, Y., M. Kotera, M. Kanehisa and S. Goto (2010). "Drug-target interaction prediction from chemical, genomic and pharmacological data in an integrated framework." Bioinformatics **26**(12): i246-i254.

Yamashita, A., S. K. Singh, T. Kawate, Y. Jin and E. Gouaux (2005). "Crystal structure of a bacterial homologue of Na+/Cl--dependent neurotransmitter transporters." Nature **437**(7056): 215-223.

Yang, L.-W. and C.-P. Chng (2008). "Coarse-grained models reveal functional dynamics-I. elastic network models–theories, comparisons and perspectives." Bioinformatics and biology insights **2**: 25.

Yang, L., J. Chen and L. He (2009). "Harvesting candidate genes responsible for serious adverse drug reactions from a chemical-protein interactome." PLoS Comput Biol **5**(7): e1000441.

Yang, L., G. Song, A. Carriquiry and R. L. Jernigan (2008). "Close correspondence between the motions from principal component analysis of multiple HIV-1 protease structures and elastic network modes." Structure **16**(2): 321-330.

Yang, L., G. Song and R. L. Jernigan (2009). "Protein elastic network models and the ranges of cooperativity." Proceedings of the National Academy of Sciences **106**(30): 12347-12352.

Yera, E. R., A. E. Cleves and A. N. Jain (2011). "Chemical structural novelty: on-targets and off-targets." Journal of medicinal chemistry **54**(19): 6771-6785.

Yıldırım, M. A., K.-I. Goh, M. E. Cusick, A.-L. Barabási and M. Vidal (2007). "Drug—target network." Nature biotechnology **25**(10): 1119-1126.

Young, D. W., A. Bender, J. Hoyt, E. McWhinnie, G. W. Chirn, C. Y. Tao, J. A. Tallarico, M. Labow, J. L. Jenkins, T. J. Mitchison and Y. Feng (2008). "Integrating high-content screening and ligand-target prediction to identify mechanism of action." Nat Chem Biol **4**(1): 59-68.

Zambrowicz, B. P. and A. T. Sands (2004). "Modeling drug action in the mouse with knockouts and RNA interference." Drug Discovery Today: TARGETS **3**(5): 198-207.

Zanelli, S. A., N. J. Solenski, R. E. Rosenthal and G. Fiskum (2005). "Mechanisms of Ischemic Neuroprotection by Acetyl‐l‐carnitine." Annals of the New York Academy of Sciences **1053**(1): 153-161.

Zhao, S. and R. Iyengar (2012). "Systems pharmacology: network analysis to identify multiscale mechanisms of drug action." Annu Rev Pharmacol Toxicol **52**: 505-521.

Zhao, Y., D. Terry, L. Shi, H. Weinstein, S. C. Blanchard and J. A. Javitch (2010). "Single-molecule dynamics of gating in a neurotransmitter transporter homologue." Nature **465**(7295): 188-193.

Zhao, Y., D. S. Terry, L. Shi, M. Quick, H. Weinstein, S. C. Blanchard and J. A. Javitch (2011). "Substrate-modulated gating dynamics in a Na+-coupled neurotransmitter transporter homologue." Nature **474**(7349): 109-113.

ZIMMER, M. and F. HOFMANN (1987). "Differentiation of the drug‐binding sites of calmodulin." European Journal of Biochemistry **164**(2): 411-420.

Zou, J., P. Ji, Y. L. Zhao, L. L. Li, Y. Q. Wei, Y. Z. Chen and S. Y. Yang (2012). "Neighbor communities in drug combination networks characterize synergistic effect." Mol Biosyst **8**(12): 3185-3196.

Zou, J., S. D. Luo, Y. Q. Wei and S. Y. Yang (2011). "Integrated computational model of cell cycle and checkpoint reveals different essential roles of Aurora-A and Plk1 in mitotic entry." Mol Biosyst **7**(1): 169-179.

Zou, J., M. W. Zheng, G. Li and Z. G. Su (2013). "Advanced systems biology methods in drug discovery and translational biomedicine." Biomed Res Int **2013**: 742835.